Photosynthetic Apparatus of Green Sulfur Bacteria Studied by Coherent Two-Dimensional Electronic Spectroscopy

Jakub Dostál

Title: Photosynthetic Apparatus of Green Sulfur Bacteria Studied by Coherent Two-Dimensional Electronic Spectroscopy

Abstract

The process of photosynthesis begins with a capture of sunlight and its quick conversion into the chemical energy. Both these primary processes take place in a specially designed photosynthetic apparatus that is present in cells of all photosynthetic organisms. In green sulfur bacteria the apparatus consists of a massive light-harvesting antenna (chlorosome), intermediate antennas (baseplate complex and FMO proteins) and of the reaction center, where the conversion into the chemical energy occurs. The energy flow through the apparatus can be monitored by time-resolved spectroscopy techniques. Coherent two-dimensional electronic spectroscopy (2DES) in one of such techniques, which combines high temporal and spectral resolution, and therefore it is especially well suited for studying multichromophoric systems such as photosynthetic apparatus. This thesis describes the principles of the 2DES technique and outlines the basic facts about the photosynthetic apparatus of green sulfur bacterium *Chlorobaculum tepidum*. Finally, it summarizes the investigation of the photosynthetic machinery using 2DES. Results presented in this thesis provide new insights into the exciton diffusion and vibrational coherences within chlorosomes, excitonic structure of the baseplate and the overall energy flow through the entire photosynthetic apparatus in whole cells.

Key words

green sulfur bacteria, primary processes of photosynthesis, energy transfer, excitons, vibrational coherence, coherent two-dimensional electronic spectroscopy

Classification system and/or index terms (if any)

Supplementary bibliographical information	Language English
ISSN and key title	ISBN 978-91-7422-352-1

Recipient's notes	Number of pages 140	Price
	Security classification	

Název práce: Studie fotosyntetického aparátu zelených sirných bakterií metodou koherentní dvourozměrné elektronové spektroskopie.

Autor: Jakub Dostál

Katedra: Katedra Chemické Fyziky a Optiky (Univerzita Karlova v Praze) a Department of Chemical Physics (Lund University)

Vedoucí doktorské práce: Jakub Pšenčík and Donatas Zigmantas

Abstrakt: Proces fotosyntézy začíná záchytem světelné energie a její rychlou konverzí na energii chemickou. Oba tyto primární procesy probíhají v evolucí specielně vyvinutých fotosyntetických aparátech, které se nacházejí v buňkách všech fotosyntetických organismů. V případě zelených sirných bakterií se tento aparát skládá z masivní světlosběrné antény – chlorosomu, intermediálních antén – základní desky chlorosomu a FMO proteinu a konečně z reakčního centra, kde se probíhá zmíněná konverze energie. Tok energie celým fotosyntetickým aparátem může být studován metodami časově rozlišené optické spektroskopie. Mezi jinými, koherentní dvourozměrné elektronová spektroskopie (2DES) kombinuje vysoké časové a spektrální rozlišení a je tedy obzvláště vhodná pro studium multichromoforických systémů jako je fotosyntetický aparát. Tato dizertační práce se skládá za tří částí. V první části jsou vysvětleny základní principy této metody a ve druhé jsou uvedena základní známá fakta o fotosyntetickém aparátu zelené sirné bakterie *Chlorobaculum tepidum*. Ve třetí části jsou shrnuty výsledky získané pro tento aparát metodou 2DES, které přinášejí nové poznatky o vibračních koherencích a difuzi excitonů v chlorosomu, o excitonové struktuře základní desky chlorosomu a o celkovém toku energie kompletním fotosyntetickým aparátem v celých buňkách.

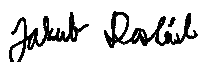**Klíčová slova:** zelené sirné bakterie, primární procesy fotosyntézy, přenos energie, excitony, vibrační koherence, koherentní dvourozměrná elektronová spektroskopie

In Prague date 7.4.2014   Jakub Dostál

Photosynthetic Apparatus of Green Sulfur Bacteria Studied by Coherent Two-Dimensional Electronic Spectroscopy

Jakub Dostál

LUND
UNIVERSITY

Contents

List of Papers

Paper I. **Two-dimensional electronic spectroscopy reveals ultrafast energy diffusion in chlorosomes**
<u>Jakub Dostál</u>, Tomáš Mančal, Ramūnas Augulis, František Vácha, Jakub Pšenčík and Donatas Zigmantas
Journal of the American Chemical Society, 134, 11611 – 11617 (2012)

Paper II. **Unraveling the nature of coherent beatings in chlorosomes**
<u>Jakub Dostál</u>, Tomáš Mančal, František Vácha, Jakub Pšenčík and Donatas Zigmantas
The Journal of Chemical Physics, 140, 115103 (2014)

Paper III. **Transfer of vibrational coherence through incoherent energy transfer process in Förster limit**
Tomáš Mančal, <u>Jakub Dostál,</u> František Vácha, Jakub Pšenčík and Donatas Zigmantas
Canadian Journal of Chemistry, 92, 135-143 (2014)

Paper IV. **2D electronic spectroscopy reveals excitonic structure in the baseplate of a chlorosome**
<u>Jakub Dostál,</u> František Vácha, Jakub Pšenčík and Donatas Zigmantas
submitted to The Journal of Physical Chemistry Letters

Paper V. **Tracking energy flow through the intact photosynthetic apparatus in vivo**
<u>Jakub Dostál</u>, Jakub Pšenčík and Donatas Zigmantas
manuscript

Papers not included in this thesis:

Paper VI. **Fast exciton dynamics and coherent oscillations revealed by coherent 2D spectroscopy in chlorosomes**
<u>Jakub Dostál</u>, Tomáš Mančal, František Vácha, Ramūnas Augulis, Jakub Pšenčík and Donatas Zigmantas
EPJ Web of Conferences, 41, 08015 (2013)

Paper VII. **Spectroscopic study of water soluble chlorophyll-binding protein from *Lepidium virginicum***
Jan Alster, Heiko Lokstein, <u>Jakub Dostál</u>, Akira Uchida and Donatas Zigmantas
The Journal of Physical Chemistry B, 118, 3524-3531 (2014)

My Contribution to the Papers

Papers I, II, IV, V and VI: I performed the experiments, data analysis and interpretation. I wrote a major part of the paper.

Paper III: I discussed the described effects. I commented on the manuscript.

Paper VII: I performed part of the experiments. I commented on the manuscript.

List of Abbreviations

2D	two-dimensional
2DES	coherent two-dimensional electronic spectroscopy
BChl	bacteriochlorophyll
Cba.	*Chlorobaculum*
Chl	chlorophyll
ESA	excited state absorption
FMO	Fenna-Matthews-Olson (protein)
FWHM	full width at half of maximum
GSB	ground state bleach
LO	local oscillator
NMR	nuclear magnetic resonance
NR	non-rephasing
PP	pump-probe (transient absorption experiment)
PS1	photosystem 1
PS2	photosystem 2
QB	quantum beatings
R	rephasing
RC	reaction center
SE	stimulated emission

8

Introduction

Photosynthesis is one of the most important processes on the planet Earth. A vast majority of plants and several groups of bacteria employ photosynthesis to build their bodies using the incoming solar energy and abundant simple inorganic material. The plant bodies in turn serve as an energy source (directly or indirectly) for almost all other organisms living on our planet, including humans. Photosynthesis is thus responsible for sustaining almost entire life on Earth.

Probably everybody has at some point seen the simple chemical equation describing photosynthesis as a light driven synthesis of water and carbon dioxide into simple sugar (glucose) and oxygen.

$$6\,H_2O + 6\,CO_2 \xrightarrow{\quad light \quad} C_6H_{12}O_6 + 6\,O_2$$
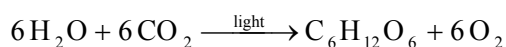
However, the actual realization of the simple-looking reaction requires a complicated sequence of tens of biochemical enzymatic sub-reactions happening at various places in the cell.

In order to supply this machinery with energy, photosynthetic organisms have adapted various forms of light-harvesting apparatus that gives most of them their characteristic green color. The apparatus typically consists of various types of antennas and reaction centers. The primary function of the antennas is to collect the energy of light and deliver it in the form of excitation energy to the reaction centers, where it is converted into electrochemical energy of separated charges and consequentially into chemical energy of reduced chemical compounds. The energy transfer within and between the individual complexes and charge separation are often referred to as the primary processes of photosynthesis.

Since the primary processes of photosynthesis are intimately connected with the absorption of visible and near infrared light, they can be studied by methods of time-resolved optical spectroscopy. A great deal can be learned by measurements of transient absorption using the well-established pump-probe experimental scheme. Even a more detailed picture can be obtained using advanced spectroscopic techniques, which were developed only recently. One such cutting-edge technique, that presently experiences a strong boom in the field of photosynthesis, is the coherent two-dimensional electronic spectroscopy (2DES).

This thesis focuses on primary processes resolved in the photosynthetic apparatus of green sulfur bacterium *Chlorobaculum tepidum* by 2DES. The thesis is organized as follows. In Chapter 1 principles of 2DES technique are explained. The focus is brought on 2DES in relation to the well-established pump-probe technique showing that 2DES is its advanced version. The advantages and

disadvantages of both approaches are thoroughly discussed. Chapter 2 summarizes the basic facts about the photosynthetic apparatus of green sulfur bacteria with special focus on its primary light-harvesting function. Chapter 3 provides an overview of the new insights into the primary processes in this photosynthetic system that were gained by application of 2DES. The detailed information can be found in the publications reprinted at the end of the thesis.

1. Coherent Two-Dimensional Electronic Spectroscopy

1.1. From Pump-Probe to Coherent Two-Dimensional Electronic Spectroscopy

Over the past decades transient absorption spectroscopy (very often referred to as pump-probe, PP) has become a well-established spectroscopic technique and is nowadays routinely used to study dynamic processes in various materials. A generic PP experiment proceeds as follows. First, the sample is illuminated by the excitation (pump) pulse. After that the induced transient change of the sample absorption is monitored, typically by using another laser pulse (probe) delayed in time (Fig. 1). This basic concept is put into practice in many different ways depending on the spectral region, the timescale and the physical character of the studied process.
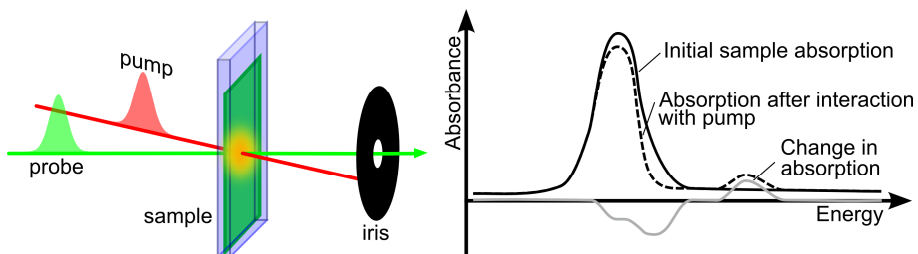
Fig. 1: Schematic illustration of pump-probe experiment

Changes in the sample absorption induced by the pump pulse consist, in theory, of three different contributions: ground state bleach (GSB), stimulated emission (SE) and excited state absorption (ESA). Firstly, the original absorption is diminished by the depletion of electrons from the molecular ground state. This ground state bleach affects not only the absorption band, excited by the pump, but also all other bands that share the common ground state. The effect lasts until electrons (not necessarily the original ones) refill vacated positions. Secondly, as Einstein predicted [1] light interaction with the excited electrons cause stimulated emission, which initially decreases the absorption of the band excited by the pump. However, as the electrons relax to the lower-lying energy levels, SE diminishes the absorption of red-shifted absorption bands instead. Thirdly, after the excitation, new absorption bands can appear in the spectrum either due to the absorption of excited electrons into the higher excited states or due to the

formation of some new absorptive species *e.g.* by a photoinduced chemical reaction. This contribution is referred to (especially in the former case) as excited state absorption. In practice, the overlap of these three contributions and their dynamic changes form in general very complex time evolution of the transient absorption spectrum.

The transient absorption technique is especially suitable for studying dynamics of photosynthetic complexes [2]. Since the primary processes of photosynthesis are triggered by the light excitation, the PP is capable of monitoring them almost in the "real time".

Various photosynthetic processes occur on a broad range of timescales varying from femtoseconds to seconds. In order to selectively excite specific absorption bands and thus consequently monitor the triggered system dynamics, it is necessary to use spectrally narrow pump pulses. However, such an approach excludes studies of the fastest processes (happening on sub-picosecond timescales), because ultrashort laser pulses, necessary to obtain the desired time resolution, cover a substantial spectral region (see Section 1.4).

On the other hand, simultaneous excitation of multiple absorption bands results in the observation of oscillatory components in the time evolution of the transient absorption. The presence of this so-called quantum coherences (or quantum beatings) is tightly connected with the very fundamentals of quantum mechanics as will be discussed in Section 1.12.

Coherent two-dimensional electronic spectroscopy (2DES) efficiently remedies the loss of spectral selectivity connected with spectrally broad pulses, while maintaining the capability to excite quantum coherences [3–6]. It is designed to bypass the Heisenberg's limitation of the ultrafast PP spectroscopy by providing additional resolution within the spectrum of the excitation pulse. As a consequence, the 2DES provides both high temporal and high spectral resolution. Simultaneously, the quantum coherences can be observed in the form of oscillatory signals located in specific regions of the 2D spectra. The character of the quantum coherences can be in principle retrieved by careful analysis of its frequency and position in the spectrum [7,8].

1.2. Experimental Setup

Principles of 2DES will be explained using the particular example of our experimental apparatus. For this purpose let us describe it first.

The core of the setup, depicted in Fig. 2, was pumped by the laser system consisting of the KGW amplified laser (Pharos, Light Conversion) and lab-made NOPA producing ultrashort (15 – 20 fs) laser pulses, tunable in the range of 450 –

850 nm with maximal repetition rate of 200 kHz. First each pulse was split by a beamsplitter into two. The time delay between resulting pulses (population time) was set by a mechanical delay line and each of the pulses was further divided into two by a transmissive diffraction grating, optimized for the $\pm 1^{st}$ order of diffraction. The resulting four laser pulses were labeled as 1, 2, 3 and the local oscillator (LO) as indicated in Fig. 2. The time delay between pulses 1 and 2 was adjusted by inserting fused silica wedges into the optical paths of individual beams. The delay between pulses 3 and LO was fixed. In addition, the LO pulse was attenuated by the OD 3 neutral density filter and beams 1 and 2 were modulated on different frequencies by a pair of optomechanical choppers. The resulting sequence of four pulses (Fig. 3) was focused into the same spot of the sample in a box-car geometry. The non-linear 3rd order signal was detected in the LO direction by a CCD camera after passing through a spectrograph. The lock-in detection on sum and difference chopper frequencies was employed to achieve a high signal to noise ratio. The apparatus is described in more details in [9,10].
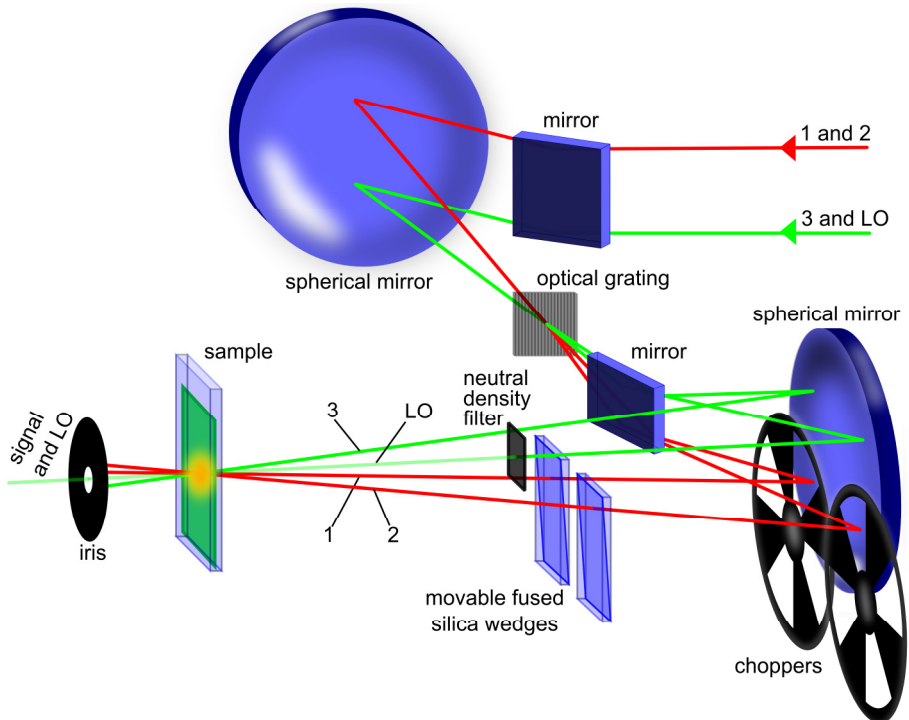
Fig. 2: Schematic picture of the experimental setup.

The purpose of all the essential parts of the experimental setup (namely, the number of beams, their arrangement in time and non-collinear geometry and the presence of choppers) will be explained in the following text together with the principles of the 2DES technique.
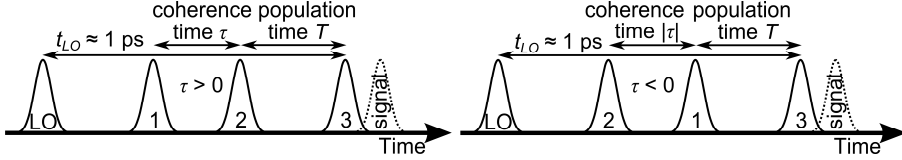
Fig. 3: Definition of delays between pulses for positive (left) and negative (right) coherence times.

1.3. Introduction to the Formalism

Let us introduce the formalism that will be used in the entire chapter. The electric field $E(t)$ of the transform-limited laser pulses is written in the time domain as

$$E(t) = \alpha\varepsilon(t)e^{i\left(\vec{k}\cdot\vec{r}-\omega_0 t\right)} + \text{c.c.}; \quad \varepsilon(t)\in\mathbb{R}, \alpha\in\mathbb{C}, \tag{1}$$

where $\boldsymbol{r}$ stands for the position vector and t for time, ω_0 is the angular frequency of the carrier wave and $\boldsymbol{k}$ its wavevector. The amplitude of the wave is characterized by the real function $\varepsilon(t)$ that determines the temporal profile of the pulse envelope which slowly varies (compared to the optical cycle) in time. Most of the times the constant α can be set to 1, however setting it to some complex number allows further adjustment of the amplitude and phase of the pulse. The symbol c.c. stands for complex conjugate of the preceding term – describing the electric field as a real quantity.

The spectrum of the electric field $E(\omega)$ is defined as the inverse Fourier transform of (1) *i.e.*

$$E(\omega) = \frac{1}{\sqrt{2\pi}}\int E(t)e^{i\omega t}\mathrm{d}t = \alpha\varepsilon(\omega-\omega_0)e^{i\vec{k}\cdot\vec{r}} + \alpha^*\varepsilon(\omega+\omega_0)e^{-i\vec{k}\cdot\vec{r}}, \tag{2}$$

where the spectral profile $\varepsilon(\omega)$ is defined as

$$\varepsilon(\omega) = \frac{1}{\sqrt{2\pi}}\int \varepsilon(t)e^{i\omega t}\mathrm{d}t \tag{3}$$

and the symbol * indicates the complex conjugation. Note that the electric field spectrum is complex quantity that spans over positive and negative frequencies. However, the fact that $\varepsilon(t)$ is a real quantity implies the symmetry of its spectral profile $\varepsilon(\omega)$

$$\varepsilon^*(\omega) = \varepsilon(-\omega). \tag{4}$$

Since it is assumed that the full width at half of maximum (FWHM) of $\varepsilon(t)$ is much longer than the optical period T_0 of the carrier wave the FWHM of $\varepsilon(\omega)$ is much smaller than the optical frequency

$$\mathrm{FWHM}\{\varepsilon(t)\} \gg T_0 \Leftrightarrow \mathrm{FWHM}\{\varepsilon(\omega)\} \ll \omega_0. \tag{5}$$

Using inverse relation to (2) and the symmetry (4), the time-dependent electric field can be alternatively expressed as a sum of harmonic waves with frequencies distributed around the central (positive) frequency ω_0

$$E(t) = \frac{1}{\sqrt{2\pi}} \int E(\omega) \mathrm{e}^{-i\omega t} \mathrm{d}\omega = \frac{1}{\sqrt{2\pi}} \int \alpha \varepsilon(\omega - \omega_0) \mathrm{e}^{i(\vec{k}\cdot\vec{r} - \omega t)} \mathrm{d}\omega + \mathrm{c.c.} \tag{6}$$

The light intensity $I(t)$ is defined through

$$I(t) = \left\langle E^2(t) \right\rangle = |\alpha|^2 |\varepsilon(t)|^2, \tag{7}$$

where the angle brackets denote such a time averaging that cancels out all terms oscillating with the optical frequency. The spectral intensity $I(\omega)$ is obtained by plugging (6) into (7) and using the property (5)

$$I(\omega) = |E(\omega)|^2 = |\alpha|^2 |\varepsilon(\omega - \omega_0)|^2 + |\alpha|^2 |\varepsilon(\omega + \omega_0)|^2. \tag{8}$$

1.4. The Origin of High Spectral Resolution – the Double Pump Pulse

2DES combines high temporal and spectral resolution – properties that are not possible to achieve in the conventional PP simultaneously. In this section we will demonstrate on a simple model system the limitations of PP as well as how they can be bypassed by the 2DES technique.

Our model system will be such that its absorption spectrum consists of two well-separated absorption bands not too far apart (Fig. 4). Moreover, it is designed in such a way that the photon absorption in any of the two bands triggers a different process that manifests itself as a transient change of absorption in some remote part of the spectrum. Finally, we invoke natural assumption that the probability of the photon absorption is proportional to the spectral intensity at the frequency of the band.

The spectral resolution of the PP technique is given by the spectral width of the excitation pulse. As long as the laser spectrum is narrow enough to excite

individual bands selectively the two processes can be studied separately. Similarly, the temporal resolution of the experiment is given by the width of the temporal profile of the excitation pulse. If we want to study ultrafast processes a short pump pulse is required. As a consequence of Heisenberg's uncertainty principle regarding time and energy (or alternatively as a consequence of elementary properties of classical electromagnetic waves) the relation between the spectral and temporal profile is the Fourier transform. A short pulse has broad spectrum and vice versa. Therefore, if the desired time resolution is high (since the processes of interest are too fast) the spectral intensity becomes broad enough to cover both absorption bands simultaneously. Such laser pulse, however, excites both bands, the selectivity is lost, and signatures of both processes, that are simultaneously triggered, are observed in the signal (Fig. 4). Since there is no way how to decompose the single signal curve into the individual components, the PP becomes ineffective. In such a situation 2DES is the method of choice.
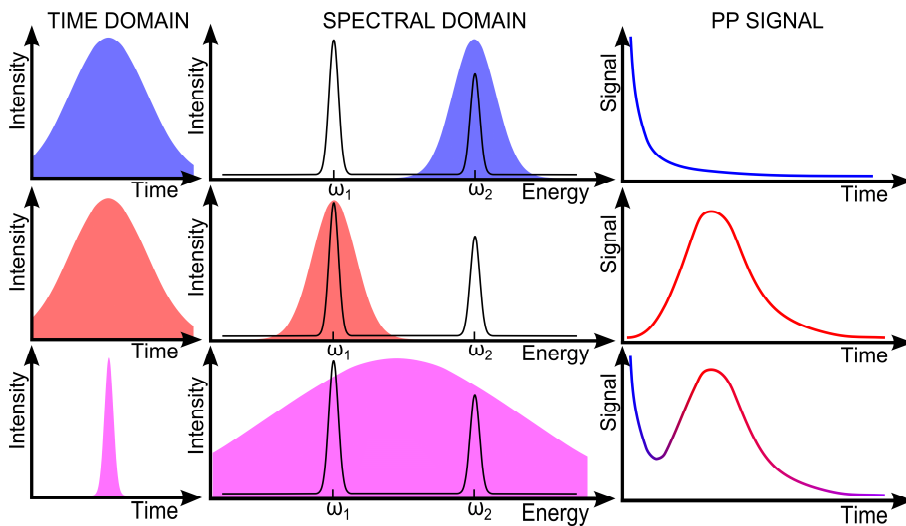
Fig. 4: Relation between the temporal (left column) and spectral (middle column) intensity of Gaussian laser pulse that serves as a pump in the transient absorption measurement. The spectral intensity in the middle column is compared to the absorption of the model system (solid line). The right column illustrates the time evolution of transient absorption detected at unspecified frequency after the system excitation by the pump pulse.

However, 2DES operates correctly only under one additional assumption concerning the studied system which for our simple model system can be formulated as follows:

Condition of linearity: *The "mixed" signal that is observed after the simultaneous excitation of both absorption bands is a simple linear combination of the individual signals that would be observed after the selective excitation of individual bands. The individual signals contribute to the linear combination proportionally to the spectral intensity at frequencies of the triggering bands.*

This condition is reasonable for many systems. Providing the condition of linearity, a separation of the signal into the individual contributions can be achieved by mutual comparison of a set of signals, in which every individual one was measured with different specially designed pump spectrum. And this is the very principle of the 2DES technique.

The 2DES technique utilizes laser pulses, the electric field E_{pump} of which looks in the time domain like two identical laser pulses E_{pulse} satisfying eq. (1), delayed with respect to each other by the time interval τ (so called coherence time)

$$E_{pump}(t) = E_{pulse}(t) + E_{pulse}(t-\tau).$$ (9)

The typical temporal profile $\varepsilon_{pulse}(t)$ of each sub-pulse has a Gaussian shape. In lab, the double pulse is generated by two laser pulses delayed in time and focused at the same spot in the sample – these are denoted as pulses 1 and 2 in Fig. 2. Electric field of the double-pulse can be transformed into the frequency domain using the Fourier shift theorem as

$$E_{pump}(\omega) = E_{pulse}(\omega)(1 + e^{i\omega\tau}),$$ (10)

which corresponds to the spectral intensity

$$I_{pump}(\omega) = 2I_{pulse}(\omega)(1 + \cos(\omega\tau)).$$ (11)

Note that it is identical to the spectral intensity of the single sub-pulse (which has Gaussian shape in case the temporal profile was also Gaussian) modulated by a cosine-shaped interference fringes (Fig. 5). Since the density of fringes is proportional to the delay between the two pulses, it can be easily varied by delaying one pulse with respect to another. In experiment, this is done by inserting the fused silica wedges into one of the laser beam paths.

Naturally, the transient absorption signal of the sample that was excited by the double pulse varies as the pulse delay is scanned. In the example of the model system, some limiting cases can be imagined. If the first absorption band falls into the fringe maximum and the second one into the minimum, the first process is preferentially triggered. The situation becomes analogous to the selective

excitation of the first band in the PP experiment (Fig. 4). A similar situation occurs for some different fringe density, in which the second band is excited. In the case when both bands are covered by fringe maxima the two processes are triggered simultaneously as in the case of the broad band PP experiment described above.

During the 2D experiment the density of spectral fringes (*i.e.* pulse time delay, or coherence time τ) is scanned. As the fringes travel through the absorption bands the signatures of both processes periodically appear and disappear in the signal with a frequency identical to the position of the absorption bands in the spectrum. This allows for retrieving the signal of the individual processes by means of Fourier analysis. As a consequence, additional resolution inside the broad spectrum of the ultrashort laser pulse is achieved.
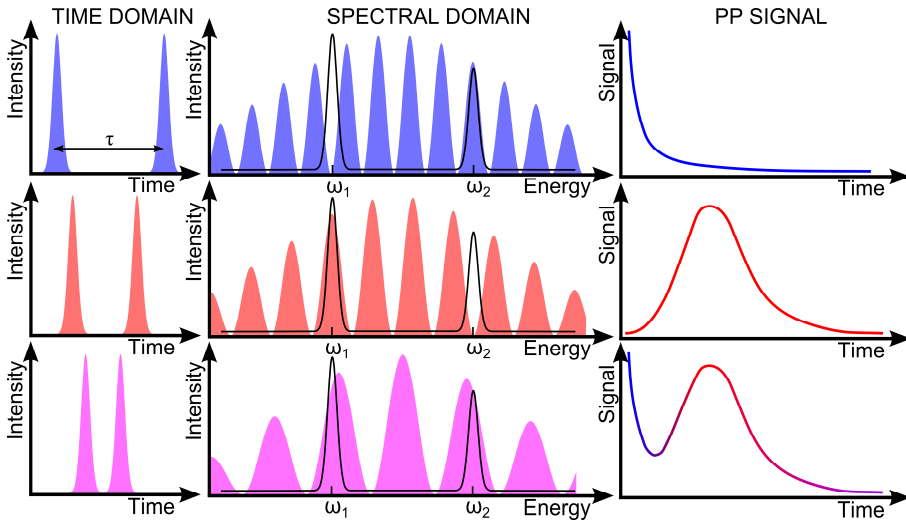
Fig. 5: Temporal (left column) and spectral (middle column) profile of laser pump pulses used by the 2DES technique. The spectral intensity in the middle column is compared to the absorption of the model system (solid line). The right column illustrates the time evolution of transient absorption detected at unspecified frequency after the system excitation by the pump pulse.

We will finish this section by a slightly philosophical discussion. In the text above the pump pulse was constructed as a composition of two laser sub-pulses delayed in time and the core principle of the 2DES technique was related to its spectral properties. From the point of view of classical optics there is no catch here, the double-pulse shape is surely as valid as any other pulse shape and its spectrum can be simply obtained by applying the Fourier transform. However, one may ask: "Why the sample is not already excited by the first sub-pulse – how can the sample know that there is another sub-pulse coming?" and "What would

18

happen if the second part actually did not arrive, possibly being somehow diverted into some other direction at the last possible moment?" In fact, there is no reason to ask such questions about the double pulse only. How can the sample know that the remaining part of the Gaussian laser pulse is still coming at the very moment the front of the pulse has just reached the sample?

None of these questions can be answered in the terms of classical physics. All the observed effects stand on the very principles of the quantum mechanics and the double-pulse case is in fact a nice demonstration of the famous double slit experiment [11]. However, in our case the "slits" are located in time, not in space as usual. The photon can be absorbed by the sample during any of the two different times and there is no way to determine when the absorption actually happens. The result is the spectral interference described by relation (11). [*] If the second pulse had not arrived, the interference pattern would have been lost, analogously to the double slit experiment where interference also vanishes once one slit is covered. In fact, there will always be some photons absorbed from the first or second pulse only – but they trigger processes that are not of concern here. In 2DES we are after the processes triggered by the excitation done at "two different times simultaneously". The way how to distinguish these processes from others is described in the next section.

1.5.   3rd Order Signal Selectivity – Non-Collinear Geometry

In the previous section it was shown that the 2DES signal originates by the interaction of the sample with three laser pulses – the first two collectively acting as a pump and the third one probing the sample absorption. However, the 2DES signal is not the only signal generated by the pulse sequence. For example, each pair of pulses acts as a conventional PP experiment – the second pulse of the pair probing the change of absorption induced by the first one. If all the beams were collinear, the signals originating from these additional processes would be detected together with the desired 2DES signal as they would propagate into the same direction. The simultaneous detection of all the signals would prevent the Fourier analysis described above.

One way how to overcome this problem is to focus the three pulses along three non-collinear wavevectors k_1, k_2 and k_3 as indicated in the schematic picture of the apparatus (Fig. 2). In such an arrangement, the spatial distribution of the

---

[*] It is interesting to note that the temporal double-slit experiment has been demonstrated for massive particles as well [12] and it is not limited to photons only.

light intensity of the first two beams I_{pump} creates a periodic interference pattern in their focus (see Fig. 6)

$$I_{pump}(\omega,\vec{r}) = 2I_{pulse}(\omega)\left[1+\cos\left(\left(\vec{k}_1-\vec{k}_2\right)\cdot\vec{r}-|\omega|\tau\right)\right].\qquad(12)$$

Note that the last equation is just a generalization of (11) for the non-collinear geometry of laser beams, and therefore the spectral intensity periodically varies with the light frequency as it was shown in the previous section.
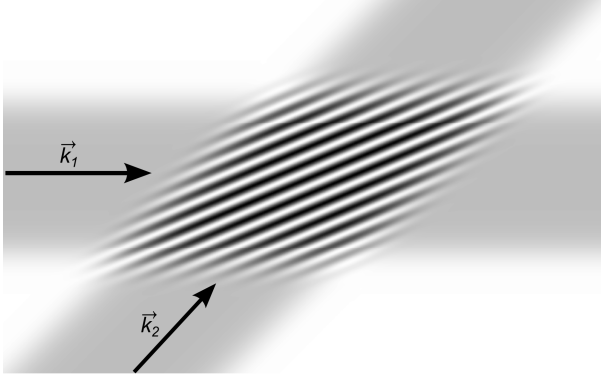
Fig. 6: The light intensity distribution of two crossing laser beams in space

Consequently, the concentration of molecules $\rho_{es}(\omega_{exc},r)$ that are excited by a photon of the particular frequency ω_{exc} creates a periodic structure that copies the light intensity distribution through the sample and that acts similarly to an optical grating

$$\rho_{es}(\omega_{exc},\vec{r}) = A(\omega_{exc})I_{pump}(\omega_{exc},\vec{r}),\qquad(13)$$

where $A(\omega)$ is the sample absorption profile. Naturally, the concentration of molecules $\rho_{gs}(r)$ that were left in the ground state (*i.e.* not excited by any frequency) forms a complementary grating given by

$$\rho_{gs}(\vec{r}) = \rho_{total} - \int \rho_{es}(\omega_{exc},\vec{r})\,\mathrm{d}\omega_{exc},\qquad(14)$$

where ρ_{total} is the total concentration of molecules that is assumed to be uniform through the entire sample.

The third (probe) pulse drives the oscillatory motions of the molecular dipole moments that consequently radiate secondary waves, having same frequency as the driving electric field. In other words, the incoming radiation is elastically scattered by molecules of the sample. The phase and amplitude of the

scattered radiation depends on microscopic properties of the molecules and is generally different for molecules in the ground state and in the excited state. The total radiation scattered by the periodically distributed molecules in the excited state adds up to a planar wave propagating into a direction **k** (so-called phase matching direction) that is different from the direction **k₃** of the probing beam. The same is valid for the radiation scattered by molecules in the ground state.

Let us focus first on the electric field E_{gs} scattered by the molecules in the ground state. Since, due to (6), the probe electric field E_{probe} at position **r'** in the sample can be written as

$$E_{probe}(t,\vec{r}') = \frac{1}{\sqrt{2\pi}} \int \varepsilon_{probe}(\omega_3 - \omega_0) e^{i(\vec{k}_3 \cdot \vec{r}' - \omega_3 t)} d\omega_3 + \text{c.c.},\qquad(15)$$

the secondary wave scattered by unexcited molecules located in the infinitesimal volume element d^3r' in the sample and observed at position **r** is given by

$$E_{gs}(t,\vec{r}-\vec{r}')d^3r' = \frac{1}{\sqrt{2\pi}} \int s_{gs}(\omega_3)\varepsilon_{probe}(\omega_3 - \omega_0) e^{i\vec{k}\cdot(\vec{r}-\vec{r}')} e^{i(\vec{k}_3 \cdot \vec{r}' - \omega_3 t)} d\omega_3$$

$$\times \rho_{gs}(\vec{r}')d^3r' + \text{c.c.}\qquad(16)$$

Here the amplitudes and phases of the scattered and driving waves are related by the complex response function $s_{gs}(\omega)$. In addition, the scattered wave is modeled by a plane wave propagating into the direction **k** by adding the phase term $e^{ik(r-r')}$, which is a good approximation if the detector is placed far away from the sample.

The total electric field, scattered by molecules in the ground states, is obtained by combining (16) with (12), (13) and (14) and integrating over the whole grating volume (that is considered very large), which gives

$$E_{gs}(t,\vec{r}) = \frac{1}{\sqrt{2\pi}} \int s_{gs}(\omega_3)\varepsilon_{probe}(\omega_3 - \omega_0) e^{i(\vec{k}\cdot\vec{r}-\omega_3 t)} d\omega_3$$

$$\times \left\{ \left[\rho_{total} - \int \rho_{es}^0(\omega_{exc})d\omega_{exc} \right] \delta(\vec{k}_3 - \vec{k}) \right.$$

$$-\frac{1}{2}\int \rho_{es}^0(\omega_{exc})e^{-i|\omega_{exc}|\tau}d\omega_{exc}\delta(\vec{k}_1 - \vec{k}_2 + \vec{k}_3 - \vec{k})$$

$$\left. -\frac{1}{2}\int \rho_{es}^0(\omega_{exc})e^{i|\omega_{exc}|\tau}d\omega_{exc}\delta(-\vec{k}_1 + \vec{k}_2 + \vec{k}_3 - \vec{k}) \right\} + \text{c.c.},\qquad(17)$$

where we use the notation $\rho^0_{es}(\omega) = 2A(\omega)I_{pulse}(\omega)$. It follows from (17) that the part of the electric field carrying information about molecules in the ground state is emitted into phase-matching directions $\boldsymbol{k} = \boldsymbol{k_1} - \boldsymbol{k_2} + \boldsymbol{k_3}$ and $\boldsymbol{k} = -\boldsymbol{k_1} + \boldsymbol{k_2} + \boldsymbol{k_3}$.

The radiation scattered by excited molecules can be derived analogously. The only difference is that molecules excited by different frequencies do not have the same properties. In fact, there exist uncountably many different gratings of molecules excited by different frequencies on top of each other. Correspondingly, the response function of excited molecules $s_{es}(\omega_3,T,\omega_{exc})$ is a function of excitation frequency and, generally, of the time delay T between the second excitation pulse and the probe pulse as well. This means that in order to get the total radiation scattered by the excited molecules the expression analogous to (16) has to be integrated over ω_{exc}, which results into

$$E_{es}(t,\vec{r}) = \frac{1}{\sqrt{2\pi}} \int\int s_{es}(\omega_3,T,\omega_{exc}) \varepsilon_{probe}(\omega_3 - \omega_0) e^{i(\vec{k}\cdot\vec{r} - \omega_3 t)} d\omega_3$$

$$\times \left\{ \rho^0_{es}(\omega_{exc})\delta(\vec{k}_3 - \vec{k}) + \frac{1}{2}\rho^0_{es}(\omega_{exc})e^{-i|\omega_{exc}|\tau}\delta(\vec{k}_1 - \vec{k}_2 + \vec{k}_3 - \vec{k}) \right. \quad (18)$$

$$\left. + \frac{1}{2}\rho^0_{es}(\omega_{exc})e^{i|\omega_{exc}|\tau}\delta(-\vec{k}_1 + \vec{k}_2 + \vec{k}_3 - \vec{k}) \right\} d\omega_{exc} + \text{c.c.}$$

Both gratings scatter the signal into identical directions, which is only natural, since the shape of gratings is identical up to the sign (see (14)). The total 2DES signal scattered by the sample is the sum of (17) and (18) that is expressed as

$$E_{signal}(t,T,\tau) = \frac{1}{2\sqrt{2\pi}} \int\int \left[s_{es}(\omega_3,T,\omega_{exc}) - s_{gs}(\omega_3) \right]$$

$$\times \varepsilon_{probe}(\omega_3 - \omega_0)\rho^0_{es}(\omega_{exc})e^{i(\vec{k}\cdot\vec{r} - \omega_3 t)} \quad (19)$$

$$\times \left\{ e^{-i|\omega_{exc}|\tau}\delta(\vec{k}_1 - \vec{k}_2 + \vec{k}_3 - \vec{k}) + e^{i|\omega_{exc}|\tau}\delta(-\vec{k}_1 + \vec{k}_2 + \vec{k}_3 - \vec{k}) \right\}$$

$$\times d\omega_3 d\omega_{exc} + \text{c.c.},$$

where the terms propagating in the original direction of the probe pulse were omitted since they are not of our interest.

Generally, it can be shown that the third order signals are emitted into any of directions $\boldsymbol{k} = \pm \boldsymbol{k_i} \pm \boldsymbol{k_j} \pm \boldsymbol{k_l}$, where i, j and l are elements of {1, 2, 3} [4]. These include already mentioned PP signals (directions $\boldsymbol{k_1}$, $\boldsymbol{k_2}$ and $\boldsymbol{k_3}$), third harmonic signals ($3\boldsymbol{k_i}$) and other processes that can be pictured as "scattering" of the ith pulse

on grating, induced by any pair of pulses j and l (i may be equal to j or l). However, none of the additional signals propagate into the phase matching directions of 2DES signal specified above. Therefore, the detection of the 2DES signal is virtually background free. It can be only contaminated by the higher order processes (prevailingly 5th order) or by the scattered radiation.

1.6. Heterodyne Detection – Local Oscillator

In Section 1.8 it will be shown that the detection of both amplitude and phase of the signal electric field is necessary in order to retrieve easily interpretable physical information. For this purpose, the experimental setup used in this work employs heterodyne detection of the 2DES signal by spectral interferometry [13]. The principle of this technique is to mix the emitted signal with an additional pulse, called local oscillator (LO), that passes through the sample into the direction of the emitted signal $k = -k_1 + k_2 + k_3$ as depicted in Fig. 2. Therefore, the spectral intensity $I_{HD}(\omega)$ detected in direction k is given by

$$I_{HD}(\omega) = \left| E_{signal}(\omega) + E_{LO}(\omega) \right|^2$$
$$= I_{signal}(\omega) + I_{LO}(\omega) + 2\Re\left\{ E_{signal}(\omega) E_{LO}^*(\omega) \right\}, \tag{20}$$

where $\Re$ marks the real part of the complex number.

The LO pulse is constructed as a replica of the third (probe) pulse of the 2DES sequence with diminished intensity (typically attenuated by OD 3 neutral density filter) and preceding in time by t_{LO}. For the sake of the ease of presentation we may neglect the attenuation factor, that is of no interest in the following, and the LO electric field can be written as

$$E_{LO}(t) = E_{probe}(t - t_{LO}), \tag{21}$$

which corresponds to the spectral density

$$E_{LO}(\omega) = E_{probe}(\omega)\mathrm{e}^{\mathrm{i}\omega t_{LO}} = \left| E_{probe}(\omega) \right| \mathrm{e}^{\mathrm{i}(\omega t_{LO} + \varphi_{probe}(\omega))}. \tag{22}$$

Here in the first equality the Fourier shift theorem is used while in the second one the electric field of the probe is expressed via its amplitude and phase φ_{probe}.

Similarly, the spectral profile of the signal electric field given by (19) can be written as

$$E_{signal}(\omega) = \left| E_{signal}(\omega) \right| \mathrm{e}^{\mathrm{i}\varphi_{signal}(\omega)}. \tag{23}$$

By plugging (22) and (23) into (20) the final expression of detected spectrum is obtained as

$$
\begin{aligned}
I_{HD}(\omega) = I_{signal}(\omega) + I_{LO}(\omega) \\
+ 2\left|E_{signal}(\omega)\right|\left|E_{probe}(\omega)\right|\cos\left(\omega t_{LO} - \Delta\varphi(\omega)\right),
\end{aligned}
\tag{24}
$$

where $\Delta\varphi \equiv \varphi_{signal} - \varphi_{probe}$.

Expression (24) reveals the advantages of the heterodyne detection. Namely, the 2DES signal is amplified by mixing it with the local oscillator, which facilitates its detection, and information about the amplitude and phase (relative to the phase of the probe pulse) becomes available.

Due to the time delay between the LO pulse and the emitted signal the detected heterodyne signal spectrum contains interference fringes – the longer the delay the higher the density of fringes. For practical reasons, it is advisable to set the fringes as dense as possible, but still well resolved by the CCD detector. This provides two possible configurations – the LO pulse can either precede or succeed the signal. The former option is chosen in most cases. Otherwise, the LO pulse would act as a probe of transient processes triggered by any of the preceding pulses. Unless these unwanted signals are filtered out (*e.g.* by a lock-in detection) they might distort measured 2D spectra.

In the experimental setup used in this work, the LO pulse precedes pulse 3 by approximately 1 ps. During the signal processing the measured spectral intensity I_{HD} is Fourier filtered by a time window to retrieve only the vicinity of the +1 ps peak in the time domain. This very powerful trick not only cuts off the constant terms of (24) but also suppresses large parts of the noise caused by sample scattering. Moreover, the filtering cuts away the contribution of the Fourier transform of (24) on the negative half-axis (that is present because of the measured signal is real). Performing inverse Fourier transform one obtains a complex expression for electric field (as defined by (23)), in which, however, the oscillatory part of the phase (due to the interference fringes) is still present. Nevertheless, it can be simply canceled out by dividing by $I_{LO}^{1/2}\exp(-i\omega t_{LO})$.

1.7. Lock-in Detection – Choppers

The 2DES technique is very sensitive to any kind of scattered radiation that accidentally reaches the detector. This leads to distortions of the 2D spectral shape and sometimes even to the observation of a periodic component in the time evolution that may be easily incorrectly interpreted as coherent beatings. This detrimental effect becomes particularly strong when the delay between any pair of

pulses is close to the t_{LO}. This is due to the fact that in this case the scattered radiation creates interference fringes on the detector identical to heterodyne detected signal and thus the unwanted signal passes through the Fourier filtering described in the previous section without any suppression.

To minimize the unwanted contributions, our experimental setup employs lock-in detection. The beams 1 and 2 are modulated by optomechanical choppers running at two different frequencies. The 2DES signal appears only if both beams are opened. Such an event periodically happens with the sum and difference of the choppers frequencies. Since we control the frequencies and phases of the beam modulation, the desired signal can be clearly identified and extracted. In the employed setup this is done by a fast continuous reading of the CCD camera and a consecutive Fourier filtering of the desired components from the modulated signal (for details see [10]).

1.8. Interpretation of the 2DES Signal

At this point all the essential parts of the experimental setup have been described. What remains is to demonstrate the physical meaning of the detected signal. In this section it will be shown that the 2DES signal really contains information about the transient change of absorption as was intended from the very beginning.

For this purpose, we cut the expression (19) describing the detected signal into its final form by inserting the definition of $\rho^0_{es}(\omega) = 2A(\omega)I_{pulse}(\omega)$ and consecutively by expressing the I_{pulse} in the form (8). Relying on the symmetry (4), we may revert the direction of integration along ω_{exc}, which allows us to write the signal emitted into direction $\boldsymbol{k} = -\boldsymbol{k_1} + \boldsymbol{k_2} + \boldsymbol{k_3}$ as

$$
\begin{aligned}
E_{signal}(t,T,\tau) = \frac{1}{\sqrt{2\pi}} \int\int & \left[\Delta s(\omega_3,T,\omega_{exc}) + \Delta s(\omega_3,T,-\omega_{exc})\right] \\
& \times \varepsilon_{probe}(\omega_3 - \omega_0)\left|\varepsilon_{pulse}(\omega_{exc} - \omega_0)\right|^2 A(\omega_{exc}) \\
& \times e^{-i\omega_3 t} e^{-i\omega_{exc}\tau} d\omega_3 d\omega_{exc} + \text{c.c.,}
\end{aligned}
\tag{25}
$$

where $\Delta s(\omega_3,T,\omega_{exc}) \equiv s_{exc}(\omega_3,T,\omega_{exc}) - s_{gs}(\omega_{exc})$. The last expression is in the form of the 2D Fourier transform, which means that the integrand containing the spectrally resolved microscopic information about the sample can be easily retrieved. In fact, inverse Fourier transform along the ω_3 axis is automatically done by the spectrometer. The second dimension (along ω_{exc}) can be reconstructed by the numerical computing of inverse Fourier transform, provided the coherence time τ is scanned in a broad enough interval. The 2D spectrum is obtained by

plotting the integrand (or rather its real part – see below) into the 2D density plot with the excitation ω_{exc} axis horizontal and detection ω_3 axis vertical. Note that the conventions adapted by other groups could be opposite – resulting in "transposed" spectra. Also, the actual labeling of the axes is usually slightly different (see Section 1.10).

The key term of the signal expression is the difference between the response of the sample in the ground and the excited state $\Delta s(\omega_3, T, \omega_{exc})$. In the final formula (25) it appears in a form symmetrized along the ω_3 showing that the response to negative and positive excitation frequencies is identical. This is only expected since the negative frequencies appear only as a consequence of decomposition of physically relevant real harmonic functions into the mathematically advantageous complex Fourier basis.

Generally speaking, any of the individual response functions $s(\omega)$ relates the (complex) amplitude of scattered secondary wave ε_{sec}, radiated by oscillating dipoles in some infinitesimal volume of the sample, to the amplitude of the driving wave ε_0 as

$$\varepsilon_{\text{sec}}(\omega) = s(\omega)\varepsilon_0(\omega). \tag{26}$$

For the interpretation of the 2D spectra it is necessary to relate the function $s(\omega)$ to the absorption properties of the sample. To do so, let us reformulate the linear absorption experiment in terms of the response function $s(\omega)$.

Assume a planar electromagnetic wave propagating through a homogeneous isotropic sample. The oscillating electric field drives oscillatory motion of dipoles present in the sample radiating secondary waves that propagate into all directions. Yet, the problem can be reduced to a single dimension, since it can be shown that the secondary radiation coming from dipoles oscillating in phase along (some infinitely large) plane adds up to a planar wave propagating perpendicularly to the surface of this plane [14]. The secondary radiation interferes with the original driving wave and together they drive the motion of dipoles in the following plane and the process continues through the total volume of the sample. Thus, for the infinitesimal change of the amplitude of the electric field $d\varepsilon$ along infinitesimal element of its path through the sample dx we obtain

$$d\varepsilon = s(\omega)\varepsilon dx, \tag{27}$$

which can be easily integrated as

$$\varepsilon(x, \omega) = \varepsilon_0(\omega)e^{s(\omega)} = \varepsilon_0(\omega)e^{\Re\{s(\omega)\}+i\Im\{s(\omega)\}} . \tag{28}$$

It is easy to see that the real part of the function $s(\omega)$ is responsible for exponential decrease (or increase) of the amplitude of the electric field and it is thus proportional to the absorption coefficient. The imaginary part describes the shift of phase and therefore it is related to the refraction index. The real part of the 2DES signal is thus proportional to the transient change of the sample absorption after excitation by the pump double-pulse and its imaginary part to the change of its dispersion.

Several other properties of the 2D spectra follow directly from the relation (25):

1. The signal is proportional to the difference between the response of molecules in the excited state and in the ground state $\Delta s(\omega_3, T, \omega_{exc}) \equiv s_{exc}(\omega_3, T, \omega_{exc}) - s_{gs}(\omega_{exc})$. As a consequence, it is not necessary to separately measure the steady-state absorption of unexcited sample as it is done in the case of PP experiment – the reference is intrinsically encoded in the 2DES signal.

2. The intensity of the transient signal is modulated by the intensity profile of the excitation pulse along the excitation axis and by the spectral profile of the probe electric field along the detection axis.[†] This corresponds to the common-sense assumption that the signal can be detected only in those spectral regions that are covered by the laser light.

3. The 2D spectrum is additionally modulated along excitation axis by the linear absorption of the sample, which is proportional to the squares of the dipole moments of the individual transitions. Since the transient absorption signal is typically proportional to the same quantity too, the relative amplitudes of peaks in the 2D spectrum are expected to scale with the fourth power of the dipole moments.

4. Although the sample response is symmetrized with respect to excitation frequency the other terms in the formula are not. This implies that the detected signal is not symmetric with respect to the coherence time τ. As a consequence, the scanned coherence time range has to cover both positive and negative values in the experiment in

---

[†] The latter quantity can be considered real, because all phases are due to the heterodyne detection related to the phase of LO that is generated as a copy of the probe pulse (see (21)).

order to retrieve the total 2D spectrum. Sometimes the Fourier transform is retrieved either from the negative or positive part only, which is referred to as non-rephasing or rephasing 2D spectrum, respectively.

1.9. Phasing of 2D Spectra

The derivation of the formula describing the 2DES signal (25) relies on explicit knowledge of relations between two different pulse pairs. In particular, it was assumed that the electric field of the pulse 2 is an identical copy of the pulse 1 (replicating both the temporal envelope and its phase) displaced in time by precisely known time delay (9). The very same assumption was made about the pulses 3 and LO (21). These assumptions are essential for retrieving the physically relevant real part of the spectra. Any additional phase shift φ between the pulses belonging to one of these pairs leads to the additional factor $e^{i\varphi}$ in the formula (25). Similarly, incorrect determination of the time delay between them by Δt adds a factor $e^{i\omega\Delta t}$. Both phase factors mix the real and imaginary parts of the spectra. Therefore, the time delay and the phase difference have to be known with very high precision – a shift in phase by only one quarter of the optical cycle leads to a complete interchange between the real and imaginary parts. In practice, a precision equivalent to about one hundredth of the wavelength ($\lambda/100$) is required.

In most of the available experimental apparatus (including the one described in this work) these critical factors cannot be determined with such a high precision.[‡] As a consequence, the 2DES signal is retrieved up to the unknown phase factor that has to be fitted using additional external information (so-called phasing). The usual approach is to measure the conventional PP spectrum using identical pulses as in the 2DES experiment and compare it to the integration of the 2DES spectrum along its horizontal (excitation) axis. As the real part of a correctly phased 2D spectrum corresponds to the spectrally resolved PP experiment its integration has to be identical (after dividing by LO electric field – see (25)) to conventional PP spectrum.

Consequentially, the precision of the 2D spectrum relies heavily on the precision of phasing (in our case, on the quality of the transient absorption spectrum). Therefore, the phasing process is one of the "bottlenecks" of the 2D

[‡] Note that even if the phase relation and the time delay between the original pulses are not known, it is absolutely essential that the relations are stable during the measurement with the $\lambda/100$ precision.

data processing. In particular, featureless transient absorption spectra might lead to rather unreliable fits.

1.10. Illustration of 2D Spectrum

The real part of typical 2D spectrum of a simple system at two population times is shown in Fig. 7 (labeled as TOTAL). The energy structure of the studied system corresponds approximately to the structure of the excitonically coupled dimer in the sense that it has four levels: a single ground state g, two closely spaced single-exciton levels e_1 and e_2 and one double-exciton level f that lies approximately two times higher than $e_{1,2}$. The only allowed optical transitions are those from g to $e_{1,2}$ and from $e_{1,2}$ to f, all the transitions are assumed to be of comparable strength. Once the e_2 level is excited the population relaxation to the lower-lying level e_1 takes place, other population transfer (*e.g.* back to the ground state) is not assumed to be present.

The absorption spectrum of the system (Fig. 8) contains two separated absorption bands and looks almost identically to the absorption spectrum of the model system used to explain principles of the 2DES in previous sections (Figs. 4 and 5).

The horizontal excitation and vertical emission axes of the spectra in Fig. 7 are conventionally labeled as ω_1 and ω_3, respectively (another often used convention would be ω_τ and ω_t). As already outlined above, each vertical cut through the spectrum corresponds to a single transient absorption spectrum that would be obtained after excitation by a hypothetical ultrashort narrow-band laser pulse. Consequently, as any other transient absorption spectrum, the 2D spectrum theoretically consists of three contributions: stimulated emission (SE), ground state bleach (GSB) and excited state absorption (ESA). For historical reasons, the 2DES technique uses the sign convention opposite to the one most commonly used in PP. The SE and GSB are plotted positive while ESA negative. All three contributions can generally exhibit oscillatory behavior in time due to the simultaneous excitation of multiple levels (see Section 1.12). The oscillatory component of the whole spectrum is sometimes considered as the fourth contribution – quantum beatings (QB). Then the former three are assumed to be oscillation-free. Decomposition of the 2D spectrum into the four contributions is indicated in Fig. 7 as well. For the sake of clarity it must be emphasized that such a decomposition is based on the known properties of the model system and it cannot be performed solely on basis of the experimental data.
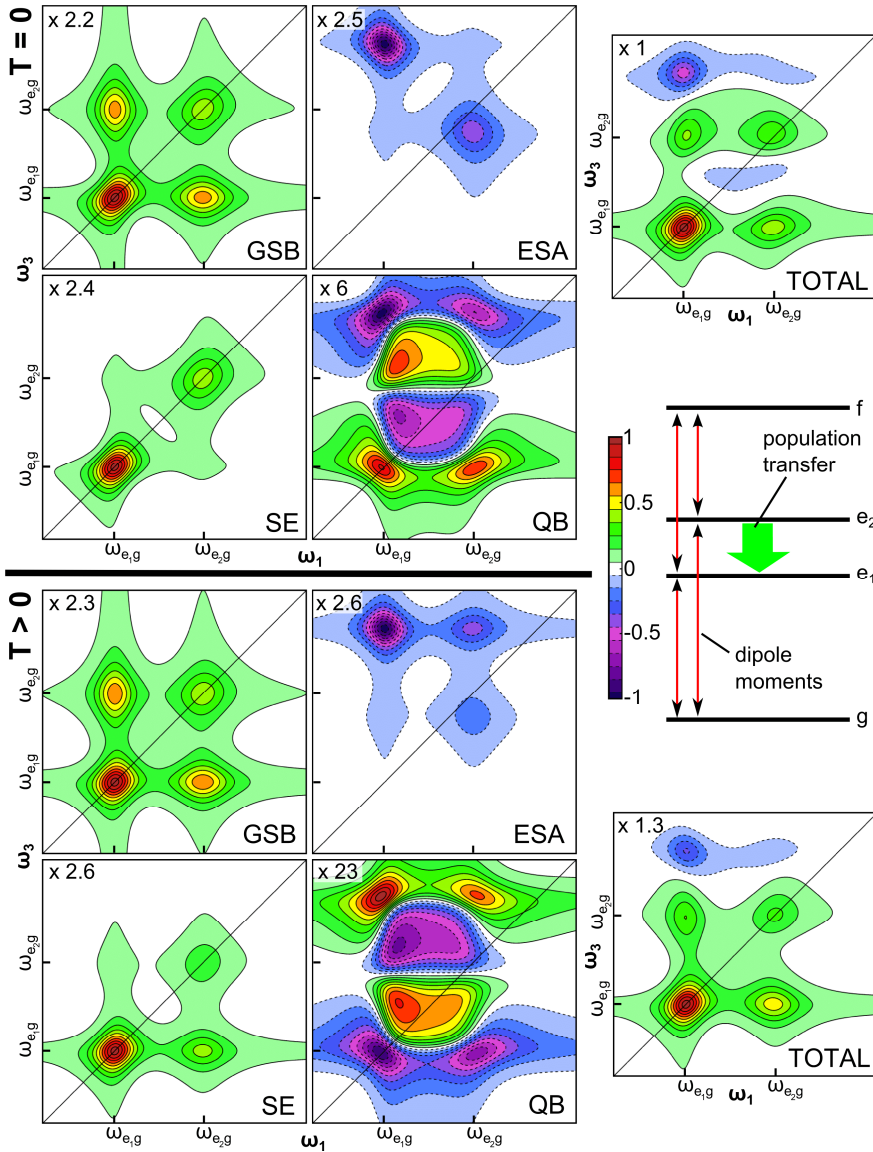
Fig. 7: Example of 2D spectrum of a simple system. The real part of the total spectrum is shown at the right hand side at zero time (top) and after some time evolution (bottom). The individual theoretical spectral contribution are shown at the left (GSB – ground state bleach, SE – stimulated emission, ESA – excited state absorption, QB – quantum beatings). The energy scheme of the simple system is shown in the center on the right hand side. All spectra are normalized; the normalization coefficient is stated in the upper left corner of each of them

The SE contribution at time right after the excitation ($T = 0$) has two diagonal peaks at the energies of individual transitions – showing that the emission

can be stimulated only from the transitions that were initially excited. The GSB contribution at the same population time manifests itself by four peaks: two lying on the diagonal, that are identical copies of the peaks of SE contribution, connected by a pair of cross-peaks. Such a pattern is typical for energy-level systems sharing a common ground state (most typically an excitonically coupled system). Exciting electrons into one of the e states automatically decreases the absorption of another one, as evidenced by the observation of the cross-peaks. Electrons present in one of the excited states e cause an additional absorption to the higher lying state f. Naturally, the additional absorption from the state e_2 appears at lower energies than from the state e_1 since the former is energetically closer to the state f than the latter. This is reflected by two off-diagonal peaks in the ESA contribution. The QB signal is a rather complicated composition of multiple positive and negative peaks.
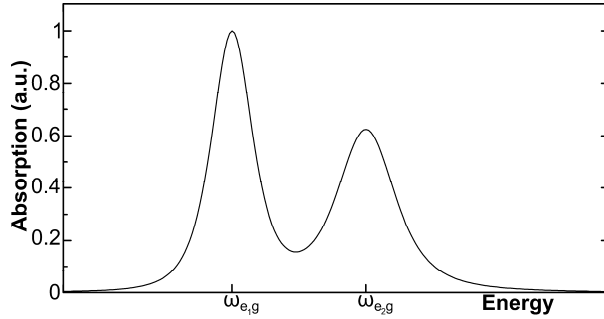
Fig. 8: Absorption spectrum of the simple system. 2D spectra of the same system are shown in Fig. 7.

The only time evolution of the model system after the excitation is the electron relaxation from the state e_2 to the state e_1. As a consequence the left half of the 2D spectrum, corresponding to excitation of the lower level e_1, remains constant (except of the QB contribution and, in our case, a very marginal intra-band dynamics). Since the return of electrons to the ground state was not assumed to be present, the GSB part does not change at all. The dynamics is documented by the disappearance of the high-energy diagonal peak, accompanied by the formation of the cross-peak bellow the diagonal in the SE part of the spectrum. The same process is reflected in the ESA signal as well. The QB term oscillates and slowly disappears with time.

As a rule of thumb, it can be generalized that positive cross-peaks present at time zero are a signature of the exciton coupling and cross-peaks appearing with time are a signature of the population transfer.

The overall dynamics of the 2D spectrum is given by the overlap of all the individual contributions. Therefore, 2D spectrum of real systems with multiple transitions might exhibit a rather complicated time evolution. In this case each point of the 2D spectrum might oscillate and decay in a multiexponential fashion. Generally, the longest timescales can be attributed to the decay of GSB that underlies the entire spectrum. On top of that, the fast changes of SE and ESA reflect the energy relaxation, that in the case of the multilevel system can be rather complex as well.

1.11. 2D Lineshapes

In the ideal case (as in the previous section) each diagonal peak in the 2D spectrum can be associated with a single optical transition between energy levels of the studied molecular system. As known from the linear absorption spectroscopy, such peaks do not appear as infinitely narrow. The reason is a combination of the natural line broadening effect due to the finite lifetimes of the energy states and the system interaction with the surrounding environment (so called thermal bath), causing dephasing of the transition. For reasonably long-living states the former effect can be neglected, leaving the latter as the dominating mechanism of the line broadening.

A typical experimental sample consists of studied systems (*e.g.* pigment molecules) dissolved in a solvent that is either liquid or amorphously solid (cryogenic glass). As a consequence, each molecule has a slightly different local environment that finely tunes the energies of its optical transitions. Naturally, the local environment continuously changes, which leads to constant fluctuations of the transition energy. Thus, the character of such stochastic processes is responsible for the actual lineshape of the peaks in the 2D spectrum.

In an extreme case it can be assumed that the bath exhibits no memory. This would mean that the energy of optical transition of an individual molecule at a certain time does not influence its energy at any later time at all (even if the time delay is infinitely short). In this case, the spectral line is referred to as homogenously broadened and it exhibits the well-known Lorentzian shape in the linear absorption spectrum and the characteristic star-shape in the 2D spectrum (see Fig. 9 - left).

Another extreme case would be an absolutely static local environment, in which transition energy of each molecule only slightly "homogenously" fluctuates around its individual mean position that is different for every molecule and that does not changes in time. The result would be an inhomogenously broadened line that has Gaussian shape in the linear spectrum and that is elongated along the

diagonal in the 2D spectrum. The (average) homogenous broadening is reflected by the anti-diagonal width of the line, whereas the inhomogeneity of the ensemble – by its diagonal elongation (see Fig. 9 - right).
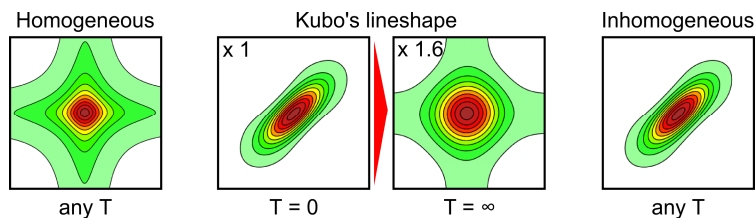

Fig. 9: Three different kinds of lineshape of a single transition as seen in the 2D spectrum.

Naturally, the intermediate case is the most abundant, where electronic transitions of the molecules quickly fluctuate around slowly varying mean values. In contrast to linear absorption and PP spectra, this situation leads to time-dependent lineshapes observed in 2D spectra (so called Kubo's lineshape). Directly after the excitation the lineshape is identical to the inhomogeneous case, however, due to the spectral diffusion it becomes round at the later times (see Fig. 9 - center). The 2DES thus allows direct monitoring the memory loss of the bath.

1.12. Quantum Coherence

An interesting phenomenon, closely connected with the excitation of the sample using spectrally broad laser pulses, is occurrence of oscillatory QB signals. So far, we have tacitly assumed that the laser pump pulse excites each molecule of studied system into exactly one of its excited states. However, since the energy of the ultrashort laser pulse is intrinsically uncertain (*i.e.* its spectrum is broad) some of the molecules may get excited into two different energy states simultaneously by the absorption of a single photon. After such an excitation the molecules appear in a coherent superposition of two excited states and the time evolution of the superposition leads to an observation of oscillatory component in PP or 2D spectra. In this respect Fig. 4 and Fig. 5 are not precise, because the oscillatory components that should be present in the time evolution after the broad band excitation were omitted for the sake of simplicity. The actual correct time evolution is depicted in Fig. 10.

For easier understanding of the situation, it is possible to draw an analogy here. The process of simultaneous photon absorption into two energy states is realization of yet another double slit experiment. The photon energy enters the system through two (or more) absorption bands and the laws of nature prevent to

say through which one this actually happened. After such an excitation the system is in a similar state as the infamous neither-dead-nor-alive Schrödinger's cat. The result of any double slit experiment is an interference pattern. In the case the "slits" are two different energies the interference appears in time as an oscillatory QB signal.
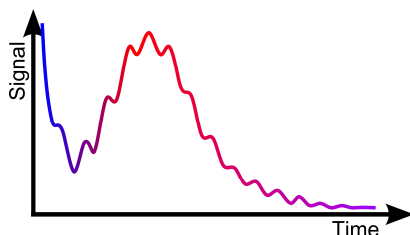

Fig. 10: Correct time evolution of transient absorption after the excitation using spectrally broad pump pulse (quantum coherence included).

The amplitude of the QB signal diminishes with time (typically on 100 fs – 1 ps timescale) due to so-called dephasing process. The most common origin of dephasing is either the random bath dynamics or the population relaxation. Both processes are responsible for the broadening of the absorption bands (see the previous section). In the language of the double slit experiment it corresponds to an opening of the slits that results in the disappearance of the interference pattern.

Two types of coherences are commonly set apart in literature: electronic coherences and vibrational coherences; the former being superposition of two different electronic (typically excitonic) states, the latter being superposition between different vibrational states. In addition, the vibrational coherences can occur between vibrational states on an electronic excited state as well as on the ground-state potential surface (ground-state or excited-state vibrational coherences, correspondingly). From the theoretical considerations it follows that the electronic coherences are generally dephased faster than the vibrational ones. Also, both types show different signatures in the 2D spectrum [7,8,15,16]. Recently, efforts to characterize vibronic coherences resulting from mixing of electronic and vibrational states have appeared in literature [15,17–19].

It is also important to note that the QB signal violates the principal "condition of linearity", introduced in Section 1.4, since it appears only after simultaneous excitation of multiple absorption bands. Fortunately, due to its oscillatory nature the QB signal can be easily discriminated from the population dynamics and therefore does not interfere with the interpretation of the 2D spectra presented in this chapter. However, as the consequence of the condition violation

the 2D-spectral shape of the QB signal does not look like any of the "absorptive" 2D peaks (see Fig. 7).

1.13. 5th and Higher-Order Contributions

The performance of 2DES relies on the "condition of linearity" introduced in the Section 1.4. If this condition is satisfied the 2DES is just a smart procedure how to identify the individual components of population dynamics and associate them to the correct absorption bands. In case the condition is violated, the 2DES analysis breaks down and the individual vertical cuts of the 2D spectrum cannot be related to the independent PP experiments anymore, because they do not exhibit the same time evolution of a system after a hypothetical ultrafast excitation with spectrally narrow pump pulse. Consequently, it would be difficult to quantitatively analyze processes happening in such 2D spectra by *e.g.* some global fitting procedure.

The physical meaning of the condition is nothing else than the situation, where simultaneously triggered processes are independent. As long as the absorption of some photon triggers a process that by no means can be affected by the absorption of another photon (into the same or different spectral band) the observed signal will be the linear combination of signals of separate processes. In most of the samples (and for reasonable excitation intensities) the number of molecules in the focus of laser beams is much higher than the number of exciting photons. In such a configuration the probability that a single molecule is excited by more than one photon is very low and therefore the condition of linearity is satisfied. However, if we assume an extreme case in which all the molecules supply a single distinctive acceptor molecule with the energy, the independence of the processes is lost. As soon as the first exciton reaches the acceptor molecule it makes it unavailable for the rest. The other excitons most likely will get stuck in the donor molecules, possibly annihilating with each other or leaving the system by another channel.

As a consequence, the 2D spectra of systems that consist of a large light-harvesting antenna supplying with excitation energy less abundant acceptor species (which happens to be the characteristics of most photosynthetic apparatus) can be affected. This problem can be solved only by decreasing the excitation light intensity to the level of less than one photon per single complex, which might be below the detection limit of the experimental apparatus.

From the point of view of the perturbation theory, the 2DES signal is a result of the 3rd order non-linear response of the sample to the electric field, during which the sample interacts exactly once with each of the three laser pulses. The first two interactions lead to a formation of a single exciton (or a quantum

coherence) that is monitored by the third pulse. However, the processes described above require formation of (at least) two excitons that can interact with each other. Therefore such problematic processes are of 5th (or higher) order of the perturbation theory.

Interestingly, the 2DES is in-a-way less sensitive to the presence of the 5th order processes than PP. Due to the phase matching condition only a part of the 5th order signal reaches the detector in the non-collinear 2DES geometry, whereas the entire 5th order signal is detected in the case of PP. As a consequence, the integration of 2D spectrum along its excitation axis may differ from corresponding PP spectrum if significant 5th order signal is present. The proper phasing of the 2D spectra might not be possible in this situation.

1.14. Advantages of 2DES over PP

The 2DES experimental setup is rather complicated; the individual measurements are time-consuming and they can be easily corrupted by a number of external influences. Therefore, if it were not for other benefits, it would be hard for the 2DES technique to compete with PP.

As already stressed in this thesis, the strength of 2DES is its capability to provide simultaneously high spectral and temporal resolution. In this sense the 2DES is utilized to resolve ultrafast processes such as ultrafast population transfer and quantum coherence in complex structures of energy states.

In practice, it is possible to reliably study population transfer processes starting at timescales slightly below 100 fs. Studying faster processes is cumbersome for two reasons. Firstly, the 2DES signal is distorted during the first 20 – 50 fs due to pulse-overlap effects and non-resonant signals coming from the cuvette and the solvent. Secondly, the absorption bands of ultrashort-living species are broadened due to the Heisenberg's uncertainty principle and therefore the high spectral resolution is not necessary any more. An example of 2DES used in this way can be found Paper I or in *e.g.* [20,21].

On the other hand, studying quantum coherences requires the full power of the 2DES technique and therefore it is probably the most common application of the method. Although oscillating signals have been observed since the early ultrafast PP experiments [22,23] the 2DES method allows for associating them (using its high spectral resolution) with the absorption bands and therefore it is possible to discuss their properties. 2DES studies focused on the quantum coherence phenomenon can be found in Paper II and *e.g.* [24–27].

The combination of the high spectral and temporal resolution is not the only unique property provided by 2DES. In fact 2D spectra contain much more

information about the system (spectrally resolved PP being only a part of it) and therefore the 2DES can be used to reveal various properties of the system. The main differences between 2DES and PP are:

1. Due to the heterodyne detection each measured 2D spectrum has a real and an imaginary parts (Fig. 11) containing the information about transient changes of absorption and dispersion, respectively. Therefore, the 2DES spectroscopy might be used to study the transient properties of the whole (complex) index of refraction (not only its absorptive part). Alternatively, the 2D spectrum can be represented by its absolute value and phase (Fig. 11). Although the physical interpretation of data in this representation is not straightforward, it still reflects the microscopic properties of the sample. The advantage of this representation is that it does not rely on the phasing process, which makes it attractive in situations where phasing is not possible (see *e.g.* [28,29]).
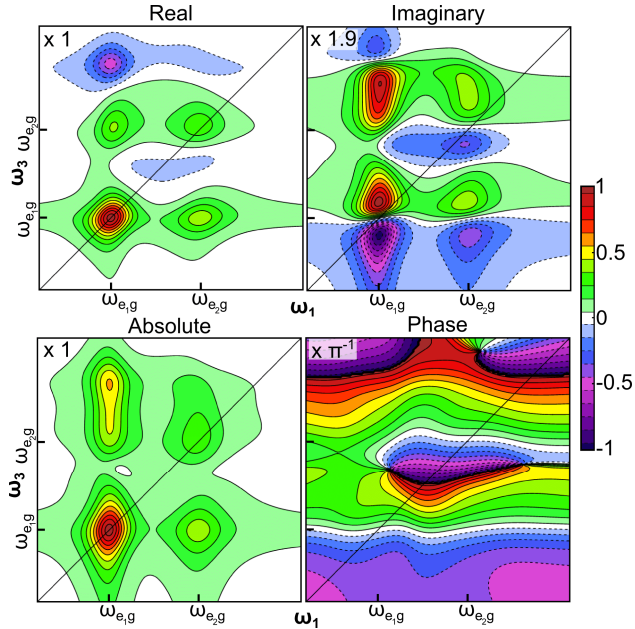

Fig. 11: Two different representation of the model 2D spectrum (T = 0) – real (absorptive) and imaginary (dispersive) part versus absolute value and phase.

2. The 2D spectrum (each of its components – real and imaginary or absolute and phase) can be decomposed into rephasing (R) and non-

rephasing (NR) parts as introduced in Section 1.8 (Fig. 12). Since the lineshapes are narrower than in the absorptive 2D spectrum such a decomposition is sometimes used to identify the exact positions of closely spaced absorption lines [25]. Moreover, the QB signal is often decomposed unevenly – leaving some peaks oscillating in R and fully static in NR and vice versa. This property can be used for distinguishing between the electronic and vibrational coherences [7,30]. Some experimental configurations allow for measurements of the R part of the spectrum only [31] (that is typically not possible to phase).
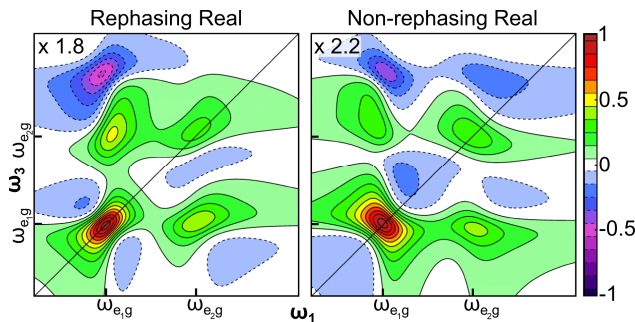
Fig. 12: Rephasing and non-rephasing component of real part of the model 2D spectrum (T = 0)

3. Each of the four pulses employed by the 2DES can have different polarization, which can be used to design polarization sequences emphasizing a different spectral contributions [26,32–34]. As an example, the sequence (–45°, 45°, 90°, 0°) suppresses all the contributions except QB connecting two states with a different orientation of their transition dipole moments. In addition, polarization sequences might be used to reveal the structural information about the relative dipole moment orientation [33]. The shortcoming of polarization 2DES is difficulty of phasing such data. However, the large potential of 2DES in this respect has not been fully explored to date.

4. All the individual transient absorption spectra composing the real part of the 2D spectrum are measured at identical conditions. In principle, provided the studied population dynamics is slow enough, the equivalent of the real part of the 2D spectrum can be composed of the multiple transient absorption spectra obtained by multiple PP

experiments. However, in reality such stitching, besides being time consuming, is quite complicated, because the individual spectra have to be normalized properly. This is provided by 2DES automatically. Also, the laser fluctuations and other irregularities are for all sub-spectra (in most cases) identical. This is beneficial for a complex global analysis of the spectra. In theory, this property opens up the possibility of directly calculating the population relaxation rate constants between the individual levels. This potential of the 2DES has not been fully explored either.

5. The 2D spectrum inherently contains pieces of information that are usually retrieved by other experimental technique. The transient absorption, transient grating, photon echo peak shift and other signals can be reconstructed from the 2D spectra – all measured at identical conditions. This should be useful for theoretical analysis.

2. Photosynthetic Apparatus of Green Sulfur Bacterium *Chlorobaculum tepidum*

2.1. Green Sulfur Bacteria

Green sulfur bacteria form one of the five major groups of photosynthetic prokaryotes [35]. Its members can be classified as obligatory anoxygenic photoautotrophs, which means that all their energy is derived from light, their cell carbon from inorganic CO_2 and they do not produce molecular oxygen as a by-product of photosynthesis. In fact, they are strictly anaerobic – they cannot grow in the presence of oxygen and typically use H_2S or other sulfuric compound as a principal reductant. This makes their habitat confined to anaerobic environments that are present *e.g.* bellow the chemocline of stratified lakes [36,37] or at the bottom of laminated bacterial mats [38], where the light conditions are often very dim. In order to conduct photosynthesis in these environments they developed a very efficient photosynthetic apparatus that allows for photosynthetic growth in as low-light conditions as found in hundred-meter depths of the Black sea [36,39] or in a vicinity of hydrothermal vents (black smokers) at the bottom of oceans, where the only source of light is the geothermal radiation [40].
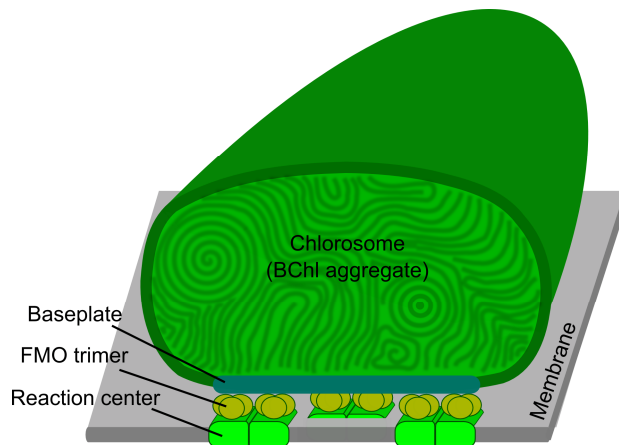

Fig. 13: Schematic picture of photosynthetic apparatus of green sulfur bacteria.

Chlorobaculum (Cba.) tepidum (formerly *Chlorobium tepidum*) serves as a model organism for the whole group due to its short replication time [41],

completely sequenced genome [42] and a possibility to grow it in laboratory conditions as a monoculture. *Cba. tepidum* is a thermophilic bacterium, with optimal grow conditions around 48 °C, that was isolated from certain acidic high sulfide hot springs of North Island, New Zealand [41,43]. The main electron donor for its photosynthetic growth is thiosulfate. The bacterial cultures grow exposed to the full daylight hence it might seem that the efficient photosynthetic apparatus is not necessary. However, bacteria form non-laminated microbial mats up to 3 mm thick, in which the steep attenuation of light is observed. Only 0.1 % of incident light is transmitted into 0.7 mm depth of the mat, reaching limiting irradiance levels for sustaining photosynthetic live of representatives belonging to other bacterial groups [43].

The schematic picture of photosynthetic apparatus of green sulfur bacteria is shown in Fig. 13. It consists of a chain of complexes that significantly differ in their overall architecture. As can be seen in the absorption spectra (Fig. 14) the electronic transitions of each complex are on lower or comparable energy than transitions of the preceding complex in the chain, thus composing together an energetic cascade, purpose of which is to efficiently capture the light energy and funnel it into the reaction center located at its bottom.
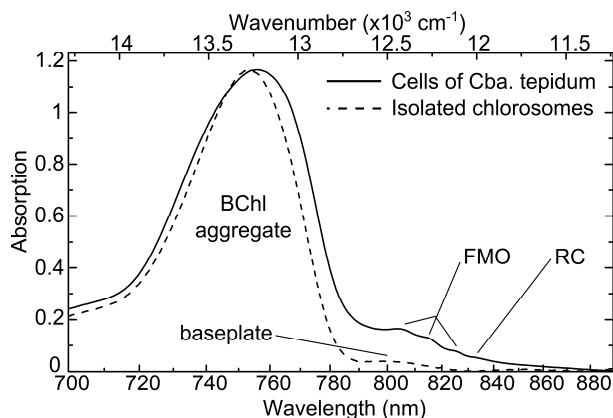
Fig. 14: Absorption spectrum of intact cells and isolated chlorosomes of Cba. tepidum at 77 K.

Most of the incoming light energy is collected by an atypically large light-harvesting antenna – chlorosome. The excitation energy is gathered from the interior of the chlorosome by a baseplate complex that is attached to its side facing the cytoplasmic membrane. Consequently, the excitation is transferred through a Fenna-Matthews-Olson (FMO) protein into the reaction center (RC) where it drives the actual photochemistry. The structure and function of the individual

components of the photosynthetic apparatus will be described in detail in the following text.

2.2. Chlorosome

Chlorosomes are the principal light-harvesting antennas that are common to representatives of green sulfur bacteria, green filamentous bacteria and acidobacteria (for a review see [44–48]). Since these bacterial groups are related only distantly it was suggested that the presence of the chlorosome in all of them might be a consequence of a lateral gene transfer [49]. Compared to light-harvesting antennas adopted by other photosynthetic species chlorosomes are unique in terms of their efficiency, size and overall architecture.

Bacteriochlorophyll *c*   Bacteriochlorophyll *a*
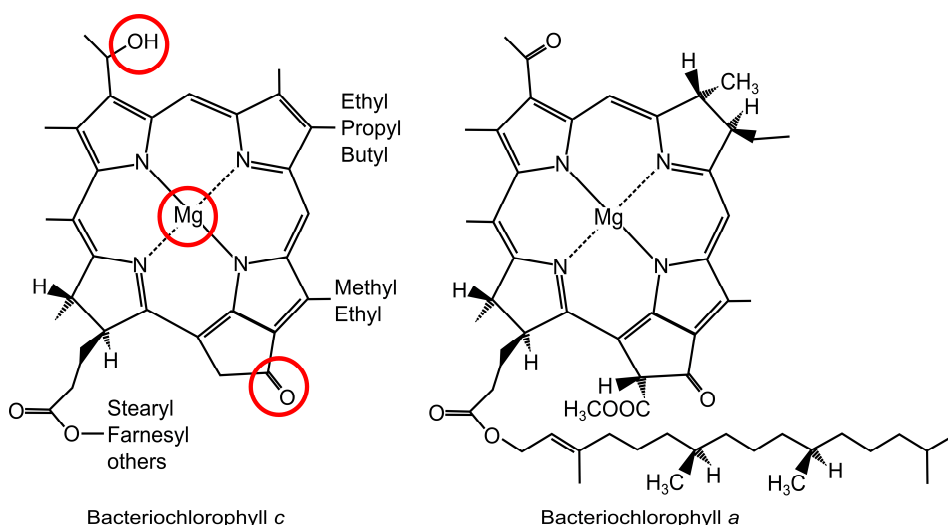
Fig. 15: Bacteriochlorophylls present in Cba. tepidum. Groups essential for BChl c aggregation are encircled (from top to bottom: hydroxy substituent at C3^1, central magnesium cation and keto group at C13^1).

The typical chlorosome has 100 – 200 nm long and 10 – 60 nm wide body that is attached to the inner side of the cytoplasmic membrane. Its interior is composed from ~10^5 bacteriochlorophyll (BChl) *c*, *d* or *e* molecules co-aggregated with smaller amounts of carotenoids and quinones. Various bacterial species typically build up chlorosomes from a single type of BChl (*c*, *d* or *e*). In particular, *Cba. tepidum* utilizes a mixture of various homologues of BChl *c* (see Fig. 15). The chlorosome is presumably surrounded by a protein-lipid envelope. On the side adjacent to the cytoplasmic membrane the proteins form the so-called baseplate

complex that binds BChl *a* and additional carotenoid molecules (see the next section for details).

It has been demonstrated that the artificially prepared BChl aggregates exhibit very similar steady-state as well as transient absorption spectra as chlorosomes (Fig. 16) [50,51]. This fact points out that the functional properties of the chlorosome are determined mainly by self-assembly and not by the pigment-protein interaction as it is common in the other types of photosynthetic antennas. The strong exciton interaction between BChl pigments (estimated to be –550 – –750 cm^{-1} [47]) leads to delocalization of excitations over multiple pigments (forming so-called excitons). The energies of individual single exciton states of large aggregate are arranged into a band that spans from energies below to energies above the energy of the electronic excited state of an isolated monomer. In the case of pigment arrangement that is close to head-to-tail arrangement (J-aggregate), only the optical transitions to the red-edge of the single exciton band are allowed [52,53]. This explains the red-shift of the near-infrared (Q_y) absorption band of the chlorosome (or aggregate) with respect to the Q_y band of monomeric BChl *c* (see Fig. 16). Interestingly, the chlorosome Q_y band is broader than the corresponding monomer band, which is in contrast to exchange narrowing predicted by exciton theory for ideal aggregate [54]. This indicates the presence of irregularity (disorder) in the chlorosome arrangement and suggests that the aggregates in chlorosome are not pure J-aggregates. Fluorescence experiments showed that emission of individual chlorosomes does not significantly differ from the ensemble emission and therefore the disorder is present within each chlorosome [55,56].
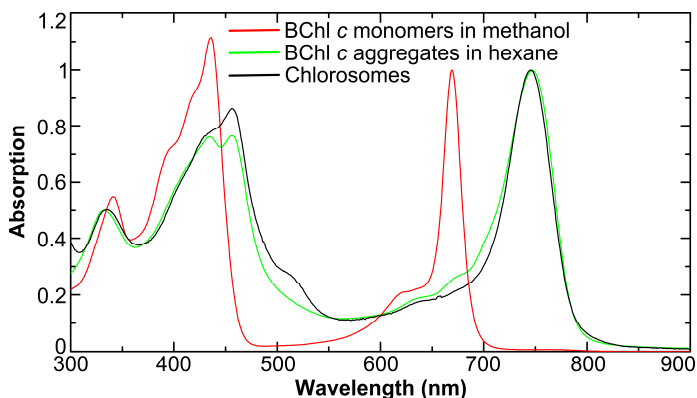

Fig. 16: Absorption spectra of chlorosomes from Cba. tepidum, artificial BChl c aggregates (in hexane) and BChl c monomers (in methanol). All spectra are normalized to the Q_y band maximum.

As a consequence the interior of every chlorosome has an unique molecular arrangement, which prevents solving its structure by the high-resolution X-ray diffraction methods. Therefore, the short-range arrangement of the pigments has to be deduced from the combination of physical properties of the BChl c molecules and constrains determined by absorption, circular dichroism, Stark and NMR spectroscopy. The short-range arrangement is apparently governed by coordination of Mg cation of one BChl molecule to the hydroxy substituent at $C3^1$ of a neighboring molecule that can be hydrogen bonded to $C13^1$ keto group of the third BChl molecule (Fig. 15). Such an arrangement can be satisfied by numerous structural motifs (for a review see [57]) and it is not clear which one(s) appear(s) in the chlorosome.

Repeating of the structural motif determines the long-range arrangement of pigments in the chlorosome, which can be visualized by electron (cryo)microscopy. Originally proposed structure consisting of hexagonally packed rods [58] was later disputed by the observation of lamellar arrangement with spacing of about 2 nm for *Cba. tepidum* [59]. The high-resolution electron cryomicroscopy end-on views of chlorosomes from wild-type strain of *Cba. tepidum* [47,60] revealed structure that was described as "multi-lamellar tubular domains extending over most of the length of the chlorosome, embedded in a less well-ordered matrix of smaller curved lamellar domains" [47].

The energy transfer processes in chlorosomes have been studied by various methods of time-resolved spectroscopy. In this context, two main factors that significantly affect the quality of the measured data have been identified. Firstly, the chlorosomes from strictly anaerobic green sulfur bacteria quickly quench the excitation when exposed to oxygen [61,62]. Therefore, in order to resolve the energy transfer pathways the chlorosome samples have to be reduced (typically by adding sodium dithionite). Secondly, the chlorosomes should be measured using very low excitation intensity [63]. The excessive excitation generates multiple excitons within a single chlorosome that annihilate with each other leading to a faster decay of the signal.

The typical dynamic processes that are resolved within the main chlorosome band using the PP technique [51,63–67] exhibit multiexponential behavior with timescales spanning the range between 0.1 – 100 ps. Mostly decay components are observed without corresponding rises, which makes them difficult to assign. The exception is the energy transfer to the baseplate complex that occurs on 10 – 100 ps timescale, depending on the species (for *Cba. tepidum* between 30 – 40 ps) [61,68] and the intra-band relaxation on a sub-picosecond timescale [63].

In addition, the work included in this thesis resolved a sub-100 fs process that we attributed to exciton diffusion in the disordered chlorosome interior (for details see Section 3.1 or Paper I).

In addition, oscillatory components were often observed in transient absorption spectra, including the early ultrafast PP experiments [23,64,67,69]. In case of *Cba. tepidum* the oscillations mainly contain two frequency components of approximately 90 and 145 cm^{-1}. Since the identical modes are observed in the resonance Raman spectra of chlorosomes and artificial aggregates [70,71], the beatings are usually attributed to the quantum coherence between vibrational states. The experiments of Ma and coworkers [23] demonstrated the presence of the coherence in the electronic ground state.

The identical oscillatory behavior was present in our 2DES experiments conducted at cryogenic 80 K (Paper II). However, the comparison of beatings located at ESA-dominated regions and GSB/SE regions has clearly indicated the vibrational coherence in the electronic excited state, whereas the ground state coherence could not be unambiguously identified. In addition, amplitude of oscillations is unusually strong. All their atypical features and their interplay with the exciton diffusion are discussed in detail in Section 3.2 or in Papers II and III.

2.3. Baseplate

The baseplate complex is an integral part of each chlorosome, and it is found on the side facing the cytoplasmic membrane (for a review see [72]). In contrast to the BChl aggregate that dominates the chlorosome interior, the baseplate is a pigment-protein complex, where the relative positions and fine spectral properties of individual pigments are controlled by the protein scaffold. Particularly, the baseplate contains BChl *a* (Fig. 15) and carotenoid molecules bound by CsmA proteins. In the case of green sulfur bacteria, BChl *a* in the baseplate accounts for about 1% of the total number of chlorosome chlorophylls.

The molecular structure of the CsmA apo-protein isolated from *Cba. tepidum* has been determined by liquid-state NMR (Fig. 17) [73]. However, neither the number of pigments bound by a single protein nor their binding geometry is known. The stoichiometry between BChl *a* and CsmA for green sulfur bacteria is estimated to be around 1 – 2 pigments per protein [74,75]. Very often the equimolar ratio is assumed, which is supported by the presence of a single conserved histidine in the CsmA sequence that is known to be capable of binding BChl molecules [72].
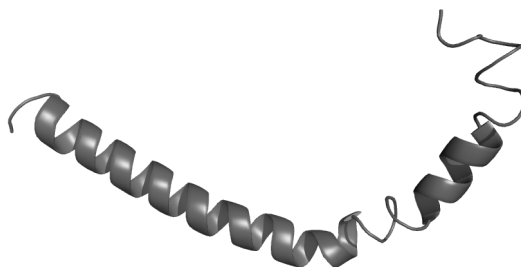
Fig. 17: Structure of CsmA protein isolated from Cba. tepidum as resolved by Pedersen et al.[73].

Analogously to the chlorosome interior the baseplate can be directly observed by electron cryomicroscopy that resolves the baseplate as a two-dimensional paracrystalline structure with 3.2 – 3.3 nm spacing [47,76]. In *Cba. tepidum* the baseplate lattice intersects the long axis of chlorosomes at ~40° angle [47]. The experimental evidence points out that the building block of the baseplate structure might be a CsmA dimer [72,77]. Similarly, the circular dichroism spectra of the *Cba. tepidum* baseplate were interpreted as a signature of BChl *a* excitonic dimer [78,79]. The putative model of a short-range baseplate structure based on the experimental evidence was proposed by Pedersen et al. [72].

Our work (Paper IV) contributed to the understanding of the baseplate structure by resolving at least four energy levels within the near-infrared baseplate band. This fact indicates that the baseplate contains an excitonically coupled BChl *a* tetramer or even more complex structure. In addition, the position of the energy levels in the context of the complete photosynthetic apparatus shows that the energy flow between the individual complexes is not as simple as was thought previously. For details see the summary Section 3.3 or Paper IV.

2.4. Fenna-Matthews-Olson Protein

The intermediate complex in the energy cascade within the photosynthetic apparatus of green sulfur bacteria and acidobacteria is the FMO protein (for a review see [80]). It is a water soluble protein that binds eight BChl *a* molecules [81,82]. [§] Interestingly, there are no carotenoids present. The FMO protein naturally appears as a trimer (Fig. 18). The FMO protein played an important role in the photosynthesis research. It was the first pigment-protein complex, molecular structure of which was determined by high-resolution X-ray crystallography [83]. It has a relatively simple structure containing only small number of pigments,

---

[§] For a long time it was believed that the FMO binds seven BChl *a* molecules. However, recent experiments identified the eighth BChl *a* in the structure [81,82].

some of them in a close interaction. These properties make FMO an ideal system for testing predictions of various methods of computational chemistry. As a consequence it is probably the most heavily theoretically and experimentally studied pigment-protein complex. Additionally, the 2DES study on FMO [84] introduced the method into the field of photosynthetic complexes. One of the following 2DES studies on FMO [24] triggered the discussion about the role of quantum coherence phenomena in the photosynthesis.
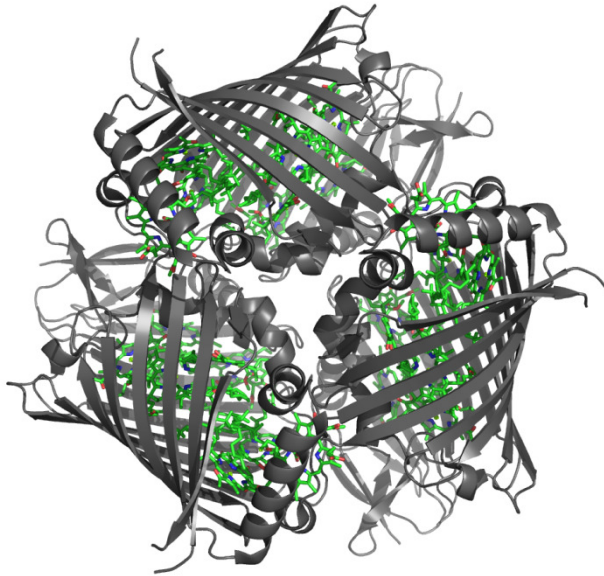
Fig. 18: Molecular structure of FMO trimer isolated from Cba. tepidum as resolved by Tronrud et al.[82].

FMO proteins are located between chlorosomes and cytoplasmic membrane where they are in close contact with both baseplate and RC. Most likely two FMO trimers are attached to a single RC complex [85,86]. The linear dichroism [87] and reconstituted 3D images based on electron microscopy data [88] indicate that the discs of FMO trimers sit flat on the cytoplasmic membrane with the C3 symmetry axis perpendicular to its surface. The exact orientation was determined by protein labeling [89]. These pieces of information together with quantum chemistry calculations [90,91] show that the higher energy states are localized on pigments in vicinity of the baseplate and the low-lying energy states near the RC. The relaxation within the exciton band of FMO thus transfers

excitation energy from the vicinity of the baseplate to the vicinity of RC. This process was unraveled to happen on a picosecond timescale at room temperature [92,93]. However, it slows down to tens of picoseconds at cryogenic temperatures [94–96].

Based on these facts it is believed that the FMO protein serves as a highly efficient molecular wire that guides the excitation energy from the baseplate to the RC. However, the energy transfer from the baseplate to FMO has never been directly observed and all experiments characterizing FMO – RC energy transfer found only surprisingly low efficiency (~30%) [97–100].

Our work (Paper V) convincingly shows the energy is transferred from the chlorosome to the RC via the FMO protein. However, the energy transfer step from FMO to the RC seems to be inefficient, as observed previously. Moreover, the comparison of baseplate energy states (Paper IV) with the states of FMO indicates that the energy transfer is not as straightforward as was thought before. For more detail see Sections 3.3 and 3.4 or Papers IV and V.

2.5. Reaction Center

The reaction center (RC) is located at the very bottom of the energy funnel. Its function is to convert the excitation energy into more stable energy of chemical bonds. The green sulfur bacteria contains the RC that is conceptually similar to the RC of photosystem 1 (PS1) of cyanobacteria and higher plants (for a review see [85]). However, its structure on a molecular level is not known and therefore many of its structural and functional properties were deduced on the basis of this similarity. The complete RC is composed from several membrane proteins. Two copies of a pigment-binding PscA and single copy of PscB protein form the RC core. The RC core contains altogether 16 BChl *a* molecules, 4 chlorophyll (Chl) *a* and two carotenoids that are equally distributed between the two copies of PscA proteins probably composing a symmetrical homodimer. This is an untypical feature since the pigments in the RCs adopted by most other photosynthetic organisms (disregarding whether they are type I or type II) are bound by two different proteins arranging them in two similar but not identical branches.

The majority of bound BChl *a* molecules serves as an internal antenna. The final destination for the excitation energy is a central special pair of closely coupled BChl *a* molecules, where it is converted into the chemical energy in the charge separation process. The excited special pair (called P840) donates an electron to a Chl *a* molecule from where the electron transfer chain continues through a sequence of intermediate electron acceptors eventually reducing a water-soluble ferredoxin protein. The oxidized special pair is re-reduced by a bound

cytochrome c_{551}. It uses electrons that originate in a sulfuric compound (such as H_2S) and is transferred to the cytochrome by a sequence of electron transfer steps.

3. Results Summary

3.1. Exciton Diffusion in Chlorosomes

In Paper I we have studied the initial ultrafast dynamics in chlorosomes from *Cba. tepidum* at room temperature. At times immediately after the excitation ($T = 0$ fs) the 2D spectrum is composed from a positive SE/GSB peak strongly elongated in the diagonal direction that is surrounded by negative ESA signal (Fig. 19). However, during the first 100 fs the positive part of the spectrum becomes rounder and fills most of the space below the diagonal. Simultaneously, the overall spectral intensity drops to approximately one half of the initial value.
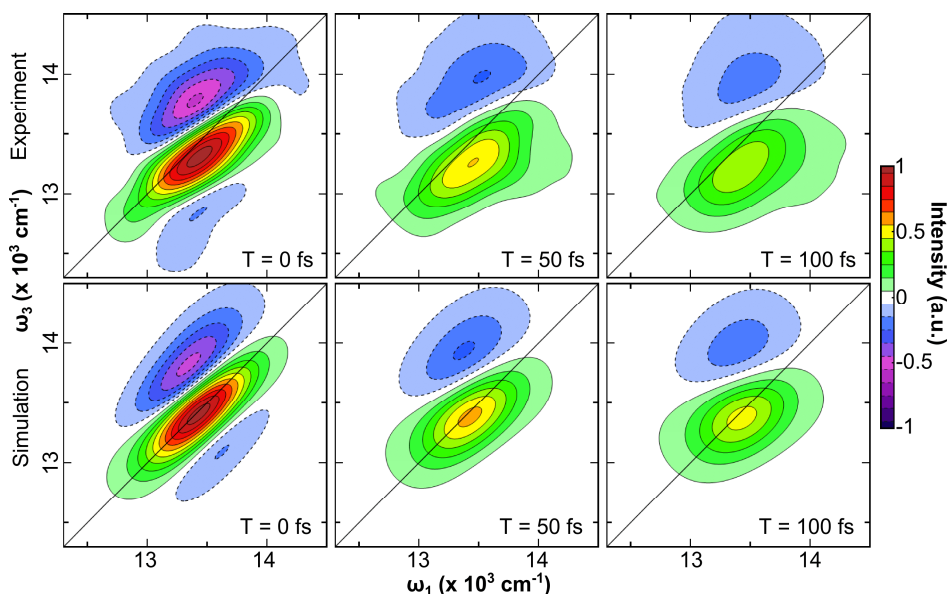
Fig. 19: 2D spectrum (real part) of chlorosomes from Cba. tepidum at room temperature compared to simulated data.

Interestingly, we found that the observed spectral dynamics of the BChl aggregate in the chlorosome containing ~10^5 pigments can be modeled by a simple phenomenological model that describes the chlorosome as a three-level system with Kubo's lineshapes. The three levels, that respectively represent the ground state, the single and double exciton bands, are almost equidistantly spaced. The allowed transition between the first two is responsible for the positive part of the signal, whereas the transition between the upper two levels leads to the negative ESA. Both positive SE/GSB and negative ESA signals fall into almost identical

spectral region. The entire ultrafast dynamics is modeled as a time evolution of the Kubo's lineshape (see Section 1.11), which correctly describes the overall change of the spectral shape including the intensity drop. Moreover, the model reproduces well the decomposition of the spectrum into a strong R part that confines most of the dynamics and a relatively weak and almost static NR part (Fig. 20).
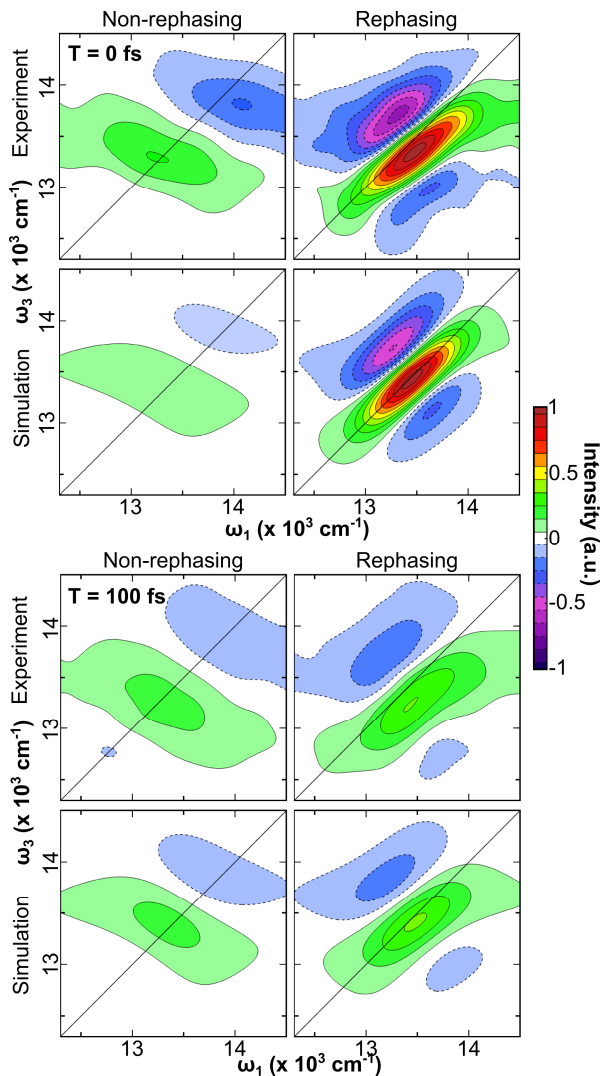

Fig. 20: Rephasing and non-rephasing parts of 2D spectra of chlorosomes from Cba. tepidum at room temperature compared to simulated data.

The ultrafast processes observed in the chlorosome have to be thus analogous to processes behind the Kubo's lineshape as described in Section 1.11. The initially elongated spectrum points out the presence of spectrally inhomogeneous subsystems in the sample. The same feature is responsible for the broad absorption spectrum of chlorosomes as discussed in Section 2.2. The time evolution is determined by the random ultrafast energy transfer between the subsystems inside the chlorosome.

On the other hand, it is typically assumed that the Kubo's lineshape is caused by the system interaction with the bath of vibrational degrees of freedom [4]. However, such explanation seems unlikely in the case of chlorosome due to the extensive width of the spectrum and the exciton nature of the chlorosome absorption band. More likely, the disorder in the arrangement of BChl molecules effectively breaks the large aggregate into smaller parts (denoted as coherent domains) that are weakly coupled to each other. Similar effect has been theoretically demonstrated for one dimensional disordered J-aggregates [101]. Additionally, fluorescence spectra from single chlorosomes have shown [55,56] that the observed inhomogeneity is present already at the level of individual chlorosome. This implies that the coherent domains have to be in close contact with each other. The observed dynamics is thus interpreted as random exciton diffusion between the individual coherent domains.

3.2. Vibrational Coherences in Chlorosomes

Our experiments conducted on chlorosomes at cryogenic temperature of 80 K led to the observation of almost identical initial behavior of the 2D spectrum attributed to the exciton diffusion as the room-temperature experiments described above (Fig. 21). Naturally, all features in the spectra are sharper due to the narrower spectral lines and the relaxation component of the exciton transfer is more prominent due to smaller thermal energy. In addition to this initial dynamics, we have resolved very strong QB component (Fig. 22). The general characteristics of these beatings correspond well to previous observations in PP experiments [22,23,64,67]. The QB signal consists of two main frequencies of about 90 and 145 cm^{-1} and it is damped in approximately 1.2 ps. However, the 2DES technique allowed us to uncover additional pieces of information about the coherent behavior in chlorosomes that are not compatible with the simplest theoretical reasoning. More thorough discussion can be found in Paper II.

The oscillations can be attributed to the vibrational coherences due to observation of the modes with very similar frequencies in resonance Raman spectra of artificial BChl aggregates [71] and chlorosomes [70]. The same low

frequency modes are present in monomeric BChl molecules, however their intensity is relatively low [71]. Apparently, the strong exciton coupling between the molecules enhances some of the modes, making them visible in resonance Raman spectra (see discussion in [71,102]) and as QB in the time-resolved experiments. The exact microscopic mechanism of the mode enhancement is not clear. As one possibility we have proposed that a resonance coupling between vibrational degrees of freedom and excitonic transitions can be a possible explanation. Similar intensity redistribution of coherences has been demonstrated on simple theoretical models [17–19]. However, the extent of simplification is unrealistic in some of these models. Another possible mechanism that we proposed in Paper II is small Hertzberg-Teller coupling (*i.e.* dependence of electronic transition dipole moment on vibrational coordinate) of these modes that in combination with the strong excitonic coupling in the aggregate enhances their apparent Huang-Rhys factor. Such an approach can explain the selective enhancement of the low-frequency modes. On the other hand, none of the proposed mechanisms is compatible with all observed features (see below).
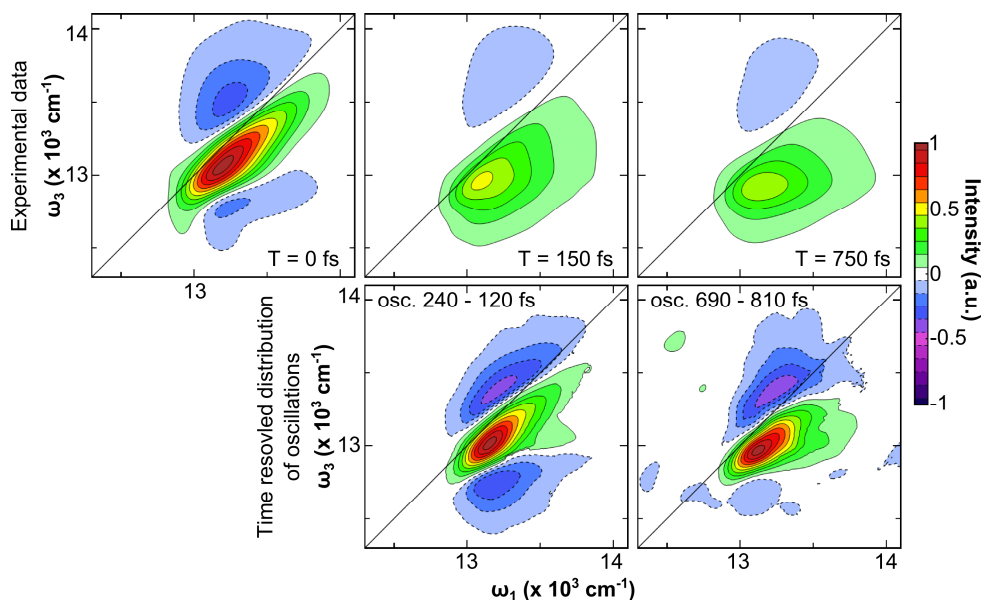
Fig. 21: 2D spectrum (real part) of chlorosomes from Cba. tepidum at 80 K (upper row) and the time-resolved distribution of oscillations in the 2D spectrum (lower row). For additional details see Paper II.

In principle, it should be possible to distinguish between vibrational coherences that are present in the potential surfaces of electronic excited states and

coherences present in the electronic ground state. The latter type is confined to the regions of the 2D spectrum with positive signal, whereas the latter type should be in addition observable in the negative ESA regions as well. More importantly, in the presence of fast diffusion process the excited state coherences should dephase much faster than the ground state ones as discussed in Papers II and III. As a consequence the oscillatory components located in the positive and negative regions of the 2D spectrum should differ from each other.

In chlorosomes the ESA oscillating signal is an almost perfect mirror image of the oscillations in SE/GSB region (Fig. 22). This implies that either the excited state coherences are much stronger or both types of coherences dephase on identical timescale. So far, we could not provide theoretical support for either option.

The overall distribution of beating amplitude in the 2D spectrum copies its initial shape and does not evolve in time despite the pronounced rapid time evolution of the monotonous 2D signal due to the excitation diffusion process. This indicates that the exciton diffusion does not transfer vibrational coherences between individual domains (see Papers II and III) and therefore only those coherent domains that were originally excited contribute to oscillatory components of the 2D spectrum.
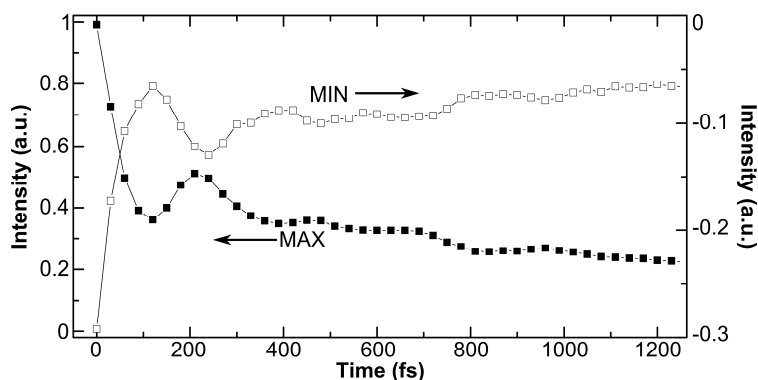
Fig. 22: Time evolution of the maximum and minimum of the 2D spectrum. Note that the relatively weak and negative minimum signal has separate ordinate axis on the right side of the graph.

3.3. Excitonic Structure of Baseplate

The absorption of BChl *a* containing baseplate complex is well separated from the dominant BChl *c* aggregate band in the chlorosome spectrum at 77 K (Fig. 14). This allows to study the properties of the baseplate by the 2DES technique.

Our experiments (summarized in Paper IV) indicate that the structure of the baseplate is more complex than was thought before. The excitation energy relaxation within the baseplate complex, as visualized by 2DES, consecutively proceeds through at least four energy states (Fig. 23). This would not be possible if BChl *a* molecules formed dimers inside the baseplate, as was previously proposed [72,78,79]. Since the 2D spectrum exhibits typical features of excitonically coupled system, we propose that the structure of the baseplate contains at least four BChl *a* molecules in a close contact.
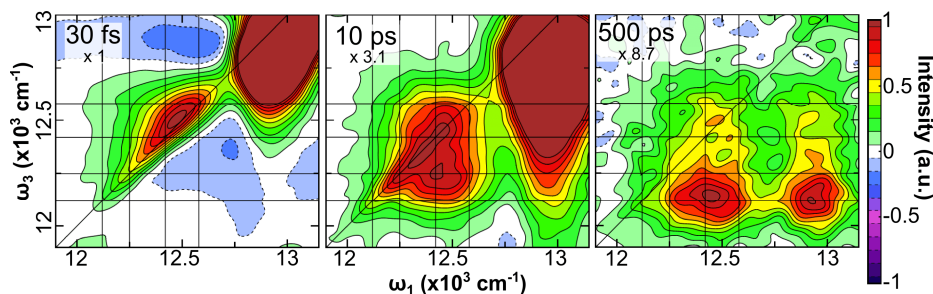
Fig. 23: 2D spectra (real part) of isolated chlorosomes from Cba. tepidum measured at 77 K. Left part of each spectrum corresponds to the baseplate complex; right part to BChl c aggregate. Each frame is normalized to the baseplate maximum signal and the corresponding multiplication factor is given. Vertical and horizontal lines indicate the presumed positions of the energy states in the baseplate.

Locating the energies of the baseplate exciton levels is important in the context of the energy flow through the entire photosynthetic apparatus. We find that energy states in the baseplate fall into the same region as energy states of the FMO protein [80]. This can be partly seen already from the absorption spectrum (Fig. 14). In addition, 2DES reveals that the excitation energy populates the lowest levels in about 20 ps and the lifetime of intermediate levels is approximately ten times shorter. Such an arrangement does not support the widely accepted opinion that the energy is donated from the baseplate complex into the highest state of the FMO. More likely the energy transfer happens in "lateral" fashion, where the energy is transferred directly to both higher and lower FMO energy states. Interestingly, the energy states of the internal antenna of the RC core are in the very same spectral region as well [85,86]. We may speculate that the energy transfer from FMO to RC happens in the similar lateral fashion. FMO would thus serve as a spacer that bridges the states of the baseplate and RC core and simultaneously allows water-soluble ferredoxin to access the RC.

The study also shows that the energy transfer from BChl *c* aggregate happens on ~70 ps timescale, which is in similar timescales as observed previously [68,103].

3.4. Energy Flow through Entire Photosynthetic Apparatus

In order to obtain information about the excitation energy flow through the entire photosynthetic apparatus we have performed 2DES experiments on whole cells of bacterium *Cba. tepidum* (see Paper V). The complexes measured *in vivo* are surrounded by their natural environment and therefore their function is not altered by the isolation procedure. Additionally, since they are part of the intact photosynthetic apparatus (and some of them are spectrally well separated – Fig. 14) the inter-complex energy transfer can be monitored.

The main experimental difficulty was to deal with the strong scattering of the sample. However, the combination of lock-in detection with Fourier filtering (as described in Chapter 1) and careful alignment of the apparatus allowed achieving good signal to noise ratio in scattering cell suspension samples.
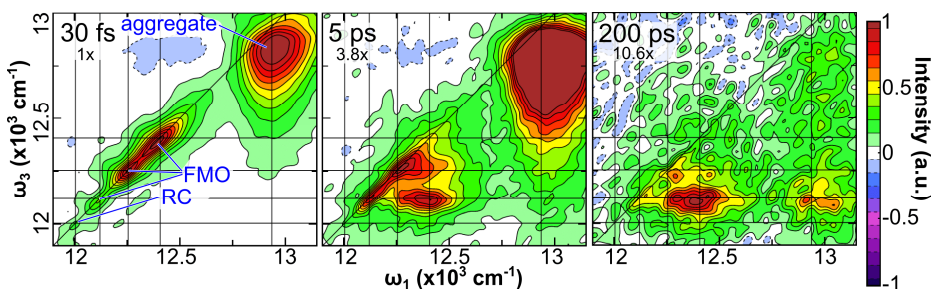
Fig. 24: 2D spectra (real part) of intact cells of Cba. tepidum measured at 77 K. Each frame is normalized to the FMO signal maximum and the corresponding multiplication factor is given.

Our experiments resolved energy transfer from the chlorosome into the FMO protein,[**] energy relaxation within the FMO protein and consecutive energy transfer to the RC (Fig. 24). These measurements provide the first experimental evidence that the energy transfer from the chlorosome to the RCs indeed occurs through the FMO proteins. The energy relaxation within individual complexes was observed to occur on faster timescales than the energy transfer between them. This seems to be a general trend and, as a consequence, the transient populations of

_____

[**] Note that the baseplate signal is not resolved since its weak absorption is covered by stronger FMO absorption

FMO and RC (and correspondingly their signals) after exciting the chlorosome are very low.

We also observed that the excitation energy accumulates on the lowest level of the FMO. We estimated that after 200 ps about 25% of the energy harvested by FMO is still not transferred into the RC. Even lower values of FMO-RC energy transfer efficiency (~30 %) were reported in previous PP experiments on isolated complexes [97,98], for which the isolation procedure was commonly blamed. However, this cannot be the case in our experiments conducted on intact cells. Most likely the effect is caused by the overly high excitation intensities. As a consequence, the photosynthetic apparatus attempts to feed multiple excitations into the RC. The first excitation closes the RC and the others remain at the bottom of the transfer chain.

In this regime the system violates the "condition of linearity" (see Section 1.4). As a consequence, exact quantitative analysis of rate constants connected with the individual processes (as was briefly discussed in Section 1.14) is not possible, since the 2D spectra contain significant amount of 5th (or higher) order contributions (see discussion in Section 1.13). This fact is confirmed by the observed different time evolution of the PP experiment (measured in order to phase the 2D spectra) and of the ω_1-integrated 2D spectrum.

Popular Scientific Summary

Almost all species on Earth including the humans directly or indirectly derive their energy from the Sun. There it is produced via thermonuclear fusion and radiated into the surroundings in the form of light. The small portion of this energy that reaches planet Earth is harvested by plants and several kinds of bacteria that can utilize it in building up their bodies. To make this process possible the evolution equipped their cells with the specially designed apparatus, composed from colored molecules – pigments (such as chlorophylls, carotenoids and related molecules) bound by proteins. The complexity of the photosynthetic apparatus spans a range from rather simple systems adopted by bacteria to highly advanced finely-tuned machinery present in the higher plants. In all cases, distinct parts of the apparatus with specialized primary functions can be identified; most importantly, light-harvesting antennas and reaction centers. The light-harvesting antenna is optimized for collecting the energy of light – the absorption of photon coming from the Sun excites pigments of the antenna into a quantum state of higher energy. However, these molecules can stay in the excited state only for a few nanoseconds and then return back to their ground state. So, the energy can be stored in this form only for a very short time, after which it is irreversibly lost. Therefore, the energy has to be extracted during this tiny fraction of time (on biological timescale) from the antenna and transferred (typically through several mediating complexes) to the reaction center, where it is converted into a more stable form of energy, namely into reactive chemical species. These are then used at different places of the cell to drive a sequence of enzymatic reactions that fixates atmospheric CO_2 in order to produce sugars.

As any substance that is capable of capturing (absorbing) part of the visible light, the photosynthetic apparatus appears to human eye as colored – most often green. A more precise picture can be gained from the absorption spectrum, a plot of the amount of light absorption with respect to the wavelength, where multiple bands appear, most of which can be attributed to the individual complexes of the photosynthetic apparatus. Moreover, a complex in the excited state, *i.e.* being active in the light-harvesting, exhibits a different absorption spectrum. Therefore, the excitation-energy flow through the photosynthetic apparatus can be monitored by the methods of time-resolved optical spectroscopy that excite the photosynthetic apparatus with a short laser pulse and measure the change of the absorption of the sample.

Until recently, these methods could not combine high spectral and high temporal resolution. This allowed for studying relatively slow processes

(timescales longer than 1 ps) after selective excitation of some particular energy states of the apparatus (often attributable to its individual complexes). However, the fastest light-harvesting processes (sub-picosecond timescales) could not be studied like this, since the selective excitation was not possible. This limitation has been overcome in recent years by an advanced spectroscopic technique – coherent two-dimensional electronic spectroscopy (2DES) – that allows for studying ultrafast processes with high spectral resolution. In addition, the method is well suited for studying highly non-classical molecular states (so-called quantum coherences) in which the molecule can simultaneously be found in more than one excited level (in analogy to famous Schrödinger's cat). The presence of such states in photosynthetic complexes after the laser excitation has been demonstrated, which triggered a heated discussion about their biological relevance.

The introductory part of this thesis explains the basic principles and features of the 2DES technique and provides the basic facts about the photosynthetic apparatus of green sulfur bacterium *Chlorobaculum tepidum*. This bacterium that serves as one of the photosynthetic model systems contains relative simple photosynthetic apparatus consisting of three complexes: chlorosome – a massive light harvesting antenna mostly composed from vast number of aggregated pigments, FMO protein – the energy conduit, and the reaction center. Moreover, a baseplate complex providing the energy interface between the chlorosome aggregate and the FMO proteins can be set apart from the rest of the chlorosome.

The main part of the thesis summarizes the author's original studies, in which the 2DES technique is applied to study the energy transfer processes in this photosynthetic apparatus. The work performed on isolated chlorosomes unraveled the ultrafast diffusion of excitons (excitations delocalized over several molecules) occurring in the aggregate of chlorosome during the first ~100 fs after excitation. Moreover, the following experiments conducted at low temperature (80 K) revealed complex interplay between this process and vibrational quantum coherences. The study focused on the baseplate complex of chlorosome pointed out that its structure is more complex than it was thought before, composed from at least four bacteriochlorophyll molecules in a close contact. In addition, the position of its energy levels indicated that the energy transfer between the chlorosome and FMO protein is not as straight-forward as was assumed previously. At last, the energy flow through the entire intact photosynthetic apparatus embedded in the full bacterial cells was unraveled.

Acknowledgements

At this point it is my pleasure to thank all those people without whom this thesis would have not been written. First and foremost, to my supervisors Jakub Pšenčík and Donatas Zigmantas for giving the project its direction and for providing their respective expertise in the fields of photosynthetic bacteria and coherent two-dimensional electronic spectroscopy that were crucial for completing this interdisciplinary work.

Other thanks belong to all co-authors whose contributions were essential for publication of papers included in this thesis. Particularly, I thank to Tomáš Mančal for the theoretical support and to František Vácha for supplying us with the samples.

Further, I would like to thank Jan Alster, Karel Žídek, David Paleček, Barbora Benešová, Tomáš Mančal and both my supervisors for reading, correcting and commenting the manuscript in various stages of preparation and, additionally, to the first two of them for aligning the NOPA for me. I also have to mention all my friends, colleagues and coworkers in Lund and in Prague that are responsible for nice atmosphere at both of these places.

And last and not least I thank to my parents and my girlfriend for their support of my work.

References

1.   Einstein A (1916) Strahlungs-Emission und Absorption nach der Quantentheorie. *Dtsch Phys Gesellschaft* **18**: 318–323.

2.   Berera R, van Grondelle R, Kennis JTM (2009) Ultrafast transient absorption spectroscopy: principles and application to photosynthetic systems. *Photosynth Res* **101**: 105–118.

3.   Jonas DM (2003) Two-dimensional femtosecond spectroscopy. *Annu Rev Phys Chem* **54**: 425–463.

4.   Mukamel S (1995) *Principles of Nonlinear Optical Spectroscopy*. Oxford University Press.

5.   Hamm P, Zanni M (2011) *Concepts and methods of 2D infrared spectroscopy*. Cambridge University Press, New York.

6.   Cho M, Brixner T, Stiopkin I, Vaswani HM, Fleming GR (2006) Two Dimensional Electronic Spectroscopy of Molecular Complexes. *J Chinese Chem Soc* **53**: 15–24.

7.   Butkus V, Zigmantas D, Valkunas L, Abramavicius D (2012) Vibrational vs. electronic coherences in 2D spectrum of molecular systems. *Chem Phys Lett* **545**: 40–43.

8.   Seibt J, Pullerits T (2013) Beating Signals in 2D Spectroscopy: Electronic or Nuclear Coherences? Application to a Quantum Dot Model System. *J Phys Chem C* **117**: 18728–18737.

9.   Augulis R, Zigmantas D (2013) Detector and dispersive delay calibration issues in broadband 2D electronic spectroscopy. *J Opt Soc Am B* **30**: 1770–1774.

10.   Augulis R, Zigmantas D (2011) Two-dimensional electronic spectroscopy with double modulation lock-in detection: enhancement of sensitivity and noise resistance. *Opt Express* **19**: 13126–13133.

11.   Feynman RP, Leighton RB, Sands M (2011) *The Feynman Lectures on Physics: Quantum Mechanics*. Basic Books.

12.   Szriftgiser P, Guéry-Odelin D, Arndt M, Dalibard J (1996) Atomic Wave Diffraction and Interference Using Temporal Slits. *Phys Rev Lett* **77**: 4–7.

13.   Gallagher SM, Albrecht AW, Hybl JD, Landin BL, Rajaram B, Jonas DM (1998) Heterodyne detection of the complete electric field of femtosecond four-wave mixing signals. *J Opt Soc Am B* **15**: 2338–2345.

14.   Feynman RP, Leighton RB, Sands M (2011) *The Feynman Lectures on Physics: Mainly mechanics, radiation, and heat*. Basic Books.

15.   Butkus V, Zigmantas D, Abramavicius D, Valkunas L (2013) Distinctive character of electronic and vibrational coherences in disordered molecular aggregates. *Chem Phys Lett* **587**: 93–98.

16.   Mančal T, Nemeth A, Milota F, Lukeš V, Kauffmann HF, Sperling J (2010) Vibrational wave packet induced oscillations in two-dimensional electronic spectra. II. Theory. *J Chem Phys* **132**: 184515.

17. Chenu A, Christensson N, Kauffmann HF, Mančal T (2013) Enhancement of Vibronic and Ground-State Vibrational Coherences in 2D Spectra of Photosynthetic Complexes. *Sci Rep* **3**: 2029.

18. Christensson N, Kauffmann HF, Pullerits T, Mančal T (2012) Origin of long-lived coherences in light-harvesting complexes. *J Phys Chem B* **116**: 7449–7454.

19. Tiwari V, Peters WK, Jonas DM (2013) Electronic resonance with anticorrelated pigment vibrations drives photosynthetic energy transfer outside the adiabatic framework. *Proc Natl Acad Sci U S A* **110**: 1203–1208.

20. Brixner T, Stenger J, Vaswani HM, Cho M, Blankenship RE, Fleming GR (2005) Two-dimensional spectroscopy of electronic couplings in photosynthesis. *Nature* **434**: 625–628.

21. Myers JA, Lewis KLM, Fuller FD, Tekavec PF, Yocum CF, Ogilvie JP (2010) Two-Dimensional Electronic Spectroscopy of the D1-D2-cyt b559 Photosystem II Reaction Center Complex. *J Phys Chem Lett* **1**: 2774–2780.

22. Savikhin S, Zhu Y, Lin S, Blankenship RE, Struve WS (1994) Femtosecond spectroscopy of chlorosome antennas from the green photosynthetic bacterium Chloroflexus aurantiacus. *J Phys Chem* **98**: 10322–10334.

23. Ma Y-Z, Aschenbrücker J, Miller M, Gillbro T (1999) Ground-state vibrational coherence in chlorosomes of the green sulfur photosynthetic bacterium Chlorobium phaeobacteroides. *Chem Phys Lett* **300**: 465–472.

24. Engel GS, Calhoun TR, Read EL, Ahn T-K, Mančal T, Cheng Y-C, Blankenship RE, Fleming GR (2007) Evidence for wavelike energy transfer through quantum coherence in photosynthetic systems. *Nature* **446**: 782–786.

25. Panitchayangkoon G, Hayes D, Fransted KA, Caram JR, Harel E, Wen J, Blankenship RE, Engel GS (2010) Long-lived quantum coherence in photosynthetic complexes at physiological temperature. *Proc Natl Acad Sci U S A* **107**: 12766–12770.

26. Westenhoff S, Paleček D, Edlund P, Smith P, Zigmantas D (2012) Coherent picosecond exciton dynamics in a photosynthetic reaction center. *J Am Chem Soc* **134**: 16484–16487.

27. Nemeth A, Milota F, Mančal T, Lukeš V, Kauffmann HF, Sperling J (2008) Vibronic modulation of lineshapes in two-dimensional electronic spectra. *Chem Phys Lett* **459**: 94–99.

28. Dahlberg PD, Fidler AF, Caram JR, Long PD, Engel GS (2013) Energy Transfer Observed in Live Cells Using Two-Dimensional Electronic Spectroscopy. *J Phys Chem Lett* **4**: 3636–3640.

29. Fransted KA, Caram JR, Hayes D, Engel GS (2012) Two-dimensional electronic spectroscopy of bacteriochlorophyll a in solution: Elucidating the coherence dynamics of the Fenna-Matthews-Olson complex using its chromophore as a control. *J Chem Phys* **137**: 125101.

30. Mančal T, Christensson N, Lukeš V, Milota F, Bixner O, Kauffmann HF, Hauer J (2012) System-dependent signatures of electronic and vibrational coherences in electronic two-dimensional spectra. *J Phys Chem Lett* **3**: 1497–1502.

31. Dahlberg PD, Fidler AF, Caram JR, Long PD, Engel GS (2013) Energy Transfer Observed in Live Cells Using Two-Dimensional Electronic Spectroscopy. *J Phys Chem Lett* **4**: 3636–3640.

32. Hochstrasser RM (2001) Two-dimensional IR-spectroscopy: polarization anisotropy effects. *Chem Phys* **266**: 273–284.

33. Read EL, Schlau-Cohen GS, Engel GS, Wen J, Blankenship RE, Fleming GR (2008) Visualization of Excitonic Structure in the Fenna-Matthews-Olson Photosynthetic Complex by Polarization-Dependent Two-Dimensional Electronic Spectroscopy. *Biophys J* **95**: 847–856.

34. Read EL, Engel GS, Calhoun TR, Mančal T, Ahn TK, Blankenship RE, Fleming GR (2007) Cross-peak-specific two-dimensional electronic spectroscopy. *Proc Natl Acad Sci U S A* **104**: 14203–14208.

35. Blankenship RE (2002) *Molecular Mechanisms of Photosynthesis*. Blackwell Science.

36. Overmann J, Cypionka H, Pfennig N (1992) An extremely low-light-adapted phototrophic sulfur bacterium from the Black Sea. *Limnol Oceanogr* **37**: 150–155.

37. Crowe SA, Jones C, Katsev S, Magen C, O'Neill AH, Sturm A, Canfield DE, Haffner GD, Mucci A, Sundby B, et al. (2008) Photoferrotrophs thrive in an Archean Ocean analogue. *Proc Natl Acad Sci U S A* **105**: 15938–15943.

38. Nicholson JAM, Stolz JF, Pierson BK (1987) Structure of a microbial mat at Great Sippewissett Marsh, Cape Cod, Massachusetts. *FEMS Microbiol Ecol* **45**: 343–364.

39. Manske AK, Glaeser J, Kuypers MMM, Overmann J (2005) Physiology and Phylogeny of Green Sulfur Bacteria Forming a Monospecific Phototrophic Assemblage at a Depth of 100 Meters in the Black Sea. *Appl Environ Microbiol* **71**: 8049–8060.

40. Beatty JT, Overmann J, Lince MT, Manske AK, Lang AS, Blankenship RE, Van Dover CL, Martinson TA, Plumley FG (2005) An obligately photosynthetic bacterial anaerobe from a deep-sea hydrothermal vent. *Proc Natl Acad Sci U S A* **102**: 9306–9310.

41. Wahlund TM, Woese CR, Castenholz RW, Madigan MT (1991) A thermophilic green sulfur bacterium from New Zealand hot springs, Chlorobium tepidum sp. nov. *Arch Microbiol* **156**: 81–90.

42. Eisen JA, Nelson KE, Paulsen IT, Heidelberg JF, Wu M, Dodson RJ, Deboy R, Gwinn ML, Nelson WC, Haft DH, et al. (2002) The complete genome sequence of Chlorobium tepidum TLS, a photosynthetic, anaerobic, green-sulfur bacterium. *Proc Natl Acad Sci U S A* **99**: 9509–9514.

43. Castenholz R, Bauld J, Jørgenson B (1990) Anoxygenic microbial mats of hot springs: thermophilic Chlorobium sp. *FEMS Microbiol Ecol* **74**: 325–336.

44. Orf GS, Blankenship RE (2013) Chlorosome antenna complexes from green photosynthetic bacteria. *Photosynth Res* **116**: 315–331.

45. Blankenship RE, Matsuura K (2003) Antenna complexes from green photsynthetic bacteria. In Green BR, Parson WW (eds.), *Light-harvesting antennas in photosynthesis* pp 195–217. Kluwer Academic Publishers, Dordrecht.

46. Blankenship RE, Olson JM, Miller M (1995) Antenna Complexes from Green Photosynthetic Bacteria. In Blankenship R, Madigan M, Bauer C (eds.), *Anoxygenic Photosynthetic Bacteria* pp 399–435. Springer Netherlands.

47. Oostergetel GT, van Amerongen H, Boekema EJ (2010) The chlorosome: a prototype for efficient light harvesting in photosynthesis. *Photosynth Res* **104**: 245–255.

48. Frigaard N-U, Bryant DA (2006) Chlorosomes: Antenna Organelles in Photosynthetic Green Bacteria. In Shively J (ed.), *Complex Intracellular Structures in Prokaryotes* pp 79–114. Springer Berlin / Heidelberg.

49. Blankenship RE (1992) Origin and early evolution of photosynthesis. *Photosynth Res* **33**: 91–111.

50. Klinger P, Arellano JB, Vácha F, Hála J, Pšenčík J (2004) Effect of carotenoids and monogalactosyl diglyceride on bacteriochlorophyll c aggregates in aqueous buffer: implications for the self-assembly of chlorosomes. *Photochem Photobiol* **80**: 572–578.

51. Savikhin S, van Noort PI, Blankenship RE, Struve WS (1995) Femtosecond probe of structural analogies between chlorosomes and bacteriochlorophyll c aggregates. *Biophys J* **69**: 1100–1104.

52. Kasha M, Rawls H, Ashraf El-Bayoumi M (1965) The exciton model in molecular spectroscopy. *Pure Appl Chem* **11**: 371–392.

53. Van Amerongen H, Valkunas L, van Grondelle R (2000) *Photosynthetic Excitons*. World Scientific.

54. Knapp EW (1984) Lineshapes of molecular aggregates, exchange narrowing and intersite correlation. *Chem Phys* **85**: 73–82.

55. Tian Y, Camacho R, Thomsson D, Reus M, Holzwarth AR, Scheblykin IG (2011) Organization of Bacteriochlorophylls in Individual Chlorosomes from Chlorobaculum tepidum Studied by 2-Dimensional Polarization Fluorescence Microscopy. *J Am Chem Soc* **133**: 17192–17199.

56. Saga Y, Shibata Y, Tamiaki H (2010) Spectral properties of single light-harvesting complexes in bacterial photosynthesis. *J Photochem Photobiol C Photochem Rev* **11**: 15–24.

57. Alster J, Kabeláč M, Tuma R, Pšenčík J, Burda J V (2012) Computational study of short-range interactions in bacteriochlorophyll aggregates. *Comput Theor Chem* **998**: 87–97.

58. Staehelin LA, Golecki JR, Drews G (1980) Supramolecular organization of chlorosomes (chlorobium vesicles) and of their membrane attachment sites in Chlorobium Limicola. *Biochim Biophys Acta* **589**: 30–45.

59. Pšenčík J, Ikonen TP, Laurinmäki P, Merckel MC, Butcher SJ, Serimaa RE, Tuma R (2004) Lamellar organization of pigments in chlorosomes, the light harvesting complexes of green photosynthetic bacteria. *Biophys J* **87**: 1165–1172.

60. Oostergetel GT, Reus M, Gomez Maqueo Chew A, Bryant DA, Boekema EJ, Holzwarth AR (2007) Long-range organization of bacteriochlorophyll in chlorosomes of Chlorobium tepidum investigated by cryo-electron microscopy. *FEBS Lett* **581**: 5435–5439.

61. Van Noort PI, Zhu Y, LoBrutto R, Blankenship RE (1997) Redox effects on the excited-state lifetime in chlorosomes and bacteriochlorophyll c oligomers. *Biophys J* **72**: 316–325.

62. Blankenship RE, Cheng P, Causgrove TP, Brune DC, Hsiao-Hsiao Wang S, Choh J-U, Wang J (1993) Redox regulation of energy transfer efficiency in antennas of green photosynthetic bacteria. *Photochem Photobiol* **57**: 103–107.

63. Pšenčík J, Ma Y-Z, Arellano JB, Hála J, Gillbro T (2003) Excitation energy transfer dynamics and excited-state structure in chlorosomes of Chlorobium phaeobacteroides. *Biophys J* **84**: 1161–1179.

64. Savikhin S, van Noort PI, Zhu Y, Lin S, Blankenship RE, Struve WS (1995) Ultrafast energy transfer in light-harvesting chlorosomes from the green sulfur bacterium Chlorobium tepidum. *Chem Phys* **194**: 245–258.

65. Martiskainen J, Linnanto J, Kananavičius R, Lehtovuori V, Korppi-Tommola J (2009) Excitation energy transfer in isolated chlorosomes from Chloroflexus aurantiacus. *Chem Phys Lett* **477**: 216–220.

66. Martiskainen J, Linnanto J, Aumanen V, Myllyperkiö P, Korppi-Tommola J (2012) Excitation energy transfer in isolated chlorosomes from Chlorobaculum tepidum and Prosthecochloris aestuarii. *Photochem Photobiol* **88**: 675–683.

67. Prokhorenko VI, Steensgaard DB, Holzwarth AR (2000) Exciton Dynamics in the Chlorosomal Antennae of the Green Bacteria Chloroflexus aurantiacus and Chlorobium tepidum. *Biophys J* **79**: 2105–2120.

68. Causgrove TP, Brune DC, Blankenship RE (1992) Förster energy transfer in chlorosomes of green photosynthetic bacteria. *J Photochem Photobiol B Biol* **15**: 171–179.

69. Savikhin S, Zhu Y, Blankenship RE, Struve WS (1996) Intraband energy transfers in the BChl c antenna of chlorosomes from the green photosynthetic bacterium Chloroflexus aurantiacus. *J Phys Chem* **100**: 17978–17980.

70. Cherepy NJ, Du M, Holzwarth AR, Mathies RA (1996) Near-infrared resonance Raman spectra of chlorosomes: Probing nuclear coupling in electronic energy transfer. *J Phys Chem* **100**: 4662–4671.

71. Diers JR, Zhu Y, Blankenship RE, Bocian DF (1996) Qy-excitation resonance Raman spectra of chlorophyll a and bacteriochlorophyll c/d aggregates. Effects of peripheral substituents on the low-frequency vibrational characteristics. *J Phys Chem* **100**: 8573–8579.

72. Pedersen MØ, Linnanto J, Frigaard N-U, Nielsen NC, Miller M (2010) A model of the protein – pigment baseplate complex in chlorosomes of photosynthetic green bacteria. *Photosynth Res* **104**: 233–243.

73. Pedersen MØ, Underhaug J, Dittmer J, Miller M, Nielsen NC (2008) The three-dimensional structure of CsmA: a small antenna protein from the green sulfur bacterium Chlorobium tepidum. *FEBS Lett* **582**: 2869–2874.

74. Bryant DA, Vassilieva E V, Frigaard N, Li H (2002) Selective protein extraction from Chlorobium tepidum chlorosomes using detergents. Evidence that CsmA forms multimers and binds bacteriochlorophyll a. *Biochemistry* **41**: 14403–14411.

75. Sakuragi Y, Frigaard N, Shimada K, Matsuura K (1999) Association of bacteriochlorophyll a with the CsmA protein in chlorosomes of the photosynthetic green filamentous bacterium Chloroflexus aurantiacus. *Biochim Biophys Acta* **1413**: 172–180.

76. Pšenčík J, Collins AM, Liljeroos L, Torkkeli M, Laurinmäki P, Ansink HM, Ikonen TP, Serimaa RE, Blankenship RE, Tuma R, et al. (2009) Structure of chlorosomes from the green filamentous bacterium Chloroflexus aurantiacus. *J Bacteriol* **191**: 6701–6708.

77. Vassilieva E V, Stirewalt VL, Jakobs CU, Frigaard N-U, Inoue-Sakamoto K, Baker MA, Sotak A, Bryant DA (2002) Subcellular localization of chlorosome proteins in Chlorobium tepidum and characterization of three new chlorosome proteins: CsmF, CsmH, and CsmX. *Biochemistry* **41**: 4358–4370.

78. Pedersen MØ, Pham L, Steensgaard DB, Miller M (2008) A reconstituted light-harvesting complex from the green sulfur bacterium Chlorobium tepidum containing CsmA and bacteriochlorophyll a. *Biochemistry* **47**: 1435–1441.

79. Gerola PD, Olson JM (1986) A new bacteriochlorophyll a-protein complex associated with chlorosomes of green sulfur bacteria. *Biochim Biophys Acta - Bioenerg* **848**: 69–76.

80. Milder MTW, Brüggemann B, van Grondelle R, Herek JL (2010) Revisiting the optical properties of the FMO protein. *Photosynth Res* **104**: 257–274.

81. Ben-Shem A, Frolow F, Nelson N (2004) Evolution of photosystem I - from symmetry through pseudo-symmetry to asymmetry. *FEBS Lett* **564**: 274–280.

82. Tronrud DE, Wen J, Gay L, Blankenship RE (2009) The structural basis for the difference in absorbance spectra for the FMO antenna protein from various green sulfur bacteria. *Photosynth Res* **100**: 79–87.

83. Fenna RE, Matthews BW (1975) Chlorophyll arrangement in a bacteriochlorophyll protein from Chlorobium limicola. *Nature* **258**: 573–577.

84. Brixner T, Stenger J, Vaswani HM, Cho M, Blankenship RE, Fleming GR (2005) Two-dimensional spectroscopy of electronic couplings in photosynthesis. *Nature* **434**: 625–628.

85. Hauska G, Schoedl T, Remigy H, Tsiotis G (2001) The reaction center of green sulfur bacteria. *Biochim Biophys Acta* **1507**: 260–277.

86. Permentier HP, Schmidt KA, Kobayashi M, Akiyama M, Hager-Braun C, Neerken S, Miller M, Amesz J (2000) Composition and optical properties of reaction centre core complexes from the green sulfur bacteria Prosthecochloris aestuarii and Chlorobium tepidum. *Photosynth Res* **64**: 27–39.

87. Melkozernov AN, Olson JM, Li Y-F, Allen JP, Blankenship RE (1998) Orientation and excitonic interactions of the Fenna—Matthews—Olson bacteriochlorophyll a protein in membranes of the green sulfur bacterium Chlorobium tepidum. *Photosynth Res* **56**: 315–328.

88. Rémigy H-W, Stahlberg H, Fotiadis D, Müller SA, Wolpensinger B, Engel A, Hauska G, Tsiotis G (1999) The reaction center complex from the green sulfur bacterium Chlorobium tepidum: a structural analysis by scanning transmission electron microscopy. *J Mol Biol* **290**: 851–858.

89.   Wen J, Zhang H, Gross ML, Blankenship RE (2009) Membrane orientation of the FMO antenna protein from Chlorobaculum tepidum as determined by mass spectrometry-based footprinting. *Proc Natl Acad Sci U S A* **106**: 6134–6139.

90.   Adolphs J, Renger T (2006) How proteins trigger excitation energy transfer in the FMO complex of green sulfur bacteria. *Biophys J* **91**: 2778–2797.

91.   Schmidt Am Busch M, Müh F, El-Amine Madjet M, Renger T (2011) The eighth bacteriochlorophyll completes the excitation energy funnel in the FMO protein. *J Phys Chem Lett* **2**: 93–98.

92.   Savikhin S, Struve WS (1994) Ultrafast energy transfer in FMO trimers from the green bacterium Chlorobium tepidum. *Biochemistry* **33**: 11200–11208.

93.   Savikhin S, Zhou W, Blankenship RE, Struve WS (1994) Femtosecond energy transfer and spectral equilibration in bacteriochlorophyll a - protein antenna trimers from the green bacterium Chlorobium tepidum. *Biophys J* **66**: 110–113.

94.   Vulto SIE, Streltsov AM, Aartsma TJ (1997) Excited state energy relaxation in the FMO complexes of the green bacterium Prosthecochloris aestuarii at low temperatures. *J Phys Chem B* **101**: 4845–4850.

95.   Zhou W, LoBrutto R, Lin S, Blankenship RE (1994) Redox effects on the bacteriochlorophyll a-containing Fenna-Matthews-Olson protein from Chlorobium tepidum. *Photosynth Res* **41**: 89–96.

96.   Gulbinas V, Valkunas L, Kuciauskas D, Katilius E, Liuolia V, Zhou W, Blankenship RE (1996) Singlet-Singlet Annihilation and Local Heating in FMO Complexes. *J Phys Chem* **100**: 17950–17956.

97.   Oh-oka H, Kamei S, Matsubara H, Lin S, van Noort PI, Blankenship RE (1998) Transient Absorption Spectroscopy of Energy-Transfer and Trapping Processes in the Reaction Center Complex of Chlorobium tepidum. *J Phys Chem B* **102**: 8190–8195.

98.   Neerken S, Permentier HP, Francke C, Aartsma TJ, Amesz J (1998) Excited states and trapping in reaction center complexes of the green sulfur bacterium Prosthecochloris aestuarii. *Biochemistry* **37**: 10792–10797.

99.   Kramer H, Kingma H, Swarthoff T, Amesz J (1982) Prompt and delayed fluorescence in pigment-protein complexes of a green photosynthetic bacterium. *Biochim Biophys Acta* **681**: 359–364.

100.   Francke C, Otte SC, Miller M, Amesz J, Olson JM (1996) Energy transfer from carotenoid and FMO-protein in subcellular preparations from green sulfur bacteria. Spectroscopic characterization of an FMO-reaction center core complex at low temperature. *Photosynth Res* **50**: 71–77.

101.   Vlaming SM, Malyshev VA, Knoester J (2009) Localization properties of one-dimensional Frenkel excitons: Gaussian versus Lorentzian diagonal disorder. *Phys Rev B* **79**: 1–8.

102.   Czarnecki K, Diers JR, Chynwat V, Erikson JP, Frank HA, Bocian DF (1997) Characterization of the strongly coupled, low-frequency vibrational modes of the special pair of photosynthetic reaction centers via isotopic labeling of the cofactors. *J Am Chem Soc* **119**: 415–426.

103. Causgrove TP, Brune DC, Wang J, Wittmershaus BP, Blankenship RE (1990) Energy transfer kinetics in whole cells and isolated chlorosomes of green photosynthetic bacteria. *Photosynth Res* **26**: 39–48.

PAPER I

Two-Dimensional Electronic Spectroscopy Reveals Ultrafast Energy Diffusion in Chlorosomes

Jakub Dostál,[†,‡] Tomáš Mančal,[‡] Ramūnas Augulis,[†,∥] František Vácha,[§] Jakub Pšenčík,[‡] and Donatas Zigmantas*,[†]

[†]Department of Chemical Physics, Lund University, Getingevägen 60, 221 00 Lund, Sweden

[‡]Faculty of Mathematics and Physics, Charles University in Prague, Ke Karlovu 3, 121 16 Prague, Czech Republic

[§]Faculty of Science, University of South Bohemia, Branišovská 31, 370 05 České Budějovice, Czech Republic

Ⓢ *Supporting Information*

ABSTRACT: Chlorosomes are light-harvesting antennae that enable exceptionally efficient light energy capture and excitation transfer. They are found in certain photosynthetic bacteria, some of which live in extremely low-light environments. In this work, chlorosomes from the green sulfur bacterium *Chlorobaculum tepidum* were studied by coherent electronic two-dimensional (2D) spectroscopy. Previously uncharacterized ultrafast energy transfer dynamics were followed, appearing as evolution of the 2D spectral line-shape during the first 200 fs after excitation. Observed initial energy flow through the chlorosome is well explained by effective exciton diffusion on a sub-100 fs time scale, which assures efficiency and robustness of the process. The ultrafast incoherent diffusion-like behavior of the excitons points to a disordered energy landscape in the chlorosome, which leads to a rapid loss of excitonic coherences between its structural subunits. This disorder prevents observation of excitonic coherences in the experimental data and implies that the chlorosome as a whole does not function as a coherent light-harvester.
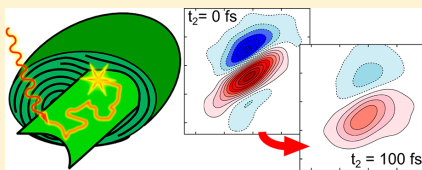
INTRODUCTION

Photosynthetic organisms developed various types of light-harvesting antennae to efficiently collect incoming sunlight. Generally, these are sophisticated protein complexes where pigments are held in appropriate positions by a protein scaffold. The only known exception to this molecular architecture is the chlorosome, an extraordinary large light-harvesting antenna found in three phyla of photosynthetic bacteria.[1−3] The chlorosome interior is composed of up to a few hundreds of thousands of strongly interacting bacteriochlorophyll (BChl) *c*, *d*, or *e* molecules self-assembled into aggregates without any direct involvement of a protein. This unique composition allows mimicking the chlorosomes by aggregates of chlorosomal BChls or their synthetic analogues prepared in vitro, which could be potentially utilized in, for example, artificial photosynthesis or photovoltaics.[4−8] Experiments employing X-ray scattering and electron cryomicroscopy revealed that BChl aggregates are organized into curved lamellar structures[9−12] ranging from disordered lamellae prevailing inside the wild-type chlorosomes, to well-organized multilayered cylinders observed mainly for a specific bchQRU mutant of *Chlorobaculum (Cba.) tepidum*.[10,12] However, the overall organization of BChl aggregates in each chlorosome is unique, and it exhibits a significant variability even inside a single chlorosome. This prevents the structure of the aggregates from being determined at the molecular level by X-ray crystallography. The exact arrangement of BChls within the chlorosome is therefore still a matter of dispute. Several models of the short-range organization have been proposed, mainly based on NMR experiments.[13−17]

Fast photophysical processes in chlorosomes were studied by several groups (for reviews, see refs 3,12). It was observed that excitation of the Q_y band of BChl aggregates is followed by a rapid exciton relaxation, which is finished in less than 1 ps.[18−20] This process is followed by long-range energy transfer within the aggregates leading to excitation equilibration over the whole chlorosome.[19] From BChl aggregates, the excitation energy is transferred to BChl *a* molecules in the baseplate, a pigment–protein complex located on the side of the chlorosome facing the cytoplasmic membrane. This step occurs on the time scale of tens of picoseconds, depending on the type of aggregated BChls.[21] Subsequently, the excitation is transferred toward the reaction centers in the cytoplasmic membrane, where charge separation occurs. In addition to relaxation processes, coherent oscillations were also observed and attributed to intramolecular vibrational wavepacket dynamics.[22−26]

To get a deeper insight into photophysical processes in chlorosomes, we have employed electronic two-dimensional (2D) spectroscopy.[27] The real part of the 2D spectrum can be interpreted as a spectrally resolved transient spectrum mapped on the two frequency axes, where ω_1 is the excitation frequency, ω_3 is the detection frequency, and t_2 is the system evolution

time. It has been demonstrated that 2D spectroscopy, apart from revealing energy transfer dynamics, has enabled observation of coherent electronic dynamics in small photosynthetic complexes,[28,29] and supplied means for tracking dynamic line shape changes due to electron−phonon interactions.[30−32] The 2D line shapes thus provide information on the spectral changes even within the homogeneous line width that are not accessible from pump−probe experiments. The limitations of the pump−probe spectra are due to the fact that they are related to 2D spectra by integration along the excitation (ω_1) axis.[27] One example of information that is lost by this integration is the pure dephasing process. This results in change of the observable 2D line shape, while the corresponding pump−probe spectrum remains unaltered.

This work explores initial dynamics (up to 200 fs after excitation) at ambient temperature within chlorosomes containing BChl c from green sulfur bacterium *Cba. tepidum*. The extra dimension of coherent 2D spectroscopy and high simultaneous spectral and time resolution have enhanced the information content of ultrafast experiments. Excitation energy dynamics have been unraveled in chlorosomes taking place on a sub-100 fs time scale. This is attributed to ultrafast energy migration between different structural units that assures extremely efficient energy flow through a lamellar layer, which is essential to the light-harvesting function of the chlorosome.

■ EXPERIMENTAL RESULTS

The NIR part of the steady-state absorption spectrum of the chlorosome from *Cba. tepidum* is shown in Figure 1. The spectrum
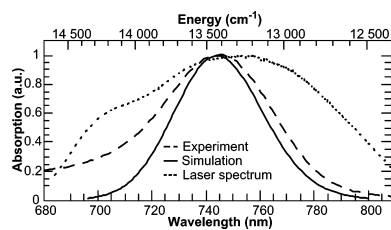

Figure 1. Absorption spectrum of chlorosomes from *Cba. tepidum* (− − −) and its simulation (−) together with a spectral profile of the laser pulses (···).

is dominated by the Q_y band of aggregated BChl c centered at 745 nm with full width at half-maximum (fwhm) of the absorption band corresponding to 930 cm^{-1}. Absorption of BChl a-rich baseplate at around 800 nm is negligible because of low abundance of BChls a (∼1%) in the chlorosome. The spectral profile of the laser pulse completely covering the absorption band is also shown. Figure 2 depicts corresponding 2D spectra (real part of the electric field) measured at population times between 0 and 200 fs. The total spectra composed of rephasing and nonrephasing parts are shown, providing an intuitive picture of emissive/absorptive signals on the map of excitation and probe frequencies. The 2D spectrum measured at 0 fs allows an upper estimate of the homogeneous line width of the exciton transition between the ground and first excited states of BChl c aggregate, which is 360 ± 20 cm^{-1}. This value is similar to the estimate of the homogeneous line width used in exciton calculations.[26]

The 2D spectrum undergoes dramatic changes during this short time period. In the beginning, the signal exhibits a strong positive feature (corresponding to ground-state bleaching and stimulated emission), which is extensively elongated along the diagonal implying

strong correlation of excitation and detection frequencies. The central positive part of the signal is surrounded by negative features due to broad excited-state absorption. During the first 100 fs, the amplitude of the positive signal drops significantly and its line shape becomes more rounded, while the negative part at the lower ω_3 frequencies disappears, because of overlap with the broadened positive signal. The amplitude of the signal at the position of its initial maximum drops to approximately one-half with an effective time constant of 40 fs (Figure 3). The overall transient absorption signal, which is obtained by integration of the 2D spectrum along its horizontal (ω_1) axis, evolves rapidly during the first 100 fs, by which time it reaches an almost stationary level (Figure 4). The time evolution of this projection reflects the fast changes of the 2D line shape; however, the exact shape evolution is not captured. Previously reported oscillating dynamics[22,24−26] were not resolved here due to their low frequency, corresponding to a typical period of ∼220 fs (comparable to the time window used here), and due to the low amplitude of the oscillations at room temperature. Qualitatively similar behavior of 2D spectra was also observed for chlorosomes from *Chloroflexus aurantiacus* (see the Supporting Information).

■ MODELING AND DISCUSSION

Role of Disorder. The chlorosome is an aggregate of tightly packed BChls, where the resonant coupling between chromophores is strong and aggregate eigenstates involve excited states of more than one molecule.[12,19,26] In a perfect large periodic aggregate, strong resonance coupling would result in energy eigenstates delocalized over the whole system. The presence of significant disorder in the aggregate structure results in a certain distribution of transition frequencies (so-called diagonal energetic disorder) and couplings between molecules (off-diagonal disorder). Thus, one may assume that the aggregate consists of a number of domains separated by a high local energetic disorder or by a significant structural dislocation. The wave function of the aggregate's excited states cannot then be fully delocalized over the aggregate, but would remain delocalized only over one domain or only over a part of the domain. Further, in this Article, we refer to these regions as coherent domains. The electronic transitions between the coherent domains would couple only relatively weakly with respect to the electron−phonon coupling, and the energy transfer between them would thus proceed in an incoherent fashion described, for example, by multichromophoric Förster rate theory.[33,34] The domain picture provides a more intuitive explanation of spectroscopic observations than treating the disordered aggregate as a whole, as we will discuss below. Also, in the situation when it is possible to theoretically treat only the two limiting cases of strong and weak resonance coupling, the partitioning into coherent domains may provide an effective tool for detailed simulations of large aggregates.

Chlorosome Structure. In all current models of chlorosomes, the BChl aggregates are organized in curved lamellar structures that can include multilayered cylinders.[9−12] The lamellar spacing was determined to be on the order of 2−3 nm.[9,10] At these distances, weak interactions lead to a negligible delocalization,[35] and the energy transfer between the lamellar layers can be described by an incoherent rate theory.[33,34] Thus, one can view the interior of the chlorosome as an ensemble of layers. The disorder within individual layers prevents delocalization of excitonic eigenstates of the system over the whole two-dimensional structure of the layer. Thus, even one lamellar layer should be viewed as an ensemble of coherent domains. The excitation could move along the two-dimensional structure in both the coherent fashion (e.g., within the coherent
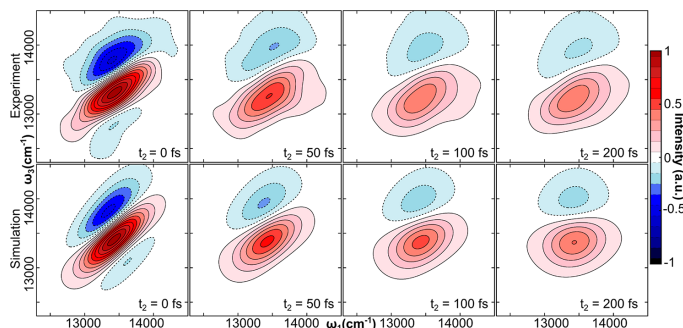
Figure 2. Measured (top) and simulated (bottom) 2D spectra (real part of electric field) of chlorosomes at different population times.
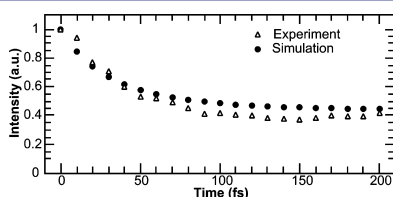

Figure 3. Amplitude decay of the positive peak in experimental ($\triangle$) and simulated ($\bullet$) 2D spectra at the point of its maximum initial signal.
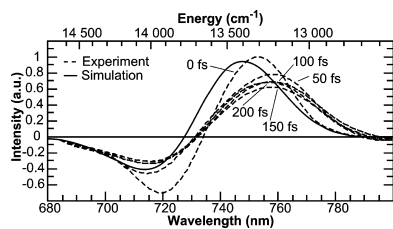

Figure 4. Transient absorption spectra of chlorosomes obtained by integration of 2D spectra along the ω_1 axis. Five different population times ($- - -$) and the time invariant simulated curve ($-$) are shown.

domains) and the incoherent fashion (between the coherent domains).

We face a situation in which measured spectra inevitably contain an averaging over a hierarchy of various types of static disorder. The highest level of disorder includes variations among chlorosomes and among individual lamellar layers within one chlorosome. The distribution associated with this highest level of disorder can be estimated from low temperature spectral hole-burning and fluorescence experiments, which can measure the distribution of the lowest excitonic levels in the ensemble of chlorosomes. The fwhm values in the range of 100−250 cm^{-1} have been determined for chlorosomal aggregates,[36,37] indicating a relatively small contribution of the highest level of disorder to the broad absorption bands (~1000 cm^{-1}) of chlorosomes from green sulfur bacteria. Similarly, single molecule spectroscopy, which shows the

variations between individual chlorosomes, revealed that low and ambient temperature fluorescence spectra of single chlorosomes from *Cba. tepidum* do not exhibit significant narrowing as compared to the bulk spectrum.[38−41] From the above discussion, it can be concluded that the differences among the individual coherent domains are responsible for the broad absorption spectrum of the chlorosome as well as for the elongated shape of 2D correlation spectrum at $t_2 = 0$ fs.

Ultrafast Line Shape Dynamics. Unlike linear and some nonlinear (transient) absorption spectroscopies, coherent 2D spectroscopy enables, to a large extent, one to overcome the loss of information due to the static disorder. It is reasonable to assume that the coherent domains in the chlorosome have a distribution of allowed transition frequencies, and that the spectral line shapes corresponding to electronic transitions associated with individual domains are significantly narrower than the ensemble line shape. The 2D spectrum at $t_2 = 0$ fs is expected to have a characteristic elongation along the diagonal. This is exactly what is observed in the experiment. Evolution of the diagonal line shape with $t_2 > 0$ fs then monitors the redistribution of the excitation in and among the domains. At very short times (sub-100 fs), no redistribution is possible on the highest level of structural hierarchy, that is, among the lamellar layers or over the whole chlorosome. The transitions between the layers in the chlorosomes were observed on the time scale of picoseconds.[19,24,26,37] Fast energy redistribution can, however, be expected within and between the domains in the same 2D lamellar layer, because of the close proximity of coherent domains.

An alternative interpretation of sub-100 fs changes might involve homogeneous line shape dynamics of excitonic transitions due to the interaction with the bath. However, in the following, we will show that this cannot be the case. Let us first estimate the homogeneous line width corresponding to electronic transitions associated with individual coherent domains. This line width has to be compared to the diagonal width of the observed 2D spectrum. To this end, we will assume a line shape function of an individual BChl molecule that has the form of an overdamped Brownian oscillator:[42]

$$g_{BChl}(t) = \frac{2\lambda_{BChl}k_B T}{\hbar\Lambda^2}(e^{-\Lambda t} + \Lambda t - 1) \approx \frac{1}{2}\Delta^2 t^2 \quad (1)$$

The two parameters of this model are the reorganization energy λ_{BChl} and the bath correlation time τ_c, which enters through the parameter $\Lambda = 1/\tau_c$. For the estimation of the line shape fwhm,

11613

dx.doi.org/10.1021/ja3025627 | *J. Am. Chem. Soc.* 2012, 134, 11611−11617

we introduced a short time expansion of the line shape function[43] and ignored the imaginary part of the line shape function, which leads only to a frequency shift. We also introduced a line shape parameter $\Delta^2 = 2\lambda_{\text{BChl}}k_B T\hbar^{-1} = C_{\text{BChl}}(0)$, where $C_{\text{BChl}}(t)$ is the energy gap correlation function of the BChl transition. The line shape of an individual electronic transition will be narrowed by exciton interaction, and, at the same time, broadened due to finite lifetime of the exciton. In a sufficiently large system of molecules interacting through nearest neighbor coupling, the line narrowing factor is $\sim 1/N$, where N is the number of interacting molecules in the system. Correspondingly the excitonic line shape would be significantly narrowed.

The reorganization energy of BChl c at 300 K can be estimated from the Q_y band's Stokes shift to be in the range 35−90 cm^{-1} depending on the solvent used.[44] The corresponding upper estimate of a BChl c homogeneous line width in solution is $\sigma_{\text{BChl}} = \Delta(8 \ln 2)^{1/2} = 457$ cm^{-1}. The lifetime broadening coming from the excitonic relaxation on the time scale of 100 fs amounts to 53 cm^{-1}, which can be neglected, leaving us with the value of 457 cm^{-1} as the least favorable upper estimate of homogeneous line width of excitonic levels. However, the actual fwhm of the Q_y band in the *Cba. tepidum* chlorosome is a factor of 2 higher (900−1000 cm^{-1}). Taking into account the close packing of the chromophores in the chlorosome, the difference is more likely to be much higher due to the narrowing effect. Another source of broadening could be the coupling of excitonic states to charge transfer (CT) states, which are expected to occur due to the close packing of the chromophores, and which were observed in Stark spectroscopy of chlorosomes.[45] However, the charge transfer from one neutral molecule to another is not energetically favorable unless the environment or external field (as in Stark spectroscopy) creates a potential that favors it. CT states can therefore be assumed to be sufficiently off resonance not to contribute in our experiment. Even if the environment did allow the CT states to have lower energy, the additional broadening due to resonance interaction of CT states with excitonic states cannot account for the very broad chlorosome absorption band.

Thus, we demonstrated that the upper estimate of the excitonic transition line width is much smaller than the diagonal line width of the observed 2D spectra. Consequently, the short time dynamics of the 2D spectrum do not reflect homogeneous line shape dynamics caused by the bath reorganization, but rather reveal excitation dynamics.

Effective Excitation Diffusion Model. As discussed above, the experimental spectra in Figure 2 reflect a significant inhomogeneous disorder in the chlorosomes and fast redistribution of transition energies on a sub-100 fs time scale. This behavior is reminiscent of spectral changes induced in a two-level system by pure dephasing due to interaction with a bath. The following analogy explores this possibility: the first excited-state manifold of a chlorosome will be considered as "one state", a superlevel, which interacts with a "bath" of electronic levels of this manifold. These electronic levels can be then included into the model by an effective energy gap correlation function, analogously to the way the bath density of states is included for a two-level system. Because of the size and the high disorder of the chlorosome, the appropriate energy gap correlation function is expected to take a relatively simple form. First, at $t_2 = 0$ fs, the correlation function has to have a value consistent with the chlorosome absorption spectrum, that is, $C(0) = \Delta^2$. Second, random hopping among the coherent

domains corresponding to spectral and spatial diffusion of the excitation would lead to an exponential decay of the correlation. One could in principle expect some more complicated contribution from a possible coherent component of the energy transfer within the coherent domains at short times, but as there are many possible substructures with similar energies, any oscillatory signal due to electronic coherences will dephase because of ensemble averaging. It is important to note that the rephasing capability of photon echo does not apply to coherences within the electronic bands. This is due the fact that the third-order spectroscopic signal involves only one time interval (so-called population time) when these coherences evolve, and not two that could lead to rephasing. To properly describe the results of ultrafast chlorosome spectroscopy, it is necessary to include consideration of the two-exciton band, which appears in the 2D and pump−probe spectra as a source of excited state absorption. This will be done by the same effective superlevel method. To calculate 2D spectra of such an effective three level system, it is necessary to know the energy gap correlation functions $C_{ee}(t)$, $C_{ff}(t)$, and $C_{fe}(t)$, where $C_{ij}(t) = \langle \delta\omega_i(t)\delta\omega_j(0)\rangle$, and the $\delta\omega_i$ is the energy gap operator of the transition between the ground state and the superlevel i. Indices e and f denote the single- and two-exciton states. The correlation function is defined as

$$C_{ij}(t) = \gamma_{ij}\Delta^2 e^{-t/\tau_c} \tag{2}$$

that leads to a real line shape function of the form:

$$g_{ij}(t) = \gamma_{ij}\Delta^2 \tau_c^2 \left(e^{-t/\tau_c} + \frac{t}{\tau_c} - 1\right) \tag{3}$$

where γ_{ij} ($\gamma_{ee} = 1$) is a prefactor, which adjusts the cross-correlation function $C_{ef}(t)$ and two-exciton correlation function $C_{ff}(t)$ relative to $C_{ee}(t)$. The same correlation time τ_c is set for all of them for simplicity. Thus, there are the following adjustable phenomenological parameters in the model: Δ, τ_c, and γ_{ij}, which are obtained by fitting simulated spectra to experimental results. Their effect on the shape of simulated 2D spectra is the following: Δ and τ_c are responsible for the overall shape and size of the 2D spectrum. In addition, τ_c provides the typical time scale of the dynamics. Parameter γ_{ff} adjusts the relative width in the diagonal and antidiagonal directions of the excited-state absorption signal, and γ_{ef} adjusts the excited-state signal shape deviation from the antidiagonal orientation.

Comparison between Simulation and Experiment. All simulations were done in the impulsive approximation, neglecting finite temporal and spectral width of the laser pulses. Values of the parameters needed to model the experimental data are summarized in Table 1. The energy gap between the ground and first excited superlevels ΔE_{ge} corresponding to 745 nm

Table 1. Values of the Parameters Used To Model the Experimental Data

ΔE_{ge} (eV)	ΔE_{ef} (eV)	μ_{ge} (au)	μ_{ef} (au)	τ_c (fs)	Δ^2 (rad^2 fs^{-2})	γ_{ee}	γ_{ff}	γ_{ef}
1.666	1.684	1	1.3	100	3.5×10^{-3}	1	4.3	1.8

dictates the position of the absorption band as well as the position of the positive signal in the 2D spectrum. The gap between the first and second excited superlevels ΔE_{ef} is set to be slightly larger than ΔE_{ge} to reproduce negative excited-state absorption signal that is more pronounced at higher energy part of the 2D and

transient absorption spectra. In the excitonic picture of the chlorosome, these energy gaps correspond to the relative energies of the strongly allowed single and double exciton bands. The values of the line shape parameter Δ, and correlation time τ_c, are chosen to correctly reproduce the elongated shape of the 2D spectrum at $t_2 = 0$ fs. In addition, the correlation time of 100 fs governs the characteristic time scale of spectral dynamics. However, the exact time evolution of the particular areas of the 2D spectrum is given by interplay between decays of positive and negative contributions. The value of transition dipole moment μ_{ef} was set larger than μ_{ge} to adequately reproduce the experimental data. The shape of the negative signal is determined by the parameters γ_{ff} and γ_{ef}. Because γ_{ff} is bigger than γ_{ee}, which is set to 1, the negative signal is broader than the positive. The parameter γ_{ef} is adjusted to provide the correct negative signal inclination toward the diagonal direction.

Results of the simulation are compared to the experimental data in Figures 1−4. The simulated spectra were normalized in such a way that the maximum amplitudes of both the simulated and the experimental 2D spectra are equal at $t_2 = 0$ fs. It can be seen that the proposed simple model reproduces well the absorption spectrum (Figure 1), as well as the general shape and evolution of the 2D spectrum (Figure 2) with its characteristic maximal intensity drop (Figure 3). The noticeable difference in the modeled and observed absorption spectra comes from limitations of the model, whose parameters were optimized to preferentially reproduce the 2D spectra. Overall success of the model confirm that observed sub-100 fs dynamics comes from stochastic exciton diffusion. However, the model does not provide an interpretation of some detailed spectral features. The differences between the model and experimentally observed dynamics discussed below will be used to make further conclusions about the nature of the excitation dynamics.

First, the discrepancies between the experimental and simulated data are listed. In particular, the slope of the nodal line separating positive and negative parts changes little during the time evolution in the experimental data. In the simulation, however, it leans from diagonal direction at $t_2 = 0$ fs to an almost horizontal orientation at $t_2 = 200$ fs. The difference is also observed in the ω_1-integrated profiles corresponding to the transient absorption signal. The general shape is similar at $t_2 = 0$ fs; only the maximum of the simulated spectrum is blue-shifted by 5 nm. The projection of the experimental spectrum at later times decays and shifts to the red side, whereas the simulated projection remains without any change.

In the following, the insight provided by the diffusion model and its limitations is combined with the coherent domain structural model to interpret the initial excitation dynamics in the chlorosome. The effective excitation diffusion model describes the chlorosome as a set of coherent domains between which random energy transfer is taking place. When energy starts diffusing between the domains in an incoherent manner, all coherence dynamics effects (if initiated by the initial excitation) are quickly dephased. Positive signal at the time immediately after excitation correlates excitation and detection frequencies from the transitions in the same coherent domain. Individual coherent domains are weakly coupled, which prevents formation of observable cross-peaks between different domains. Nevertheless, the energy transfer between the domains is very fast, because of the presence of a multitude of exciton transitions with similar energy, but likely with different oscillator strength. Strongly elongated shape at $t_2 = 0$

fs is the result of a broad energetic distribution of coherent domains. The antidiagonal width of the positive band is given by the average properties of a single domain. In general, it cannot be simply identified with the homogeneous line width of a single exciton level because there can be several excitonic transitions localized in one coherent domain sharing a common ground state. Thus, the 2D spectrum of a single coherent domain is a superposition of diagonal- and cross-peaks. In agreement with the exciton theory, which predicts comparable spacing between bands, the whole positive signal is overlaid with a broad negative signal arising from single- to double-exciton absorption. The temporal evolution of the 2D spectrum reflects energy redistribution between neighboring domains. Because stochastic energy diffusion in the simulation is completely random, without any preferred direction, the positive signal of the 2D spectrum acquires a rounded shape with a horizontal nodal line, and the red-shift dynamics in the integrated projection is not observed. The model does not take into account any oscillator strength differences between transitions belonging to different coherent domains. This prevents the decay of the transient signal and, together with the effect described above, leads to the complete lack of time evolution in the integrated projection (Figure 4). However, in the chlorosome, we observe energy diffusion in which coherent domains with allowed exciton transitions at higher energies populate similar and lower energy exciton transitions located in the neighboring domains. This downhill process results in a filling of the space under the diagonal by a positive signal. Because some high energy domains remain excited during the diffusion process, the direction of nodal line remains almost unchanged. The fact that after 200 fs the low energy side of the positive signal is not completely horizontal indicates that the excitation energy redistribution is not completed on this time scale. The preferred downhill direction can be also observed as a red shift of a transient absorption signal (Figure 4). The intensity drop of the integrated projection is explained by the fact that levels with a strong transition dipole moment are initially excited, but levels with a weaker dipole moment become populated during the energy redistribution within and between coherent domains. This observation supports the previously reported suggestion that the lowest excitonic states in the chlorosome aggregates possess small transition dipole moments.[19,26,37] Similar initial energy transfer dynamics were observed in chlorosomes from *Chloroflexus aurantiacus* as well (see the Supporting Information), indicating that this form of ultrafast energy migration is a general phenomenon in chlorosomes.

Note that the ensemble average of a broad range of dynamical processes taking place in photoexcited chlorosomes was observed. For example, the energy of the photons absorbed very close to the baseplate will be immediately transferred to the baseplate without initial energy diffusion. However, these instances are rare and do not contribute substantially to the observed signal. By observing the average excitation energy dynamics in this work, the most common and most important initial processes of the chlorosome light-harvesting function were investigated.

■ CONCLUSIONS

We report a study of initial excitation evolution in chlorosomes on a sub-100 fs time scale that has not been explored previously. Excitation dynamics monitored as spectral changes in the 2D spectra are explained by proposing a model of

effective diffusion-like behavior of the excitons. Following initial excitation, energy diffuses extremely fast among and within coherent domains of the chlorosome. Most of the inhomogeneous transition energy distribution in the chlorosome is sampled by the spectral diffusion within 200 fs. The presence of a coherent energy transfer component within the chlorosome substructures on an even shorter time scale cannot be excluded, because oscillatory contributions to the 2D spectrum are likely to be smeared out by the significant static disorder within chlorosomes. According to the proposed model, energy diffusion causes rapid dephasing between the coherent domains, and thus the electronic phase relationship between the domains is lost. This implies that the overall energy transfer through the chlorosome as a light-harvesting unit cannot proceed coherently.

MATERIALS AND METHODS

Cells of *Cba. tepidum* were grown as described previously,[9] and the chlorosomes were isolated following a standard method consisting of two successive sucrose gradient ultracentrifugation steps.[46] Before the measurement, chlorosomes were dissolved in 50 mM Tris-HCl buffer (pH 8.0), sucrose was removed using a centrifugal filter, and the sample was diluted to absorbance of about 0.4 in a 0.5 mm optical path at 745 nm. In addition, chlorosomes were reduced by 15 mM sodium dithionite and incubated at least 45 min before measurement to achieve anaerobic conditions. All experiments were carried out in a 0.5 mm optical path length flow cell. The sample was flowed at ∼10 cm/s rate. Excitation intensity was typically 100 pJ per pulse in each of excitation pulse, which corresponds to approximately 4.8×10^{12} photons per pulse per cm^2 that satisfies annihilation-free conditions.[19]

2D spectra were obtained using the double-modulation lock-in technique described in ref 47. Briefly, a 200 kHz repetition rate KGW amplified laser system (PHAROS, Light Conversion) was used to pump a homemade NOPA that produced broadband 15 fs pulses centered at 750 nm with spectral fwhm of ∼95 nm. Using a plate beam splitter and transmissive diffraction grating, the initial beam is split into four beams arranged in the boxcar geometry. One of them, the local oscillator (LO) beam is attenuated by a 3 OD filter. The other three beams are used to excite the sample in a four wave mixing experiment. The first and second beams are modulated at different frequencies, using optical choppers. Accurate time delays of the first two pulses are introduced by moving fused silica wedges with motorized translation stages. Polarization induced in the sample is emitted in the phase-matched direction, mixed with the collinear LO beam, and detected in a spectral interferometry scheme. Detection of the third-order signal is performed by locking to the sum and difference of the chopper modulation frequencies.

ASSOCIATED CONTENT

Ⓢ Supporting Information

2D spectra of chlorosomes from *Chloroflexus aurantiacus*. This material is available free of charge via the Internet at http://pubs.acs.org.

AUTHOR INFORMATION

Corresponding Author
donatas.zigmantas@chemphys.lu.se
Present Address
‖Center for Physical Sciences and Technology, Gostauto 11, LT-01108 Vilnius, Lithuania.
Notes
The authors declare no competing financial interest.

ACKNOWLEDGMENTS

REFERENCES

(1) Frigaard, N.-U.; Bryant, D. In *Complex Intracellular Structures in Prokaryotes*; Shively, J., Ed.; Springer: Berlin/Heidelberg, 2006; Vol. 2, p 79.

(2) Bryant, D. A.; Costas, A. M. G.; Maresca, J. A.; Chew, A. G. M.; Klatt, C. G.; Bateson, M. M.; Tallon, L. J.; Hostetler, J.; Nelson, W. C.; Heidelberg, J. F.; Ward, D. M. *Science* **2007**, *317*, 523.

(3) Blankenship, R. E.; Matsuura, K. In *Light-Harvesting Antennas in Photosynthesis*; Green, B. R., Parson, W. W., Eds.; Kluwer Academic Publishers: Dordrecht, 2003; p 195.

(4) Katterle, M.; Prokhorenko, V. I.; Holzwarth, A. R.; Jesorka, A. *Chem. Phys. Lett.* **2007**, *447*, 284.

(5) Roger, C.; Miloslavina, Y.; Brunner, D.; Holzwarth, A. R.; Wurthner, F. *J. Am. Chem. Soc.* **2008**, *130*, 5929.

(6) Huijser, A.; Marek, P. L.; Savenije, T. J.; Siebbeles, L. D. A.; Scherer, T.; Hauschild, R.; Szmytkowski, J.; Kalt, H.; Hahn, H.; Balaban, T. S. *J. Phys. Chem. C* **2007**, *111*, 11726.

(7) Miyatake, T.; Tamiaki, H. *Coord. Chem. Rev.* **2010**, *254*, 2593.

(8) Alster, J.; Polivka, T.; Arellano, J. B.; Chabera, P.; Vacha, F.; Psencik, J. *Chem. Phys.* **2010**, *373*, 90.

(9) Psencik, J.; Ikonen, T. P.; Laurinmaki, P.; Merckel, M. C.; Butcher, S. J.; Serimaa, R. E.; Tuma, R. *Biophys. J.* **2004**, *87*, 1165.

(10) Oostergetel, G. T.; Reus, M.; Chew, A. G. M.; Bryant, D. A.; Boekema, E. J.; Holzwarth, A. R. *FEBS Lett.* **2007**, *581*, 5435.

(11) Psencik, J.; Torkkeli, M.; Zupcanova, A.; Vacha, F.; Serimaa, R. E.; Tuma, R. *Photosynth. Res.* **2010**, *104*, 211.

(12) Oostergetel, G. T.; van Amerongen, H.; Boekema, E. J. *Photosynth. Res.* **2010**, *104*, 245.

(13) Holzwarth, A. R.; Schaffner, K. *Photosynth. Res.* **1994**, *41*, 225.

(14) Nozawa, T.; Ohtomo, K.; Suzuki, M.; Nakagawa, H.; Shikama, Y.; Konami, H.; Wang, Z. Y. *Photosynth. Res.* **1994**, *41*, 211.

(15) Egawa, A.; Fujiwara, T.; Mizoguchi, T.; Kakitani, Y.; Koyama, Y.; Akutsu, H. *Proc. Natl. Acad. Sci. U.S.A.* **2007**, *104*, 790.

(16) Ganapathy, S.; Oostergetel, G. T.; Wawrzyniak, P. K.; Reus, M.; Gomez Maqueo Chew, A.; Buda, F.; Boekema, E. J.; Bryant, D. A.; Holzwarth, A. R.; de Groot, H. J. *Proc. Natl. Acad. Sci. U.S.A.* **2009**, *106*, 8525.

(17) Jochum, T.; Reddy, C. M.; Eichhofer, A.; Buth, G.; Szmytkowski, J.; Kalt, H.; Moss, D.; Balaban, T. S. *Proc. Natl. Acad. Sci. U.S.A.* **2008**, *105*, 12736.

(18) Savikhin, S.; Zhu, Y. W.; Blankenship, R. E.; Struve, W. S. *J. Phys. Chem.* **1996**, *100*, 17978.

(19) Psencik, J.; Ma, Y. Z.; Arellano, J. B.; Hala, J.; Gillbro, T. *Biophys. J.* **2003**, *84*, 1161.

(20) Martiskainen, J.; Linnanto, J.; Kananavicius, R.; Lehtovuori, V.; Korppi-Tommola, J. *Chem. Phys. Lett.* **2009**, *477*, 216.

(21) Causgrove, T. P.; Brune, D. C.; Blankenship, R. E. *J. Photochem. Photobiol., B* **1992**, *15*, 171.

(22) Savikhin, S.; Zhu, Y. W.; Lin, S.; Blankenship, R. E.; Struve, W. S. *J. Phys. Chem.* **1994**, *98*, 10322.

(23) Savikhin, S.; Vannoort, P. I; Blankenship, R. E.; Struve, W. S. *Biophys. J.* **1995**, *69*, 1100.

(24) Savikhin, S.; Vannoort, P. I; Zhu, Y. W.; Lin, S.; Blankenship, R. E.; Struve, W. S. *Chem. Phys.* **1995**, *194*, 245.

(25) Ma, Y. Z.; Aschenbrucker, J.; Miller, M.; Gillbro, T. *Chem. Phys. Lett.* **1999**, *300*, 465.

(26) Prokhorenko, V. I.; Steensgaard, D. B.; Holzwarth, A. R. *Biophys. J.* **2000**, *79*, 2105.

(27) Jonas, D. M. *Annu. Rev. Phys. Chem.* **2003**, *54*, 425.

(28) Engel, G. S.; Calhoun, T. R.; Read, E. L.; Ahn, T. K.; Mancal, T.; Cheng, Y. C.; Blankenship, R. E.; Fleming, G. R. *Nature* **2007**, *446*, 782.

(29) Collini, E.; Wong, C. Y.; Wilk, K. E.; Curmi, P. M.; Brumer, P.; Scholes, G. D. *Nature* **2010**, *463*, 644.

(30) Mancal, T.; Nemeth, A.; Milota, F.; Lukes, V.; Kauffmann, H. F.; Sperling, J. *J. Chem. Phys.* **2010**, *132*, 184515.

(31) Nemeth, A.; Milota, F.; Mancal, T.; Lukes, V.; Hauer, J.; Kauffmann, H. F.; Sperling, J. *J. Chem. Phys.* **2010**, *132*, 184514.

(32) Nemeth, A.; Milota, F.; Mancal, T.; Lukes, V.; Kauffmann, H. F.; Sperling, J. *Chem. Phys. Lett.* **2008**, *459*, 94.

(33) Sumi, H. *J. Phys. Chem. B* **1999**, *103*, 252.

(34) Scholes, G. D.; Fleming, G. R. *J. Phys. Chem. B* **2000**, *104*, 1854.

(35) Zigmantas, D.; Read, E. L.; Mancal, T.; Brixner, T.; Gardiner, A. T.; Cogdell, R. J.; Fleming, G. R. *Proc. Natl. Acad. Sci. U.S.A.* **2006**, *103*, 12672.

(36) Fetisova, Z. G.; Mauring, K.; Taisova, A. S. *Photosynth. Res.* **1994**, *41*, 205.

(37) Psencik, J.; Polivka, T.; Nemec, P.; Dian, J.; Kudrna, J.; Maly, P.; Hala, J. *J. Phys. Chem. A* **1998**, *102*, 4392.

(38) Saga, Y.; Wazawa, T.; Mizoguchi, T.; Ishii, Y.; Yanagida, T.; Tamiaki, H. *Photochem. Photobiol.* **2002**, *75*, 433.

(39) Furumaki, S.; Vacha, F.; Habuchi, S.; Tsukatani, Y.; Bryant, D. A.; Vacha, M. *J. Am. Chem. Soc.* **2011**, *133*, 6703.

(40) Saga, Y.; Shibata, Y.; Tamiaki, H. *J. Photochem. Photobiol., C* **2010**, *11*, 15.

(41) Tian, Y.; Camacho, R.; Thomsson, D.; Reus, M.; Holzwarth, A. R.; Scheblykin, I. G. *J. Am. Chem. Soc.* **2011**, *133*, 17192.

(42) Mukamel, S. *Principles of Nonlinear Optical Spectroscopy*; Oxford University Press: New York, 1995.

(43) Cho, M. H.; Yu, J. Y.; Joo, T. H.; Nagasawa, Y.; Passino, S. A.; Fleming, G. R. *J. Phys. Chem.* **1996**, *100*, 11944.

(44) Brune, D. C.; Blankenship, R. E.; Seely, G. R. *Photochem. Photobiol.* **1988**, *47*, 759.

(45) Frese, R.; Oberheide, U.; van Stokkum, I.; van Grondelle, R.; Foidl, M.; Oelze, J.; van Amerongen, H. *Photosynth. Res.* **1997**, *54*, 115.

(46) Steensgaard, D. B.; Matsuura, K.; Cox, R. P.; Miller, M. *Photochem. Photobiol.* **1997**, *65*, 129.

(47) Augulis, R.; Zigmantas, D. *Opt. Express* **2011**, *19*, 13126.

■ NOTE ADDED AFTER ASAP PUBLICATION

Table 1 contained an error in the version published ASAP July 2, 2012. The heading in column 3 was corrected and this paper reposted on July 5, 2012.

Two-dimensional electronic spectroscopy reveals ultrafast energy diffusion in chlorosomes

Jakub Dostál,[1,2] Tomáš Mančal,[2] Ramūnas Augulis,[1] František Vácha,[3] Jakub Pšenčík,[2] and Donatas Zigmantas[1]

[1]*Department of Chemical Physics, Lund University, Getingevägen 60, 221 00 Lund, Sweden*
[2]*Faculty of Mathematics and Physics, Charles University in Prague, Ke Karlovu 3, 121 16 Prague, Czech Republic*
[3]*Faculty of Science, University of South Bohemia, Branišovská 31, 370 05 České Budějovice, Czech Republic*

2D spectra of chlorosomes from Chloroflexus aurantiacus

The time evolution of the 2D spectrum of chlorosomes from *Chloroflexus (Cfl.) aurantiacus* is shown in Fig. S1. It can be clearly seen that the general features of the initial 2D spectrum dynamics are very similar to the ones observed in the 2D spectra sequence of *Cba. tepidum* (Fig. 2). Initially elongated along diagonal 2D spectrum becomes more round on sub-100 fs time scale. This process is accompanied by the significant maximum intensity drop (Fig. S2). The Q_y band absorption spectrum of *Cfl. aurantiacus* chlorosomes (FWHM of 644 cm^{-1}) is narrower than absorption band of *Cba. tepidum*. Correspondingly, the 2D spectrum diagonal width of *Cfl. aurantiacus* is smaller than of *Cba. tepidum* (Fi. S2). This can be explained by the more regular short-range arrangement of BChls within the *Cfl. aurantiacus* chlorosome, which results in less disorder within the aggregate. More ordered short-range organization is due to the presence of only one main BChl *c* homologue in the *Chloroflexaceae* chlorosomes [1].

Materials and methods. Cells of *Cfl. aurantiacus* were cultured anaerobically as described in [2], but at lower light intensity (~10 – 15 μE/m^{2}s incident on the surface of 14 L fermenter with a ~30 cm diameter). Culture was grown for 11 days at 50°C and the chlorosomes were prepared by a method of [3] with minor modifications. 2D spectroscopy experiments were carried under aerobic

SUPPORTING INFORMATION

conditions. Otherwise all experimental details are the same as in the case of *Cba. tepidum* measurements.
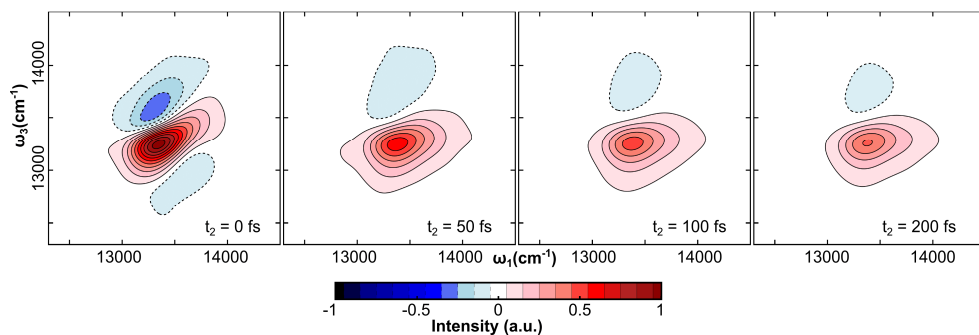
Fig. S1: 2D spectra (real part of the electric field) of chlorosomes from Cfl. aurantiacus at different population times.
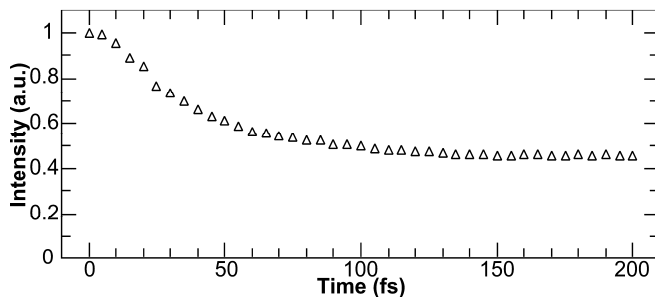
Fig. S2: Amplitude decay at the point of maximal signal at $t_2 = 0$ fs in the 2D spectrum of chlorosomes from Cfl. aurantiacus.

1. Blankenship RE, Olson JM, Miller M (1995) Antenna Complexes from Green Photosynthetic Bacteria. In Blankenship R, Madigan M, Bauer C (eds.), *Anoxygenic Photosynthetic Bacteria* pp 399–435. Springer Netherlands.

2. Pšenčík J, Collins AM, Liljeroos L, Torkkeli M, Laurinmäki P, Ansink HM, Ikonen TP, Serimaa RE, Blankenship RE, Tuma R, et al. (2009) Structure of chlorosomes from the green filamentous bacterium Chloroflexus aurantiacus. *J Bacteriol* **191**: 6701–6708.

3. Feick RG, Fitzpatrick M, Fuller RC (1982) Isolation and characterization of cytoplasmic membranes and chlorosomes from the green bacterium Chloroflexus aurantiacus. *J Bacteriol* **150**: 905–915.

PAPER II

Unraveling the nature of coherent beatings in chlorosomes

Jakub Dostál,[1,2] Tomáš Mančal,[2] František Vácha,[3] Jakub Pšenčík,[2]
and Donatas Zigmantas[1,a)]

[1]*Department of Chemical Physics, Lund University, P.O. Box 124, SE-22100 Lund, Sweden*
[2]*Faculty of Mathematics and Physics, Charles University in Prague, Ke Karlovu 3, 121 16 Prague,
Czech Republic*
[3]*Faculty of Science, University of South Bohemia, Branišovská 31, 370 05 České Budějovice, Czech Republic*

Coherent two-dimensional (2D) spectroscopy at 80 K was used to study chlorosomes isolated from green sulfur bacterium *Chlorobaculum tepidum*. Two distinct processes in the evolution of the 2D spectrum are observed. The first being exciton diffusion, seen in the change of the spectral shape occurring on a 100-fs timescale, and the second being vibrational coherences, realized through coherent beatings with frequencies of 91 and 145 cm^{-1} that are dephased during the first 1.2 ps. The distribution of the oscillation amplitude in the 2D spectra is independent of the evolution of the 2D spectral shape. This implies that the diffusion energy transfer process does not transfer coherences within the chlorosome. Remarkably, the oscillatory pattern observed in the negative regions of the 2D spectrum (dominated by the excited state absorption) is a mirror image of the oscillations found in the positive part (originating from the stimulated emission and ground state bleach). This observation is surprising since it is expected that coherences in the electronic ground and excited states are generated with the same probability and the latter dephase faster in the presence of fast diffusion. Moreover, the relative amplitude of coherent beatings is rather high compared to non-oscillatory signal despite the reported low values of the Huang-Rhys factors. The origin of these effects is discussed in terms of the vibronic and Herzberg-Teller couplings. © *2014 AIP Publishing LLC*. [http://dx.doi.org/10.1063/1.4868557]

I. INTRODUCTION

In order to efficiently collect incoming sunlight, photosynthetic organisms have developed various types of light-harvesting antennas. These are usually sophisticated pigment-protein complexes, where the properties of the pigment molecules are finely tuned by the encapsulating protein structure. Notable exception to this architecture is represented by chlorosomes—light-harvesting antennas adopted by the species belonging to three phyla of photosynthetic bacteria. While the number of pigments in other photosynthetic antennas usually does not exceed several hundred, the interior of a single chlorosome is composed of a much larger number ($\sim 10^5$) of strongly coupled bacteriochlorophyll (BChl) *c*, *d*, or *e* molecules (depending on species) without any direct interaction with proteins.[1–4] Steady-state and transient absorption spectra of chlorosomes bear a close resemblance to the corresponding spectra of *in vitro* self-assembled BChl aggregates,[5] which proves the dominating contribution of the aggregates to the optical properties of chlorosomes. In addition to BChl molecules as a major constituent, chlorosomes contain a smaller amount of quinone, carotenoid, lipid, and protein molecules. Attached to the chlorosome side, facing cytoplasmic membrane, is the baseplate—a pigment-protein complex containing hundreds of BChl *a* molecules acting as mediators of excitation energy transfer from the chlorosomal body towards the reaction centers.[1,3,4]

Energy transfer within chlorosomes has been studied using femtosecond spectroscopy techniques by several groups, and many different decay components have been identified on the 100 fs to 100 ps time scale depending on the species, growth, and experimental conditions (for review see Refs. 3, 4, and 6). These decays were often observed without a corresponding rise in the spectral region of the excitation acceptor, making it difficult to reliably assign them to energy transfer steps within the chlorosome. One exception is the energy transfer from BChl aggregates to the baseplate, which in *Chlorobi* species containing BChl *c*, such as *Chlorobaculum* (*Cba.*) *tepidum* studied in this work, occurs with the main time constant of 30–40 ps.[4] The second exception is the energy transfer from the blue part of the Q$_y$ absorption band of BChl aggregates to their redshifted states, which was observed in chlorosomes from different species with transfer times between 100 and 1000 fs.[7–10] This process corresponds to exciton relaxation from higher to lower exciton levels. Particularly for *Cba. tepidum* chlorosomes, it is rather fast (100–250 fs),[9] which is perhaps due to their better ordered BChl *c* aggregates as compared to other bacteria species. In addition, our previous two-dimensional (2D) spectroscopy study resolved even a faster, sub-100-fs process, attributed to the exciton diffusion in the highly disordered interior of the chlorosomes.[11] It was proposed that due to a strong disorder in the BChl arrangement the chlorosomal aggregate is effectively broken into smaller parts (coherent domains) that in the first approximation can be viewed as independent systems weakly coupled to each other. The observed ultrafast process corresponds

a)Author to whom correspondence should be addressed. Electronic mail:
donatas.zigmantas@chemphys.lu.se

to the energetically downhill-biased diffusion between such neighboring domains.

A typical feature observed in ultrafast experiments is the presence of the short-lived oscillations.[5,12–15] In the case of *Cba. tepidum* two major frequencies of 70–90 cm^{-1} and 130–160 cm^{-1} are usually resolved,[12,15] which approximately coincide with the group of low-frequency modes observed in the resonance Raman scattering data on chlorosomes[16] or artificial thin-solid-film BChl *c* aggregates.[17] The observed oscillations in transient spectra were thus assigned to the coherent beatings between vibrational levels of these modes.[5,12–15] Cherepy *et al.*[16] speculated that these coherences are mostly of excited state origin, however, Ma *et al.*[14] convincingly showed the presence of ground state vibrational coherences by the means of two-color transient absorption measurements on chlorosomes from *Chlorobium phaeobacteroides*, where the Q_y transition was probed after Soret band excitation.

In addition, the resonance Raman study by Bocian and coworkers[17] identified that the same modes are also present in the BChl-related molecules that are incapable of aggregation, but their intensity was very low. Based on this observation it was concluded that these modes belong to the individual pigments and are coupled to the Q_y electronic transition of the supramolecular assembly, which enhances particular resonance Raman transitions. These modes were assigned to out-of-plane deformations of the chlorin macrocycle.

In this work we have studied coherent oscillations in the chlorosomes from *Cba. tepidum* at 80 K using coherent 2D electronic spectroscopy.[18] This method measures third-order polarization response of the sample and provides simultaneous high spectral and temporal resolution. It is thus especially suitable for studying fast photophysical processes in multichromophoric systems, e.g., in photosynthetic complexes. Moreover, 2D spectroscopy provides detailed insight into the quantum coherence phenomenon as has been demonstrated in many studies (see, e.g., Refs. 19–22). We performed the amplitude and phase analysis of the oscillations in two dimensions, which provided us with comprehensive information on coherent beatings and their origin.

II. MATERIALS AND METHODS

Cba. tepidum cells were grown as described previously[23] and the chlorosomes were isolated following the standard method consisting of two successive sucrose gradient ultracentrifugation steps.[24] Before the measurement, the chlorosomes were dissolved in the 2:1 (v/v) mixture of glycerol and 50 mM Tris-HCl buffer (pH 8.0) to achieve absorbance of about 0.35 at 745 nm in a 0.5 mm optical cuvette. We have shown that observed quantum coherences were not dependent on the redox conditions of the sample[25] and therefore in the presented experiments samples were used without addition of any agent controlling the electrochemical potential. All experiments were carried out in a nitrogen continuous flow cryostat (STVP-400, Janis Research Company) kept at a constant temperature of 80 K. Excitation intensity of each laser pulse was set to 100 pJ (photon density of $\sim$4.8 × 10^{12} photons/pulse cm^2).

The detailed description of the experimental setup used to obtain 2D spectra can be found in Refs. 26 and 27. Briefly, the 15 fs long laser pulses centered at 750 nm with FWHM of $\sim$90 nm were generated by the laser system consisting of 200 kHz KGW amplified laser (Pharos, Light Conversion) pumping lab-made non-collinear optical amplifier. The initial beam was split into four parts using a beamsplitter and a transmissive diffraction grating. Pulses were sequenced in time using a conventional optical delay line and inserting fused silica wedges mounted on motorized translation stages. The beams were focused and overlapped in a box-car geometry onto a single spot of the sample. The four-wave mixing signal resulting from the sample interaction with three pumping pulses was emitted into the phase-matching direction. The signal was mixed with the fourth beam (local oscillator), attenuated by an OD 3 filter, and interferometrically detected after transmission through a spectrograph on a CCD camera. Two excitation pulses were modulated at different frequencies by optomechanical choppers. Lock-in detection of the sum and difference chopping frequencies allowed discrimination of the four-wave mixing signal against scattering signals. During the measurements the coherence time (delay between the first two pulses) was scanned in the range from −120 fs to 180 fs with a step of 1 fs, which ensured the resolution of 90 cm^{-1} along the excitation (coherence) frequency axis. The same resolution was achieved along the detection frequency axis, determined by the time domain window used in Fourier analysis.

III. RESULTS AND DISCUSSION

Two distinct processes can be resolved in the time evolution of the real part of the experimental 2D spectrum (Fig. 1(a)). One of them is the exciton diffusion in the highly disordered interior of the chlorosome previously observed in room temperature experiments.[11] This process is manifested by a fast signal amplitude drop during the first 100 fs to approximately half of its initial value (Fig. 2). The decay of the signal is accompanied by the pronounced change of the 2D spectrum shape. Within $\sim$100 fs the diagonally elongated positive part of the 2D spectrum (surrounded at the top and bottom by the negative excited state absorption) extends downwards, completely filling the space under the diagonal. The downhill relaxation part of the diffusion process, which manifests itself as a rounding and shift of the 2D spectrum to the lower detection frequencies, is more distinct at 80 K (Fig. 1) than at room temperature.[11]

Other phenomena, which are well pronounced at low temperature, are coherent beatings damped during the first 1.2 ps (Fig. 2). Note that we have also observed much weaker oscillations in the 2D spectra measured at room temperature.[25] To get a better insight into the properties of the oscillating signals, kinetics at individual points of the 2D spectrum were fitted with three decaying exponentials. Residuals after subtraction of multiexponential fits from the kinetic traces together with their Fourier transform amplitudes are shown in Fig. 3. Remarkably, the oscillatory patterns are very similar throughout the whole 2D spectrum and the variations between different regions are limited mainly to the amplitude
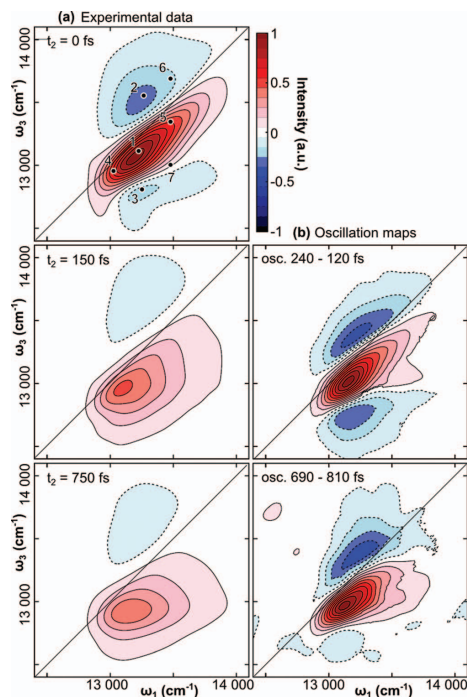
FIG. 1. (a) Time evolution of the 2D spectrum (real part of the electric field). The numbered points indicate the places from where trajectories for further analysis were taken. (b) Time-resolved maps of the distribution of the oscillatory patterns in the 2D spectra, all normalized to their maxima. These maps are obtained by calculating the difference of the oscillatory component from two 2D spectra at indicated population times.

and sign. This similarity allows simple construction of the time-resolved maps demonstrating distribution of the oscillations in the 2D spectra. This is achieved by plotting the signal difference between two consecutive extremes of a large am-
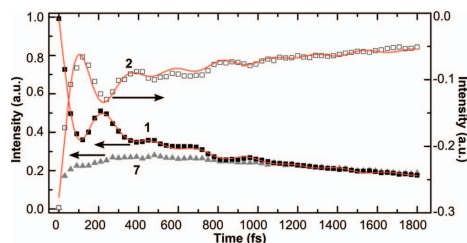

FIG. 2. Time evolution at the selected points in the 2D spectrum. Solid squares correspond to the point in the $t_2 = 0$ fs 2D spectrum with initial signal maximum; open squares—initial signal minimum; gray triangles—initial signal lower nodal line (for the assignment of the numbers to different points in the 2D spectrum see Fig. 1). Lines are the best simultaneous fits by the Eq. (1). Note that the weaker and negative trace 2 has a separate ordinate axis on the right side of the graph.
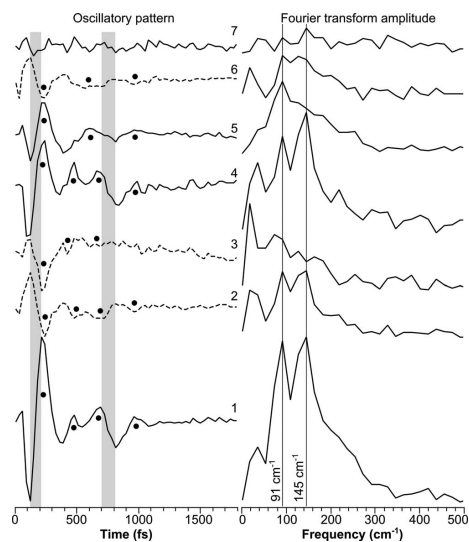

FIG. 3. Oscillatory pattern after subtraction of the three-exponential fit at different points of the 2D spectrum, corresponding to GSB/SE (solid line) or ESA (dotted line) and their Fourier transform amplitude. Numbers assigned to trajectories are introduced in Fig. 1. The black dots mark the main oscillatory features and aid visual reading of the picture. The meaning of the grey regions is explained in the text.

plitude change observed in all oscillatory patterns at the same population times (see gray regions in Fig. 3). Resulting oscillation distribution maps (Fig. 1(b)) resemble very closely the shape of the 2D spectrum at $t_2 = 0$ fs (correlation spectrum). The relative phase of the oscillations follows the sign of the correlation spectrum, i.e., the oscillations appearing in the 2D spectral regions, where the signal is positive, have the opposite phase to the oscillations appearing in the 2D spectral regions, where the sign is negative. Even though the shape of the 2D spectrum changes substantially during the first 100 fs, the oscillation maps do not follow this change. The oscillating signal evolution in the rephasing and non-rephasing parts is very similar to that of the total signal as described above and is given in the supplemental material.[25]

Fourier transform analysis of individual oscillatory traces (Fig. 3) reveals the presence of two main frequencies at ~91 cm^{-1} and ~145 cm^{-1}. Coherent beatings with similar frequencies were observed in the previous investigations of chlorosomes.[12, 15] The relative amplitudes of the two modes are very similar, but not completely uniform. The lower-frequency mode tends to dominate in the higher excitation energy side of the spectrum (trajectory 5), whereas the higher-frequency mode prevails in the lower-energy side (trajectory 4). This causes small excitation-frequency-dependent variations in the otherwise very similar oscillatory dynamics. Fourier transformation of the sequences of the 2D spectra residuals in t_2 results in the oscillation maps (Fig. 4). Again, the Fourier amplitude maps of the two dominant frequencies
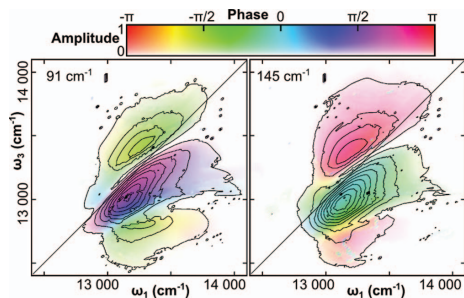
FIG. 4. Amplitude and phase distribution of the individual modes in the 2D spectra obtained from the Fourier transform of the oscillatory part of the data. Contours and the color saturation mark the amplitude, the color hue codes the phase.

at 91 cm^{-1} and 145 cm^{-1} are similar to the elongated shape of the 2D spectrum at $t_2 = 0$ fs. The phase of each mode flips by π between positive and negative regions of the 2D spectrum. Interestingly, these modes do not oscillate in phase, but their relative phases are shifted by approximately $\pi/2$.

A. Origin of the coherent beatings

Since the frequencies of the observed coherent oscillations in the 2D spectra coincide well with the group of lines observed in the resonance Raman experiments (within the resolution of 18 cm^{-1}, given by the t_2 scan),[16, 17] the oscillations can be attributed to the coherent vibrational wavepacket motion. For the possible assignment of the modes we follow the detailed work of Czarnecki *et al.*[28] on the reaction centers from purple bacteria containing BChl *a*. Some Raman spectral features in the reaction centers are similar to the features observed in the BChl *c* aggregates.[17] Particularly, the group of modes around 137 cm^{-1} is amplified in the resonance Raman spectrum of a strongly coupled special pair, as compared to the identical modes of weakly coupled accessory BChl *a* pigments. Based on *ab initio* calculation and the isotope labeling, these modes were assigned to the macrocycle doming mode, out-of-plane deformations of the pyrrole rings and in-plane deformation of the acetyl group at C3 (according to the IUPAC nomenclature); all effective at modulating the electronic structure of the dimer. Due to the structural similarity between BChl *c* and *a* molecule the qualitatively similar modes could be responsible for the 145 cm^{-1} mode observed in chlorosomes. Obviously, vibration of the acetyl group at C3 does not contribute because this group is replaced by the 1-hydroxyethyl group in BChl *c*. The modes with frequencies similar to 90 cm^{-1} were also observed in the reaction centers, but their intensity was weak. These modes were assigned to the out-of-plane deformations of peripheral groups, most notably the methyl group at C3^1 and keto oxygen at C13^1. Both groups (the former being part of the hydroxyethyl group at C3 in the BChl *c* molecule) are essential for formation of the BChl *c* aggregates.[29] It is reasonable to assume that their vibrations affect the interaction strength between excitonically coupled BChl *c* pigments, thus making them sensitive to the electronic state changes and therefore being enhanced in the resonance Raman scattering.

Vibrational coherence oscillations in the 2D spectra occur due to the three types of contributions to the transient signal: ground state bleaching (GSB), stimulated emission (SE), and excited state absorption (ESA). Oscillations with different phase can appear in all parts of the spectrum when vibrational quantum energy is comparable to the extent of the 2D spectrum.[30, 31] Note that in the case of chlorosomes, vibrational quanta of the modes (~91 cm^{-1} and ~145 cm^{-1}) are much smaller than the ω_3 difference between the positive and negative parts in the 2D spectra (points 1 and 2 in Fig. 1), which is approximately 500 cm^{-1}. This leads to the conclusion that the beatings in the regions where the oscillation phase is opposite to the phase at the maximum of the positive signal should originate from ESA. This is also supported by almost identical shapes of the negative regions in the correlation 2D spectrum and oscillation distribution maps. It implies that the part of the oscillations that are simultaneously observed in the positive region as oscillatory SE and in the negative region as oscillatory ESA come from the vibrational wavepacket dynamics in the excited electronic states. On the other hand, vibrational coherences in the ground state (previously documented in Ref. 14) manifested as oscillatory GSB should be located in the region of positive signal.

The ratio between the excited and ground state contributions to the oscillatory signals is not completely clear. The basic theoretical considerations of an electronic system with vibrational progression predict an equal intensity of coherences from the ground and excited states due to the (anti)symmetry of Franck-Condon factors. Excited and ground state contributions should in principle differ in their dephasing times in the presence of the fast energy relaxation to the ground state (possibly connected with the Förster energy transfer to a neighboring molecule), during which the excited state coherence disappears completely, while the one in the ground state may dephase only partially.[32] From Fig. 2 it is apparent that the oscillatory ESA is almost a perfect mirror image of the oscillations obtained from the central part of the positive signal. One of two possible implications is that the fast diffusion process is either capable of dephasing the ground and excited state coherences on the same timescale, making both types indistinguishable even on the basis of their dynamic properties. The other implication could be that the excited state coherences are much stronger making the ground state coherences observable only in the specially designed experiments, such as two-color transient absorption measured with relatively long laser pulses.[14]

Another notable observation is that the amplitude of coherences is relatively high compared to the intensity of the exponentially decaying non-oscillatory part of the signal. This could indicate a rather high value of the Huang-Rhys (HR) factors. However, the values of the HR factor of the low frequency modes in the chlorosomes from *Chloroflexus aurantiacus* have been estimated to lie in the range of 10^{-2} by simultaneous fitting of the linear absorption and the resonance Raman spectra.[16] The absolute intensities of the resonance Raman lines of the chlorosomes from *Cba. tepidum*

reported in the same work are lower, indicating even lower values of the HR factors. Moreover, only the modes around 50–170 cm^{-1} are observed as coherent beatings in the femtosecond experiments, whereas the other modes of comparable and even higher intensities in the resonance Raman experiments are not observed in time-resolved studies.[12, 14, 15] In contrast to the chlorosome data reported by Cherepy *et al.*,[15] the resonance Raman spectra of the BChl *c* thin-solid-film aggregates[17] are dominated by two distinctive peaks at frequencies of ∼115 cm^{-1} and ∼145 cm^{-1}. These modes represent a close match to the Fourier transforms frequencies of the oscillatory components observed in the ultrafast experiments. This correspondence suggests that the HR factor of these modes in chlorosomes could be rather high. The discrepancy between the resonance Raman spectra of chlorosomes and BChl *c* aggregates is quite striking, since many other spectroscopic properties (including coherent beatings) are almost identical for these two systems.[5] In addition, the correspondence between enhanced low-frequency resonance Raman modes and strong coherent beatings with the same frequencies have been previously reported for porphyrin J-aggregates.[33] From all the mentioned cases it can be implied that the enhancement of the low frequency modes is quite a general phenomenon in large aggregates of porphyrin based molecules.

To explain why only certain low-frequency modes are enhanced in the chlorosome experiments we provide a couple of interpretations. One possible explanation could be the enhancement of the vibrational coherences by the intensity borrowing from the resonant electronic transition. Such enhancement mechanisms have been recently explored in idealized dimer systems,[34–36] and we can speculate that in the case of more complicated systems such as chlorosomes the induced effects can grow in complexity, possibly causing the contribution of the excited state coherences to enhance disproportionally. The advantage of this interpretation is that the mechanism does not require a big HR factor. The necessary resonant electronic transition can be readily present in the single exciton manifold due to the complex coupling between the molecules in the three-dimensional aggregate. On the other hand, a strong and disproportional enhancement of only the excited state part of the oscillations cannot be inferred from the current theoretical models.

Another option would be to consider theoretical models which go beyond the Franck-Condon approximation. The Herzberg-Teller coupling of the nuclear vibrations to the electronic transition has been previously used by Kano *et al.*[33] to explain very similar observations of coherences in porphyrin J-aggregates. Here we show that strong coupling of the Herzberg-Teller (HT) active low-frequency mode leads to an increase of their HR factor. The effect is demonstrated in an excitonically coupled homodimer of molecules with the Huang-Rhys factors equal to zero. Let us assume that the strength of the transition dipole moments μ of the molecules weakly depends on the vibrational coordinate q of some particular mode (Herzberg-Teller effect):[37, 38]

$$\mu = \mu_0 \left(1 + \xi \frac{q}{q_0} \right), \tag{1}$$

where the small dimensionless parameter ξ characterizes the strength of the HT effect, μ_0 is the transition dipole moment in the Condon approximation, and q_0 provides the unit of vibrational coordinate. Standard representation of q_0 is given by

$$q_0 = \sqrt{\frac{2\hbar}{m\omega}}, \tag{2}$$

where m stands for the effective mass of the oscillator with the angular frequency ω. Due to the dipole moment dependence on the vibrational coordinate, coupling between molecules J becomes dependent on the vibrational coordinate as well. For simplicity assume dipole-dipole coupling

$$J = \mu(q_1)\mu(q_2)\frac{\kappa}{r^3} = \mu_0^2 \frac{\kappa}{r^3} \left(1 + \frac{\xi}{q_0}(q_1 + q_2) + \frac{\xi^2}{q_0^2} q_1 q_2 \right)$$

$$= J_0 \left(1 + \frac{\sqrt{2}\xi}{q_0} q_+ + \frac{\xi^2}{2q_0^2} \left(q_+^2 - q_-^2 \right) \right), \tag{3}$$

where the subscripts 1 and 2 index individual molecules, κ stands for the orientational factor, r - for the distance between the molecules, and J_0 - for the the dipole-dipole coupling in the Condon approximation. In the last equality we used the basis transformation $q_\pm = 2^{-1/2}(q_1 \pm q_2)$ into the collective symmetric (+) and antisymmetric (−) vibrational coordinates that represent the synchronized in-phase and off-phase vibrations of both molecules, respectively.

The exciton coupling between the molecules leads to the splitting of the single exciton levels $E_\pm = E_0 \pm J(q_+, q_-)$.[39] Evolution of the symmetric mode on the $E_\pm$ potential energetic surface is thus governed by the Hamiltonian (neglecting all small terms quadratic in ξ):

$$H_{vib} = \frac{p_+^2}{2m} + \hbar\omega \frac{q_+^2}{q_0^2} \pm J_0 \frac{\sqrt{2}\xi}{q_0} q_+$$

$$\approx \frac{p_+^2}{2m} + \hbar\omega \left(\frac{q_+}{q_0} \pm \frac{\xi J_0}{\sqrt{2}\hbar\omega} \right)^2, \tag{4}$$

which corresponds to the Hamiltonian of the harmonic oscillator displaced by the HR factor

$$S = \frac{1}{2} \left(\frac{\xi J_0}{\hbar\omega} \right)^2. \tag{5}$$

Thus, although we assumed that the HR factor of each molecule is equal to zero, the collective delocalized symmetric oscillation in the dimer gains the non-zero HR factor by the HT coupling. Consequently, vibrational coherences of the HT mode in electronic ground and excited sates of the dimer can be excited. From Eq. (5) follows that the HR factor enhancement effect is strong only for the low-frequency modes of strongly coupled molecules that have some HT activity. These requirements are well in line with what has been observed in chlorosomes.

The derivation is valid for the large aggregate (like chlorosome) as well with an exception that the energy level splitting approaches $4J$ instead of $2J$ and all the formulas would have to be modified accordingly. If we plug the typical values for chlorosome ($2J_0 \approx 1200$ cm^{-1}, $\hbar\omega \approx 100$ cm^{-1}) in

(5), we obtain reasonably high value for the HR factor of 0.18 even for the small HT coupling parameter $\xi = 0.05$.

The proposed HT mechanism explains the selective enhancement of the low-frequency modes in chlorosomes and in other big aggregates.[33] However, it does not provide a mechanism that could either dephase both the excited and ground state coherences on the same timescale or substantially diminish the ground state coherence.

B. Dephasing of the coherences by the diffusion process

The common description of the transfer process between weakly coupled domains, formulated in terms of (multi-chromophoric) Förster rates, assumes an exponential damping of the donor signal, while the ESA, SE, and GSB of the acceptor exponentially rise. In principle, excited state vibrational coherences could be transferred between the electronic states in the chlorosomes because vibrational oscillation periods (220–370 fs) are longer than the typical transfer time observed in the diffusion processes ($\sim$100 fs).[11] However, the observation that the oscillation amplitude map copies the initial shape of the 2D spectrum implies that the random energy diffusion process is not capable of transferring coherences between different coherent domains. In our previous work[32] we used the theory developed in Ref. 40 to show that a single step of energy transfer leads (for the oscillation frequency 150 cm^{-1} and depopulation rate 1/100 fs^{-1}) to a 70% loss of the amplitude of the oscillations. Since during the diffusion-like energy transfer in chlorosomes such a transfer step is rapidly followed by further steps, it leads us to a conclusion that the transfer of the coherent nuclear oscillations between excited states of the molecules should not be observable.

We conclude that the initially excited domains can be the only source of the oscillatory signals in the 2D spectra of the chlorosomes. The vibrational coherences in the domains are quickly attenuated with the diffusion time of $\tau_1 \sim 100$ fs. We denote the probability that the vibrational coherence is created in the domain that quickly diffuse energy by p. A small fraction of domains $(1 - p)$ that do not undergo diffusion keep beating, and they are dephased on a slower time scale. The value for the slower dephasing time $\tau_2 = 1$ ps was estimated from the fitting procedure described below and it is in agreement with the time component observed previously in several studies.[5, 12, 13, 15, 41] The origin of this component is widely discussed and is generally attributed to the slower energy transfer processes in chlorosomes. Two characteristic oscillating traces, corresponding to the maximum positive and maximum negative 2D signals (and having the highest oscillation amplitudes) that are presented in Fig. 2, were simultaneously fitted with the model that describes the main observed features:

$$I(t) = \left[p e^{\frac{-t}{\tau_1}} + (1 - p)e^{\frac{-t}{\tau_2}} \right] \left[A_1 \cos\left(\omega_1 t + \frac{\pi}{2}\right) \right.$$
$$\left. + A_2 \cos(\omega_2 t) \right] + B_1 e^{\frac{-t}{\tau_1}} + B_2 e^{\frac{-t}{\tau_2}} + C. \quad (6)$$

The two main oscillating modes have frequencies $\omega_{1,2}$ (92 cm^{-1} and 142 cm^{-1}) and their phases are shifted by $\pi/2$

TABLE I. Set of parameters of model (1) that best simultaneously fit the evolution of the 2D spectrum maximum and minimum (traces 1 and 2).

τ_1 (fs)	τ_2 (fs)	ω_1 (cm^{-1})	ω_2 (cm^{-1})	p
101	1031	92	142	0.93

from each other. Both oscillations are dephased by a pair of independent processes with time constants $\tau_{1,2}$. The same time constants describe the two-exponential decay of the signal intensity, consistently binding together diffusion and dephasing processes. The corresponding fitted curves are plotted in Fig. 2. The fitting parameters are summarized in Table I showing that the fraction $(1 - p)$ of the domains that do not dephase during the 100-fs diffusion is of the order of a few percent.

IV. CONCLUSIONS

We report a low temperature coherent 2D spectroscopy study of the chlorosomes from bacterium *Cba. tepidum*. The observations are consistent with the theoretical model previously presented in Ref. 11, describing the chlorosomes as light harvesters composed of weakly coupled domains mutually exchanging the energy by a random ultrafast diffusion process. In addition to this distinctive process manifested by the pronounced evolution of the 2D spectrum shape, the quantum beatings caused by the coherent vibrational wavepacket motion is resolved at 80 K. Remarkably, some of the beatings are able to significantly outlive the diffusion process, being observable as long as 1.2 ps. However, distribution of the oscillation amplitudes during their entire lifetime persistently copies the initial shape of the 2D spectrum, which identifies their origin in a fraction of domains unaffected by the diffusion. This also demonstrates that the diffusion process is not capable of transferring vibrational coherences between domains. In addition we discuss interpretation of the high relative amplitude of the coherent beatings and the uniformity of the dephasing rates across the whole 2D spectrum.

[1]N.-U. Frigaard and D. A. Bryant, in *Complex Intracellular Structures in Prokaryotes*, edited by J. Shively (Springer, Berlin, 2006), pp. 79–114.
[2]D. A. Bryant, A. M. G. Costas, J. A. Maresca, A. G. M. Chew, C. G. Klatt, M. M. Bateson, L. J. Tallon, J. Hostetler, W. C. Nelson, J. F. Heidelberg, and D. M. Ward, Science **317**, 523 (2007).
[3]R. E. Blankenship and K. Matsuura, in *Light-Harvesting Antennas in Photosynthesis*, edited by B. R. Green and W. W. Parson (Kluwer Academic Publishers, Dordrecht, 2003), pp. 195–217.
[4]R. E. Blankenship, J. M. Olson, and M. Miller, in *Anoxygenic Photosynthetic Bacteria*, edited by R. Blankenship, M. Madigan, and C. Bauer (Springer Netherlands, 1995), pp. 399–435.
[5]S. Savikhin, P. I. van Noort, R. E. Blankenship, and W. S. Struve, Biophys. J. **69**, 1100 (1995).

[6] G. T. Oostergetel, H. van Amerongen, and E. J. Boekema, Photosynth. Res. **104**, 245 (2010).

[7] S. Savikhin, Y. Zhu, R. E. Blankenship, and W. S. Struve, J. Phys. Chem. **100**, 17978 (1996).

[8] J. Martiskainen, J. Linnanto, R. Kananavičius, V. Lehtovuori, and J. Korppi-Tommola, Chem. Phys. Lett. **477**, 216 (2009).

[9] J. Martiskainen, J. Linnanto, V. Aumanen, P. Myllyperkiö, and J. Korppi-Tommola, Photochem. Photobiol. **88**, 675 (2012).

[10] J. Pšenčík, Y.-Z. Ma, J. B. Arellano, J. Hála, and T. Gillbro, Biophys. J. **84**, 1161 (2003).

[11] J. Dostál, T. Mančal, R. Augulis, F. Vácha, J. Pšenčík, and D. Zigmantas, J. Am. Chem. Soc. **134**, 11611 (2012).

[12] S. Savikhin, P. I. van Noort, Y. Zhu, S. Lin, R. E. Blankenship, and W. S. Struve, Chem. Phys. **194**, 245 (1995).

[13] S. Savikhin, Y. Zhu, S. Lin, R. E. Blankenship, and W. S. Struve, J. Phys. Chem. **98**, 10322 (1994).

[14] Y.-Z. Ma, J. Aschenbrücker, M. Miller, and T. Gillbro, Chem. Phys. Lett. **300**, 465 (1999).

[15] V. I. Prokhorenko, D. B. Steensgaard, and A. R. Holzwarth, Biophys. J. **79**, 2105 (2000).

[16] N. J. Cherepy, M. Du, A. R. Holzwarth, and R. A. Mathies, J. Phys. Chem. **100**, 4662 (1996).

[17] J. R. Diers, Y. Zhu, R. E. Blankenship, and D. F. Bocian, J. Phys. Chem. **100**, 8573 (1996).

[18] D. M. Jonas, Annu. Rev. Phys. Chem. **54**, 425 (2003).

[19] G. S. Engel, T. R. Calhoun, E. L. Read, T.-K. Ahn, T. Mančal, Y.-C. Cheng, R. E. Blankenship, and G. R. Fleming, Nature (London) **446**, 782 (2007).

[20] A. Nemeth, F. Milota, T. Mančal, V. Lukeš, H. F. Kauffmann, and J. Sperling, Chem. Phys. Lett. **459**, 94 (2008).

[21] D. B. Turner, K. E. Wilk, P. M. G. Curmi, and G. D. Scholes, J. Phys. Chem. Lett. **2**, 1904 (2011).

[22] S. Westenhoff, D. Paleček, P. Edlund, P. Smith, and D. Zigmantas, J. Am. Chem. Soc. **134**, 16484 (2012).

[23] J. Pšenčík, T. P. Ikonen, P. Laurinmäki, M. C. Merckel, S. J. Butcher, R. E. Serimaa, and R. Tuma, Biophys. J. **87**, 1165 (2004).

[24] D. B. Steensgaard, K. Matsuura, R. P. Cox, and M. Miller, Photochem. Photobiol. **65**, 129 (1997).

[25] See supplementary material at http://dx.doi.org/10.1063/1.4868557 for data measured at room temperature and anaerobic conditions and for oscillation distribution in rephasing and non-rephasing parts of the 2D spectrum.

[26] R. Augulis and D. Zigmantas, Opt. Express **19**, 13126 (2011).

[27] R. Augulis and D. Zigmantas, J. Opt. Soc. Am. B **30**, 1770 (2013).

[28] K. Czarnecki, J. R. Diers, V. Chynwat, J. P. Erikson, H. A. Frank, and D. F. Bocian, J. Am. Chem. Soc. **119**, 415 (1997).

[29] T. S. Balaban, H. Tamiaki, and A. R. Holzwarth, Top. Curr. Chem. **258**, 1 (2005).

[30] T. Mančal, N. Christensson, V. Lukeš, F. Milota, O. Bixner, H. F. Kauffmann, and J. Hauer, J. Phys. Chem. Lett. **3**, 1497 (2012).

[31] V. Butkus, D. Zigmantas, L. Valkunas, and D. Abramavicius, Chem. Phys. Lett. **545**, 40 (2012).

[32] T. Mančal, J. Dostál, J. Pšenčík, and D. Zigmantas, Can. J. Chem. **92**, 135 (2014).

[33] H. Kano, T. Saito, and T. Kobayashi, J. Phys. Chem. A **106**, 3445 (2002).

[34] N. Christensson, H. F. Kauffmann, T. Pullerits, and T. Mančal, J. Phys. Chem. B **116**, 7449 (2012).

[35] A. Chenu, N. Christensson, H. F. Kauffmann, and T. Mančal, Sci. Rep. **3**, 2029 (2013).

[36] V. Tiwari, W. K. Peters, and D. M. Jonas, Proc. Natl. Acad. Sci. U.S.A. **110**, 1203 (2013).

[37] G. Herzberg and E. Teller, Z. Phys. Chem. **21**, 410 (1933).

[38] G. Orlandi and W. Siebrand, J. Chem. Phys. **58**, 4513 (1973).

[39] M. Kasha, H. Rawls, and M. Ashraf El-Bayoumi, Pure Appl. Chem. **11**, 371 (1965).

[40] M. Yang and G. R. Fleming, J. Chem. Phys. **111**, 27 (1999).

[41] J. Pšenčík, T. Polívka, P. Němec, J. Dian, J. Kudrna, P. Malý, and J. Hála, J. Phys. Chem. A **102**, 4392 (1998).

Unraveling the nature of coherent beatings in chlorosomes

Jakub Dostál,[1,2] Tomáš Mančal,[2] František Vácha,[3] Jakub Pšenčík,[2] and Donatas Zigmantas[1]

[1]*Department of Chemical Physics, Lund University, P.O. Box 124, SE-22100 Lund, Sweden*
[2]*Faculty of Mathematics and Physics, Charles University in Prague, Ke Karlovu 3, 121 16 Prague, Czech Republic*
[3]*Faculty of Science, University of South Bohemia, Branišovská 31, 370 05 České Budějovice, Czech Republic*

S I.   COMPARISON BETWEEN THE MEASUREMENTS AT ROOM-TEMPERATURE AND 80 K

The room-temperature sample was prepared and measured as described in [1] with an exception that no sodium dithionite was added.
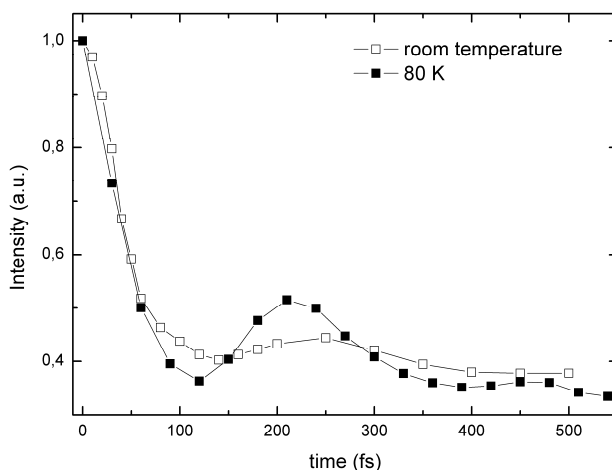

Fig. S1: Time traces of the 2D spectrum maximum at 80 K (solid squares) and at room temperature (open squares) normalized at $t_2 = 0$ fs. While the amplitude of the oscillating signal is very strong at 80 K, it is rather weak at room temperature.

S II. COMPARISON BETWEEN MEASUREMENTS AT AEROBIC AND ANAEROBIC CONDITIONS

For anaerobic conditions the sample was prepared and measured as descibed in the main text. In addition, sodium dithionite was added in the amount to achieve a 15 mM concentration in the sample. The sample was incubated at room temperature for 1.5 hours prior to freezing it in the cryostat.

2D spectra measured at anaerobic conditions are almost identical to the spectra obtained at aerobic conditions. The oscillatory decay kinetics are shown in Fig. S2. Most of the small differences observed between corresponding traces are likely caused by the slightly different laser spetra used in the measurement at aerobic and anaerobic conditions.
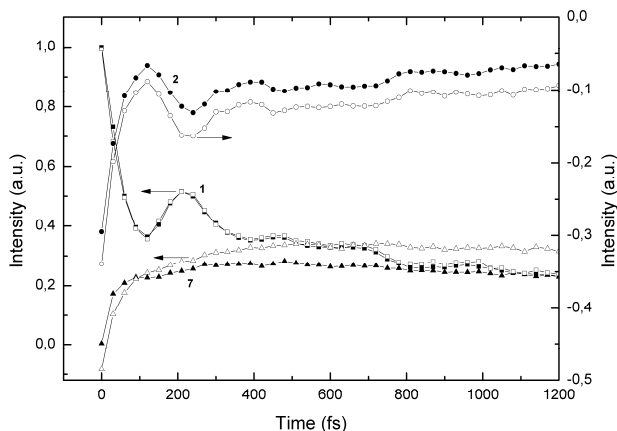
Fig. S2: Kinetic traces from selected points in 2D spectra measured at aerobic (solid markers) and anaerobic (open markers) conditions. The data sets were normalized to trace 1 at $t_2 = 210$ fs. The numbering of the traces was introduced in the main text (see Fig 1).

S III. DISTRIBUTION OF OSCILLATIONS IN THE REPHASING AND NON-REPHASING PARTS OF THE SPECTRA

Allmost all monotonious time evolution of the 2D spectrum is confined in its rephasing (R) part. Interestingly, the distributions of oscillations in the R and non-rephasing (NR) parts follow the same trends as found for the total spectrum (see the main text).The R and NR oscllation maps copy the shape of R and NR spectral parts at $t_2 = 0$.

SUPPLEMENTAL MATERIAL
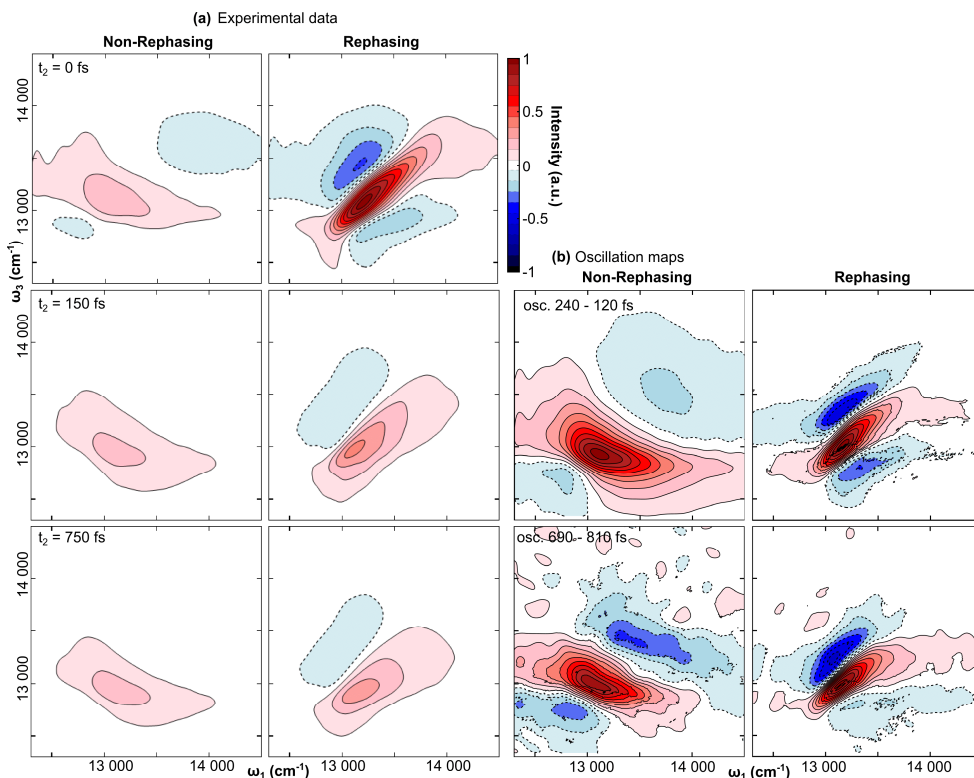
Fig. S3: (a) Time evolution of the rephasing and non-rephasing parts of the 2D spectrum with indicated population times. (b) Time-resolved maps of the distribution of the oscillatory patterns in the 2D spectra, all normalized to their maxima. These maps are obtained by calculating the difference of the oscillatory component from two 2D spectra at indicated population times.

REFERENCES

1. Dostál J, Mančal T, Augulis R, Vácha F, Pšenčík J, Zigmantas D (2012) Two-dimensional electronic spectroscopy reveals ultrafast energy diffusion in chlorosomes. *J Am Chem Soc* **134**: 11611–11617.

PAPER III

ARTICLE

Transfer of vibrational coherence through incoherent energy transfer process in Förster limit

Tomáš Mančal, Jakub Dostál, Jakub Pšenčík, and Donatas Zigmantas

Abstract: We study transfer of coherent nuclear oscillations between an excitation energy donor and an acceptor in a simple dimeric electronic system coupled to an unstructured thermodynamic bath and some pronounced vibrational intramolecular mode. Our focus is on the nonlinear optical response of such a system, i.e., we study both excited state energy transfer and the compensation of the so-called ground-state bleach signal. The response function formalism enables us to investigate a heterodimer with monomers coupled strongly to the bath and by a weak resonance coupling to each other (Förster rate limit). Our work is motivated by recent observation of various vibrational signatures in two-dimensional coherent spectra of energy-transferring systems including large structures with a fast energy diffusion. We find that the vibrational coherence can be transferred from donor to acceptor molecules provided the transfer rate is sufficiently fast. The ground-state bleach signal of the acceptor molecules does not show any oscillatory signatures, and oscillations in ground-state bleaching signal of the donor prevail with the amplitude, which is not decreasing with the relaxation rate.

Key words: 2D coherent spectroscopy, vibrational coherence, coherence transfer, energy transfer.

Résumé : Nous étudions le transfert d'oscillations nucléaires cohérentes entre un donneur d'énergie d'excitation et un accepteur dans un système électronique dimère simple couplé à un bain thermodynamique non structuré et à un mode prononcé de vibration nucléaire intramoléculaire. Nous nous intéressons à la réponse optique non linéaire de ce système, c'est-à-dire que nous étudions le transfert d'énergie à l'état excité ainsi que la compensation de ce qu'on appelle le signal de blanchiment de l'état fondamental. Le formalisme de la fonction de réponse nous permet d'étudier un hétérodimère dont les monomères sont fortement couplés au bain et couplés l'un à l'autre par une résonance faible (limite de vitesse de Förster). Nos travaux sont motivés par l'observation récente de diverses signatures vibrationnelles dans les spectres cohérents à deux dimensions de systèmes de transfert d'énergie incluant de grandes structures à diffusion rapide d'énergie. Nous constatons que la cohérence vibrationnelle peut être transférée des molécules donneuses aux molécules accepteuses à condition que la vitesse de transfert soit suffisamment grande. Le signal de blanchiment de l'état fondamental des molécules accepteuses ne présente aucune signature oscillatoire, et les oscillations dans le signal de blanchiment de l'état fondamental du donneur prédominent avec une amplitude qui ne diminue pas avec le taux de relaxation. [Traduit par la Rédaction]

Mots-clés : spectroscopie cohérente à deux dimensions, cohérence vibrationnelle, transfert de cohérence, transfert d'énergie.

I. Introduction

Ultrafast time-resolved nonlinear spectroscopy of electronic transitions represents an indispensable tool for the study of photoinduced dynamic and kinetic processes in a wide range of interesting molecular and solid state systems.[1–11] While the degrees of freedom of the studied systems that are directly addressed in these experiments are electronic, the fine details of the time-resolved spectra depend crucially on the characteristics of the surrounding nuclear modes. It was recognized early on that some ultrafast techniques yield unprecedented time-dependent information about the nuclear modes, even though these might form a thermodynamic bath with broad spectral density. For instance, the so-called photon echo peakshift experiment yields almost directly the form of the energy gap correlation function (also termed bath correlation function).[12–14] With the advent of the two-dimensional (2D) coherent Fourier transformed spectroscopy,[15,16] it was hoped shortly that one obtained a method that would provide insight into electronic coupling between chro-

mophores forming a molecular complex. Instead, the strength of the method proved to be in allowing observation of coherent oscillatory features of electronic and nuclear origin.[4,6,17–23] In particular, a large effort has been made to understand the vibrational features revealed by 2D spectroscopy and to contrast them with the electronic features.[22,24–27] Motivation for this work can be found in the ongoing debate on the origin of the long-lived coherent oscillations observed in the 2D spectra of some molecular complexes[4,6,19,28] for which models employing nuclear vibrational modes are also suggested.[29–32] Setting aside this particular debate, the study of the vibrational features of 2D spectra has its own importance. The vibrational degrees of freedom are ubiquitous in molecular aggregates and almost all ultrafast time-resolved spectroscopic methods are sensitive to them. A notable exception would be an ideal frequency integrated pump-probe spectroscopy for which one can show that it is insensitive to the nuclear vibrations.[33] 2D spectroscopy, however, can be shown to have a specific sensitivity to vibrational features,[34] and the

frequency-resolved pump-probe spectroscopy with finite pulses keeps sufficient sensitivity to vibrational features, also.

Our theoretical work in this paper is motivated by our recent observation of coherent oscillations in low-temperature 2D spectra of the chlorosome.[35] Previous measurements by pump-probe technique on this system showed convincingly that nuclear oscillations occur in the electronic ground state after an ultrafast excitation.[36] The chlorosome is the largest known bacterial photosynthetic antenna, containing ~10^5 aggregated chlorophylls that are subject to large disorder in optical gaps. Correspondingly, a plausible explanation of the oscillations observed in 2D spectra at low temperature are nuclear oscillations, as these could survive the disorder in the electronic transition energies. In our previous room temperature measurements of the chlorosome,[11] we observed an initial ultrafast time scale that could be associated with the fast diffusion of the excitation between certain coherent domains formed in the disordered energetic landscape of the chlorosome. We are therefore motivated to study the influence of an ultrafast energy transfer on the evolution of the nuclear oscillatory features in the 2D spectra.

To understand the properties of nuclear oscillations observed by 2D spectroscopy of photosynthetic energy-transferring systems, one needs to know spectroscopic properties and time-dependent signatures of nuclear vibrations of at least the two limiting cases in which these systems occur, namely the case of the Förster energy transfer between spatially localized excitons and the case of the delocalized Frenkel excitons. In photosynthetic energy-transferring antennae, these cases never occur in their pure form, as many photosynthetic antennae fall in between the two limiting regimes. Nevertheless, when trying to understand experimentally observed behaviors, it is useful to understand spectroscopic signatures that could be assigned to these two limiting cases. In this paper, we start with the simpler of the two regimes, namely with the Förster energy transfer between spatially localized excitations. With regard to our previous work, this corresponds to the energy transfer between the coherent domains of the chlorosome.[11]

To simplify the theoretical treatment, we study a weakly coupled dimeric system that possesses one pronounced intramolecular nuclear vibrational mode with a sufficient Huang–Rhys factor to be observable by electronic nonlinear spectroscopy, coherent 2D electronic spectroscopy in our case. We avoid the situation of a resonance between the vibrational frequency and the donor–acceptor energy gap in which the selected intramolecular nuclear vibrational mode would influence the energy transfer rate. This dimer interacts with its environment (solvent, protein surroundings, etc.). We ask the question whether the vibrational coherence excited by a sequence of two short pulses (the first two of the three pulses of the 2D electronic spectroscopy technique) on one molecule (denoted as donor here) can be transferred to a neighboring molecule (an acceptor). We also study the fate of the oscillations induced on the donor after it relaxes to the electronic ground state when its excitation is transferred to the acceptor. The answers to these questions could in principle shed some light on the behavior of the coherent oscillations observed in chlorosomes.

The paper is organized as follows. In the next section, we introduce the model molecular Hamiltonian and we discuss the model of system–bath interaction. We introduce the weak intermolecular coupling limit — the Förster limit. In Section III, we derive response functions for all of the signal components of the coherent 2D spectra of a dimer system with a weak resonance coupling and we discuss their properties. In Section IV, we discuss particular numerical results and the dependence of the amplitude of the transferred vibrational coherence on the energy transfer rates. We present our conclusions in Section V.

II. Molecular model

In this work, we consider a molecular dimer. We will describe unidirectional energy transfer from one molecule to another. We therefore denote the molecule that we consider to be the excitation donor by "D", while the other molecule (the excitation acceptor) will be denoted by "A". In actual molecular systems, both molecules can be donors and acceptors, e.g., when they have similar transition frequency and the energy transfers in one or the other direction are close to equally probable. A general theory of excitation energy transfer has to account for the possible back transfer of an excitation to the donor molecule. However, as will be shown later, the oscillation amplitude decays during the energy transfer, and it is enough to demonstrate this on a single step of the energy transfer. In systems in which the transition frequency of the acceptor molecule will be similar to that of the donor, such as in a chlorosome, the probability of back transfer will be diminished by the presence of other possible neighbors. Most of the relevant conclusions about the likelihood of vibrational coherence transfer can therefore be reached from studying unidirectional energy transfer. The theory developed below applies directly to a heterodimeric system where back transfer is small due to large energy difference between the donor and the acceptor.

We will describe the donor (acceptor) molecule in the dimer as a two-level system with electronic ground states $|g_D\rangle$ ($|g_A\rangle$) and excited state $|e_D\rangle$ ($|e_A\rangle$). To describe a complete nonlinear spectrum of such a system, it might be necessary to add even higher lying excited states or band of states $|f_D\rangle$ ($|f_A\rangle$). The two molecules interact through a resonance coupling J so that the electronic excitation can be exchanged between them. This means that the electronic states of the individual molecules are not eigenstates of the dimer. When, however, the interaction with the environment is stronger than the resonance coupling, the identity of the molecules is approximately preserved. Any delocalization possibly established by resonance coupling is destroyed by fluctuations induced by the environment. This is the limit of a strong bath influence, $\lambda_{bath} > J$, where λ_{bath} is the bath reorganization energy — the parameter characterizing the system–bath coupling. In the strong system–bath coupling limit, the appropriate description of the energy transfer process is the Förster rate theory and its modifications.[37–39] The Förster rate can be calculated from the known absorption and fluorescence spectra of the donor and acceptor molecules, respectively, and it carries a prefactor proportional to $|J|^2$. In this work, we will be interested in the influence that the value of the rate has on the transfer of the vibrational coherence. We will not calculate the rates; rather, we will use them as a free parameter assuming that different rates correspond to different values of J. The dynamics of the bath, which determines the line shape of the absorption and the fluorescence, will be specified in terms of the bath correlation function, also known as energy gap correlation function.

The total Hamiltonian of the dimer reads as

$$(1) \qquad H = H_{bath} + \sum_{i=A,D} H_i^{(1)} + J(|A\rangle\langle D| + |D\rangle\langle A|) + H^{(2)}$$

where H_{bath} is the Hamiltonian of the bath, $H_i^{(1)}$ are the Hamiltonians corresponding to the singly excited states of noninteracting dimmer $H_i = (\epsilon_i + \Delta V_i)|i\rangle\langle i|, i = A,D$, the states $|A\rangle$ and $|D\rangle$ are the singly excited states of the noninteracting dimer:

$$(2) \qquad |A\rangle = |e_A\rangle|g_D\rangle$$

$$(3) \qquad |D\rangle = |g_A\rangle|e_D\rangle$$

and $H^{(2)} = (\epsilon_A + \epsilon_B + \Delta V_A + \Delta V_D)|e_A\rangle|e_D\rangle\langle e_D|\langle e_A|$ is the Hamiltonian

of the doubly excited state of the dimer. If needed, it may include the higher excited states $|f_D\rangle$ and $|f_A\rangle$ of the donor and acceptor, respectively. The energy gap operators ΔV_A and ΔV_B describe the interaction of the acceptor and donor with the their surrounding environment, respectively. We set the ground-state electronic energy ϵ_g to zero. We will ignore the doubly excited state in our treatment because for weak coupling J (which is assumed in our Förster-type treatment), the excited-state absorption (ESA) cancels with the ground-state contributions, which would otherwise lead to crosspeaks in the 2D spectra.[40]

The description of the electron–phonon coupling (the coupling of the electronic states $|A\rangle$ and $|D\rangle$ with the bath of nuclear degrees of freedom) will be done in terms of the bath correlation functions $C_A(t) = \text{tr}\{\Delta V_A(t)\Delta V_A(0)W_{\text{eq}}^{(A)}\}$ and $C_D(t) = \text{tr}\{\Delta V_D(t)\Delta V_D(0)W_{\text{eq}}^{(D)}\}$, which describe the fluctuation of the transition energy on the acceptor and the donor, respectively. The time argument on the energy gap operators in the definitions of the bath correlation functions denotes the interaction picture with respect to the bath Hamiltonian and $W_{\text{eq}}^{(A)}$ ($W_{\text{eq}}^{(D)}$) denotes the equilibrium density operator of the acceptor (donor). For simplicity, we will assume that they are equal, $C_A(t) = C_D(t) \equiv C(t)$, but the fluctuations on different molecules remain uncorrelated. The absorption and fluorescence spectra as well as nonlinear optical spectra including 2D spectra can be expressed using a double integral of the bath correlation function, the so-called line shape function:[41]

$$(4) \qquad g(t) = \frac{1}{\hbar^2} \int_0^t \mathrm{d}\tau \int_0^\tau \mathrm{d}\tau' C(\tau')$$

We consider the bath correlation function, and correspondingly the line shape function, containing two components:

$$(5) \qquad g(t) = g_{\text{bath}}(t) + g_{\text{vib}}(t)$$

where $g_{\text{bath}}(t)$ describes the energy gap fluctuations due to interaction with a large harmonic bath and $g_{\text{vib}}(t)$ describes the contributions of underdamped oscillations due to individual intramolecular vibrational modes. We choose to treat the case of a single vibrational mode and we use

$$(6) \qquad g_{\text{osc}}(t) = \frac{\lambda}{\omega}(\Theta(T)(1 - \cos(\omega t)) + i\sin(\omega t) - i\omega t)$$

where $\Theta(T) = \coth(\hbar\omega/2k_B T)$ (see Mukamel[41]). We will assume the bath to be characterized by Debye spectral density with some correlation time τ_{bath} and reorganization energy λ_{bath}. The line shape function $g_{\text{bath}}(t)$ corresponding to this bath correlation function is linear at large values of $t > \tau_{\text{bath}}$, i.e., $g_{\text{bath}}(t) \approx \alpha t$. In particular, for the imaginary part, we have $\text{Im} g_{\text{bath}}(t) \approx -i\lambda t$ at long times.[41]

The energy transfer rate K_{AD} from the donor to acceptor is in principle time dependent and can be calculated with the help of correlation functions (line shape functions) of the donor and acceptor.[42] We assume that the part $g_{\text{vib}}(t)$ of the energy gap fluctuation does not participate in the transfer rate, and we assume that the rate quickly becomes time independent. Later in this paper, we study the dependence of various vibrational features in spectroscopic signals on the magnitude of the rate K_{AD}, which we always assume to be constant.

III. Nonlinear response functions with energy transfer

Nonlinear spectroscopic signals can be calculated conveniently using the response function formalism.[41] In the following, we will

Fig. 1. Diagram of the levels of a weakly coupled dimer system and the Feynman diagrams of the rephasing Liouville pathways used in this paper.
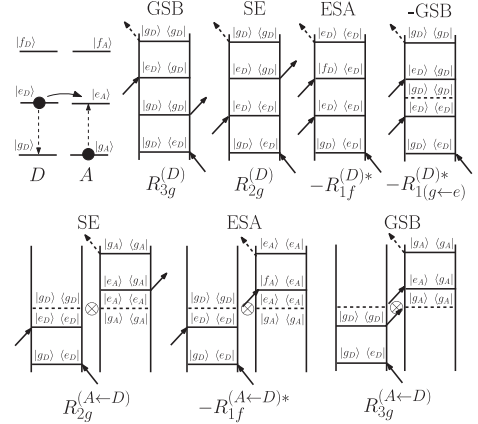
use the theory developed in Yang and Fleming[43] to describe the nonlinear optical signal of an acceptor–donor system. In Yang and Fleming,[43] the nuclear degrees of freedom are treated via a second cumulant expansion of the response functions. For Gaussian baths, such as the bath of an infinite number of harmonic oscillators coupled linearly to the electronic transition, this approach leads to exact expressions for the response. Adding a single independent vibrational mode, which is well pronounced in the nonlinear response, allows us to model the transfer of the nuclear oscillations during energy exchange between the monomers.

In Yang and Fleming,[43] two two-level systems connected through a transfer rate K_{AD} were studied. In our case, we need to formally include ESA to a higher excited state other than the two-exciton states discussed above. However, this addition does not change the treatment of the energy transfer because higher excited states do not contribute to the energy transfer dynamics observed by third-order spectroscopic methods (such as 2D coherent spectroscopy).[41] We will study the transfer in one direction, from a donor molecule D to an acceptor molecule A. We will denote nonlinear response functions corresponding to the experimental signal by superindices (D) and (A), or (A ← D) if the response contains energy transfer. We will show that this process leads to a partial loss of the amplitude of the oscillations due to vibrational coherence.

There are four types of double-sided Feynman diagrams representing four general types of response functions. These are usually denoted by lower index $n = 1, \ldots, 4$ in the literature (see, e.g., Mukamel[41]). In addition, we distinguish the pathways that include the ground state $|g\rangle$ and the excited state $|e\rangle$ only and those involving the higher excited state $|f\rangle$. To the former, we add a lower index g, while to the latter, we add a lower index f. Some pathways involve relaxation from the excited state $|e\rangle$ to the ground state $|g\rangle$ and we denote them with a lower index $(g \leftarrow e)$. The list of rephasing pathways and their corresponding Feynman diagrams are presented in Fig. 1.

In this section, without the loss of generality, we consider only the rephasing part of the response. All calculations presented later in Section IV will be based on a complete set of pathways. We assume that originally only the donor is excited, although in reality, the process where the roles of the donor and the acceptor

are exchanged occurs simultaneously. There are seven rephasing Liouville pathways with the following interpretations. (*i*) The ground-state bleach (GSB) signal from the donor is attributed to the pathway $R_{3g}^{(D)}$. During the population time, this contribution evolves due to the bath reorganization and the oscillation of the vibrational mode, but it does not change due to the energy transfer process. (*ii*) The donor-stimulated emission (SE), which exponentially decays with the energy transfer rate K_{AD}, is described by the response function $R_{2g}^{(D)}$ multiplied by the corresponding decay factor. (*iii*) When the donor decays to the ground state due to energy being transferred to the acceptor, the bleach is filled with the decayed population. This process is described by the response function $R_{1(g \leftarrow e)}^{(D)^*}$ where the asterisk denotes complex conjugation. This response function has an overall type of an R_1 pathway, but it carries a minus and a complex conjugation. It rises with a factor $(1 - e^{-K_{AD}t_2})$. The minus leads to cancellation of the GSB contribution of $R_{3g}^{(D)}$. (*iv*) Together with the energy transfer, there is a corresponding rise of the GSB of the acceptor. This is described by the response function $R_{3g}^{(A \leftarrow D)}$ and the rise is the same as in pathway *iii*. (*v*) and (*vi*) Similar to the GSB, also the SE and the ESA of the acceptor rise. These processes are described by the response functions $R_{2g}^{(A \leftarrow D)}$ and $R_{1f}^{(A \leftarrow D)}$, respectively. (*vii*) Finally, the ESA of the donor is decaying in exactly the same way as its SE and is described by the response function $R_{1f}^{(D)^*}$ multiplied by the corresponding exponentially decaying factor.

A. Transfer of the excited-state vibrational coherence

Using the matrix elements of the Liouville space density matrix propagators for optical coherences $U_{eg}(t) \equiv U_{egeg}(t)$ and the ground- and excited-state density matrix elements $U_{ee}(t) \equiv U_{eeee}(t)$ and $U_{gg}(t) \equiv U_{gggg}(t)$, where we abbreviated the number of electronic indices to two, we can express the above-discussed response functions in the following way (see, e.g., Mančal[40]):

$$(7) \quad R_{2g}^{(D)} \approx \langle \mathcal{U}_{e_D g_D}(t_3) \mathcal{U}_{e_D e_D}(t_2) \mathcal{U}_{ge}(t_1) \rangle_D e^{-K_{AD}t_2}$$

$$(8) \quad R_{3g}^{(D)} \approx \langle \mathcal{U}_{e_D g_D}(t_3) \mathcal{U}_{g_D g_D}(t_2) \mathcal{U}_{g_D e_D}(t_1) \rangle_D$$

$$(9) \quad R_{1f}^{(D)^*} \approx -\langle \mathcal{U}_{f_D e_D}(t_3) \mathcal{U}_{e_D e_D}(t_2) \mathcal{U}_{g_D e_D}(t_1) \rangle_D e^{-K_{AD}t_2}$$

$$(10) \quad R_{1(g \leftarrow e)}^{(D)^*} \approx -K_{AD} \int_0^{t_2} d\tau \langle \mathcal{U}_{e_D g_D}(t_3) \mathcal{U}_{g_D g_D}(t_2 - \tau) \\ \times \mathcal{U}_{e_D e_D}(\tau) \mathcal{U}_{g_D e_D}(t_1) \rangle_D e^{-K_{AD}\tau}$$

$$(11) \quad R_{2g}^{(A \leftarrow D)} \approx K_{AD} \int_0^{t_2} d\tau \langle \mathcal{U}_{e_A g_A}(t_3) \mathcal{U}_{e_A e_A}(t_2 - \tau) \rangle_A \\ \times \langle \mathcal{U}_{e_D e_D}(\tau) \mathcal{U}_{g_D e_D}(t_1) \rangle_D e^{-K_{AD}\tau}$$

$$(12) \quad R_{3g}^{(A \leftarrow D)} \approx K_{AD} \int_0^{t_2} d\tau \langle \mathcal{U}_{e_A g_A}(t_3) \mathcal{U}_{g_A g_A}(t_2 - \tau) \rangle_A \\ \times \langle \mathcal{U}_{g_D g_D}(\tau) \mathcal{U}_{g_D e_D}(t_1) \rangle_D e^{-K_{AD}\tau}$$

$$(13) \quad R_{1f}^{(A \leftarrow D)^*} \approx -K_{AD} \int_0^{t_2} d\tau \langle \mathcal{U}_{f_A e_A}(t_3) \mathcal{U}_{e_A e_A}(t_2 - \tau) \rangle_A \\ \times \langle \mathcal{U}_{e_D e_D}(\tau) \mathcal{U}_{g_D e_D}(t_1) \rangle_D e^{-K_{AD}\tau}$$

Here, we omitted the prefactors containing transition dipole moments, and $\langle ... \rangle_D = \mathrm{tr}_{bath}\{... W_{eq}^{(D)}\}$ corresponds to the averaging over the equilibrium environmental degrees of freedom of the donor. The sign $\langle ... \rangle_A = \mathrm{tr}_{bath}\{... W_{eq}^{(A)}\}$ represents the same averaging for the acceptor. Expressions for the standard pathways of eqs. 7, 8, and 9 are well known from the literature (see, e.g., Mukamel[41]). The response of eq. 10 will be treated in more detail later. Let us first address eqs. 11 to 13. The averaging on the donor in these equations leads to an elimination of the dependence on the variable τ in the donor part of the response because

$$(14) \quad \langle \mathcal{U}_{e_D e_D}(\tau) \mathcal{U}_{g_D e_D}(t_1) \rangle_D = \mathrm{tr}_{bath}\{\mathcal{U}_{e_D e_D}(\tau) \mathcal{U}_{g_D e_D}(t_1) W_{eq}\} \\ = \mathrm{tr}_{bath}\{\mathcal{U}_{g_D e_D}(t_1) W_{eq}\}$$

This is because the superoperator $\mathcal{U}_{e_D e_D}(\tau)$ acting on an arbitrary operator A corresponds to an action of two ordinary evolution operators:

$$(15) \quad \mathcal{U}_{e_D e_D}(\tau) A = U_{e_D}(t) A U_{e_D}^\dagger(t)$$

and the operators can be reordered in a cyclic way under the trace operation. In addition, in $R_{3g}^{(A \leftarrow D)}$, the τ dependence can be eliminated also on the acceptor part of the response because

$$(16) \quad \mathcal{U}_{g_A g_A}(t_2 - \tau) W_{eq}^{(A)} = W_{eq}^{(A)}$$

due to invariance of the equilibrium to the ground-state propagation. Correspondingly, we have

$$(17) \quad R_{3g}^{(A \leftarrow D)} \approx e^{-g_A(t_3) - g_D(t_1)}(1 - e^{-K_{AD}t_2})$$

In the bleach signal, there is therefore no transfer of any dependency of the response on t_2. Other transfer pathways can now be expressed through the purely acceptor pathways, which have a standard form, with the first time argument (from the right) equal to zero:

$$(18) \quad R_{2g}^{(A \leftarrow D)} \approx e^{-g_D(t_1)} K_{AD} \int_0^{t_2} d\tau R_{2g}^{(A)}(t_3, t_2 - \tau, 0) e^{-K_{AD}\tau}$$

$$(19) \quad R_{1f}^{(A \leftarrow D)^*} \approx -e^{-g_D(t_1)} K_{AD} \int_0^{t_2} d\tau R_{1f}^{(A)^*}(t_3, t_2 - \tau, 0) e^{-K_{AD}\tau}$$

For the stimulated emission, this leads to

$$(20) \quad R_{2g}^{(A \leftarrow D)} \approx e^{-g_D(t_1) - g_A^*(t_3)} \times K_{AD} \int_0^{t_2} d\tau \, e^{2i\mathrm{Im}[g_A(t_2 - \tau) - g_A(t_2 + t_3 - \tau)] - K_{AD}\tau}$$

which can be relatively easily evaluated. The ESA contribution depends on the particular assumptions that we make about the higher excited states and cannot therefore be evaluated without introducing further assumptions. We can consider this contribution to be similar in oscillatory features to the SE because the source of the oscillation is the same excited state of the acceptor.

B. Refilling of the bleaching signal

The GSB contribution to the rephasing signal, which we denote by $R_{3g}^{(D)}$, appears stationary and, at the first sight, unaffected by the

energy transfer process. However, the transfer process is accompanied by deexcitation of the donor domain, and correspondingly, there is a signal countering the one of the $R_{3g}^{(D)}$ pathway. Above, we denoted this signal by $R_{1(ge \leftarrow e)}^{(D)*}$ above. The diagram of this pathway has a form of the R_1 diagram mirror imaged and is used with the minus sign. According to Yang and Fleming,[43] this pathway reads

$$(21) \quad R_{1(ge \leftarrow e)}^{(D)*}(t_3, t_2, t_1) = R_{3g}^{(D)}(t_3, t_2, t_1) e^{-2i\mathrm{Im}(g_D(t_2+t_3) - g_D(t_2))}$$
$$\times K_{AD} \int_0^{t_2} dt' e^{-K_{AD}t'} e^{2i\mathrm{Im}(g_D(t_2+t_3-t') - g_D(t_2-t'))}$$

The signal canceling the GSB contains the GSB response function $R_{3g}^{(D)}$. Later in this paper, we will evaluate all of the response functions numerically. Let us, however, attempt a slightly more involved analysis of eq. 21 assuming its long t_2 approximation. Because the g_{bath} and the g_{osc} components of the total donor line shape function are independent, one can factorize the response function into the bath and the vibrational parts. In addition, the bath line shape function $g_{\mathrm{bath}}(t)$ is linear at its arguments larger than τ_{bath} and correspondingly, the t' dependence on the bath part of the line shape function vanishes. With these assumptions, we can write for $t_2 > \tau_{\mathrm{bath}}$:

$$(22) \quad R_{1(ge \leftarrow e)}^{(D)*}(t_3, t_2, t_1) \approx R_{3g}^{(D)}(t_3, t_2, t_1) e^{-2i\mathrm{Im}(g_{\mathrm{osc}}(t_2+t_3) - g_{\mathrm{osc}}(t_2))}$$
$$\times K_{AD} \int_0^{t_2} dt' e^{-K_{AD}t'} e^{2i\mathrm{Im}(g_{\mathrm{osc}}(t_2+t_3-t') - g_{\mathrm{osc}}(t_2-t'))}$$

i.e., the influence of the bath evolution is completely hidden in the $R_{3g}^{(D)}(t_3, t_2, t_1)$ function. In the integral in eq. 22, we see only contributions originating from the intramolecular vibrations.

Integrating eq. 22 by parts, we obtain

$$(23) \quad R_{1(ge \leftarrow e)}^{(D)*}(t_3, t_2, t_1)$$
$$\approx R_{3g}^{(D)}(t_3, t_2, t_1)(1 - e^{-K_{AD}t_2} e^{-2i\mathrm{Im}(g_{\mathrm{osc}}(t_2+t_3) - g_{\mathrm{osc}}(t_2) - g_{\mathrm{osc}}(t_3))})$$
$$- 2i\frac{\lambda}{\omega} R_{3g}^{(D)}(t_3, t_2, t_1) e^{-2i\mathrm{Im}(g_{\mathrm{osc}}(t_2+t_3) - g_{\mathrm{osc}}(t_2))}$$
$$\times \int_0^{t_2} dt' \omega[\cos\omega(t_2 + t_3 - t') - \cos\omega(t_2 - t')]$$
$$\times e^{-K_{AD}t'} e^{2i\mathrm{Im}(g_{\mathrm{osc}}(t_2+t_3-t') - g_{\mathrm{osc}}(t_2-t'))}$$

Under the integral, we used explicitly the form of the g_{osc}, eq. 6. At long times t_2, when $e^{-K_{AD}t_2} \approx 0$, the donor contribution to the overall signal consists only of the integral term

$$(24) \quad S^{(D)}(t_3, t_2 > K_{AD}^{-1}, t_1) = R_{3g}^{(D)}(t_3, t_2, t_1) - R_{1(ge \leftarrow e)}^{(D)*}(t_3, t_2, t_1)$$
$$\approx -2i\frac{\lambda}{\omega} R_{3g}^{(D)}(t_3, t_2, t_1) e^{-2i\mathrm{Im}(g_{\mathrm{osc}}(t_2+t_3) - g_{\mathrm{osc}}(t_2))}$$
$$\times \int_0^{t_2} dt' \omega[\cos\omega(t_2 + t_3 - t') - \cos\omega(t_2 - t')]$$
$$\times e^{-K_{AD}t'} e^{2i\mathrm{Im}(g_{\mathrm{osc}}(t_2+t_3-t') - g_{\mathrm{osc}}(t_2-t'))}$$

We can see that the difference between the original GSB signal and the signal coming from the filling of the GSB is proportional to the Huang–Rhys factor with a factor the a form of an

Fig. 2. Potential energy surfaces of the dimer model with Förster regime of energy transfer. Donor molecule D is initially excited and the excitation is transferred with a transfer constant K_F to the acceptor molecule A. This process corresponds to a deexcitation of the donor and excitation of the acceptor with the same rate K_F. The excited state wavepacket is projected to a nonequilibrium position of the ground state during the energy transfer to the acceptor.
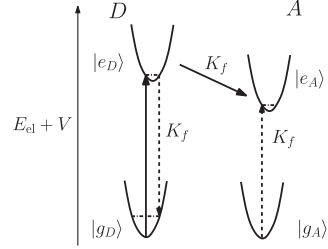
integral over oscillating function. The whole factor will obviously be an oscillating function of t_2. Its numerical analysis for the range of Huang–Rhys factors between 0 and 1 shows that it has a leading imaginary contribution. Correspondingly, the GSB signal on a donor does not vanish after the excitation leaves the donor molecule. The remaining signal is similar to the ground-state contribution $R_{3g}^{(D)}$ multiplied by i and modulated by an oscillating real function. The numerical results presented in Section IV confirm this conclusion.

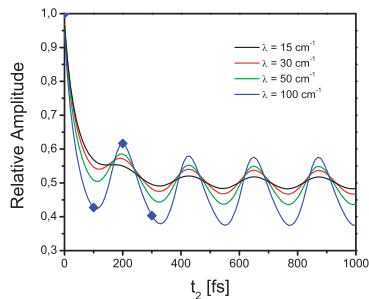**C. Origin of the bleach signal**

Interestingly, after an ideal impulsive excitation of a molecular system, no dynamic GBS (i.e., dependent on t_2) would arise. This can be seen directly from the form of the response function while setting $t_1 = 0$ or from an intuitive picture summarized in Fig. 2. In terms of the response function, the beach corresponds to an excitation and then deexcitation of one of the sides of the Feynman diagram (see pathway $R_{3g}^{(D)}$ of Fig. 1). The beating that we observe in t_2 is then the beating between the static unexcited ground-state wavepacket (or more precisely an equilibrium mixed state) and a perturbed wavepacket that was excited, evolved for a short time t_1 on the excited-state potential energy surface, and then transferred back to the ground state into a nonequilibrium position. If the delay $t_1 = 0$, the wavepacket does not have time to evolve on the excited-state potential energy surface and is returned back to its original equilibrium state. Hence, no dynamical signal arises.

During the excitation transfer, the GSB signal is compensated by an excited-state population returning to the ground state. In the nonlinear response corresponding to the excited states, there are in principle two wavepackets (in the ket and the bra of the Feynman diagram) that were created in the excited state at two times occurring with a delay t_1. These wavepackets are projected to the ground state of the donor during the excitation transfer, and they are unlikely to have a phase as to cancel the oscillations that already occur in the ground state. It is therefore not surprising that the GSB signal will remain after the excitation is transferred. In the next section, we will study the amplitude of these remaining oscillations and its dependence on the value of the energy transfer rate.

IV. Discussion

In this section, we will present results of numerical calculations of 2D coherent Fourier transformed spectra. The definition of the 2D spectrum as well as the description of the experimental technique can be found, e.g., in Brixner et al.[15] and Jonas[44]. Throughout

Fig. 3. Oscillations due to underdamped vibrations of nuclear mode with frequency $\omega = 150$ cm^{-1} for various reorganization energies. The diamonds denote the positions for which the real part of the 2D spectrum is plotted in Fig. 4.

Fig. 4. Time evolution of the real part of the 2D coherent spectrum of a donor molecule in the absence of energy transfer to an acceptor. The snapshots are taken at $t_2 = 0$, 100, 200, and 300 fs. The reorganization energy λ of the vibrational mode is 100 cm^{-1}. The figures correspond to the positions on the blue curve (color in online version only) in Fig. 3 that are marked by diamonds. The figures are normalized to maximum of the 2D spectrum at $t_2 = 0$ fs, and there are 12 contours between zero and the maximum.

this section, we use one parameter set for the bath correlation function, namely, $\lambda_{bath} = 200$ cm^{-1}, $\tau_{bath} = 100$ fs. The temperature is assume to be $T = 300$ K. These parameters ensure a realistically broad 2D spectrum on which a typical frequency of an intramolecular vibrational mode $\omega = 150$ cm^{-1} and an oscillator reorganization frequency $\lambda < \omega$ lead to characteristic line shape modulation (see, e.g., Nemeth et al.[21]). It is customary to present the real part of the spectrum, which corresponds to the absorption–absorption/stimulated emission plots.[40,44] Similar to the situation in the chlorosome, the presence of the vibrational mode does not lead here to any discernible crosspeak, but the spectral amplitude at its center and the overall line shape are modulated. Figure 3 shows the characteristic oscillations of the amplitude of the 2D spectrum at the resonance for the donor molecule with no excitation energy transfer ($K_{AD} = 0$). Figure 4 presents the corresponding 2D spectra at some selected points (denoted by diamonds in Fig. 3). All 2D spectra are represented with respect to the resonant optical transition frequency, and they are therefore centered around the (0,0) point. On both figures, we can notice the initial drop of the amplitude and broadening, which occurs with the time scale of the bath correlation time τ_{bath}. For delay times longer than τ_{bath}, the 2D spectrum shows a characteristic pattern of line shape oscillation that corresponds to an oscillation of the amplitude. The oscillations are more pronounced with increasing reorganization energy of the oscillator, i.e., with increasing Huang–Rhys factor.

When the energy transfer from the donor to the acceptor is allowed, the total donor signal quickly disappears as the stimulated emission pathway decays exponentially and the GSB is compensated for by the signal from the population arriving to the ground state from the excited state. Figure 5 shows, however, that the donor signal remains oscillating around zero. The signal on the acceptor, on the other hand, rises to an amplitude corresponding to the one exhibited by the donor without energy transfer (cf. Fig. 3). One can notice by eye that the amplitude of the oscillations decreases with the increasing transfer time (decreasing transfer rate). One can also notice that this is not the case for the GSB. Characteristic 2D spectra of the donor contribution are presented in Fig. 6. An originally almost completely positive signal quickly disappears on the time scale of the energy transfer, and what remains is a signal with a characteristic shape of the imaginary part of the 2D spectrum (see, e.g., Nemeth et al.[21]), but with an alternating sign. The rising acceptor signal (Fig. 7) shows only the characteristic line shape modulations accompanied with the change of the maximum amplitude of the spectrum.
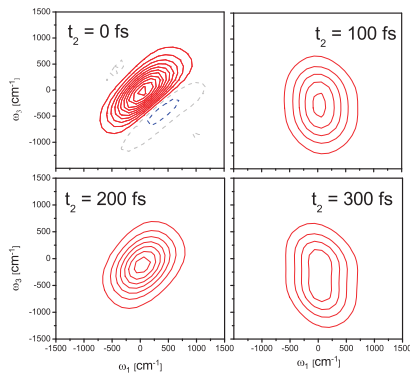
Fig. 5. Oscillations of the 2D spectrum at the optical resonance. The amplitude of the spectrum at $\omega_1 = \omega_3$ is plotted for the donor molecule and for the acceptor molecule for different values of the transfer time $T_{AD} = 1/K_{AD}$ and the reorganization energy $\lambda = 100$ cm^{-1}. The vibrational mode has a frequency $\omega = 150$ cm^{-1}. The diamonds indicate the positions for which the real part of the 2D spectrum is plotted in Fig. 6, and squares indicate the positions for which the real part of the 2D spectrum is plotted in Fig. 7.
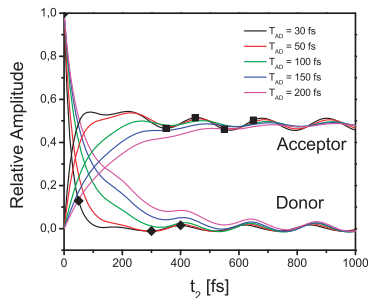
The relative amplitude of the coherent oscillations transferred to the acceptor or left on the donor with respect to the amplitude expected on the nontransferring donor is plotted in Fig. 8. We compare relative amplitudes for four different values of the oscillator reorganization energy. We find that the transfer of oscillations to the acceptor for all reorganization energies follows roughly the same exponential decay with the transfer time. This behavior is expected because a slow feeding rate leads to more destructive interference between various contributions of the transferred nuclear wavepacket. For electronic coherence, this effect was recently discussed in Chenu et al.[45] Similar behavior is observed when electronic coherence is induced in a multilevel molecular system by pulsed light with increasing duration as

Fig. 6. Decay of the signal on the donor. The short time behavior ($t_2 = 0$ and 50 fs) corresponds to the bath dephasing and the loss of population. When the population is completely lost and the system has relaxed back to the ground state electronically, the mismatch between the returning excited state nuclear wavepacket and the groud-state wavepacket yields a dispersion patern known from the imaginary part of the 2D spectra. The dispersion patern changes sign with the period of the oscillation. The snapshots correspond to the positions on the curve in Fig. 5 that are marked by diamonds. The figures are normalized to maximum of the 2D spectrum at $t_2 = 0$ fs, and there are 12 contours between zero and the maximum. At times $t_2 = 50, 300,$ and 400 fs, we use four times as many contours as in the $t_2 = 0$ fs spectrum to enhance the small amplitude of the spectrum.
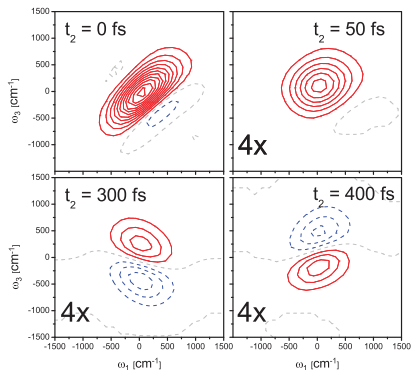

Fig. 7. Time evolution of coherences transferred to the acceptor molecule. After the rise of the 2D signal is completed (see Fig. 5), the spectrum keeps evolving due the nuclear motion in the excited state of the acceptor molecule. The figures are normalized to the maximum of 2D spectrum at $t_2 = 450$ fs (largest amplitude of the four spectra), and there are 12 contours between zero and its maximum.
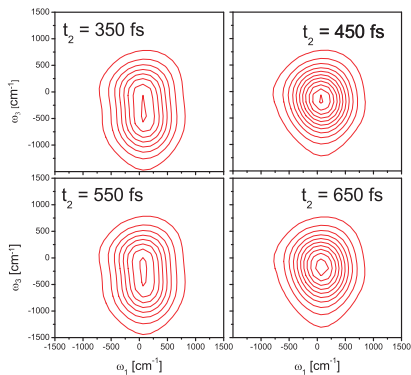
shown by Jiang and Brumer[46]. This trend is, however, not followed by the GSB signal remaining on the donor. Figure 8 demonstrates that the relative amplitude of the oscillations on the resonance does not decay with increasing transfer time. It even

Fig. 8. Efficiency of the coherence transfer. Curves denoted as "Transfer": ratio of the amplitude transferred to the acceptor to the original amplitude of the oscillations on the donor. Curves denoted as "Relaxation": ratio of the amplitude of the ground-state bleaching oscillations on the donor to the original amplitude of the oscillations on the donor. All parameters are as in Fig. 5.
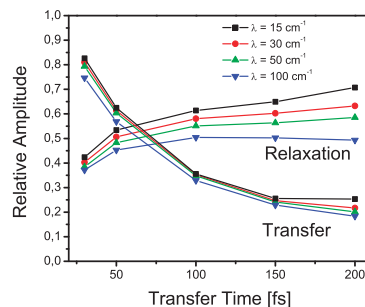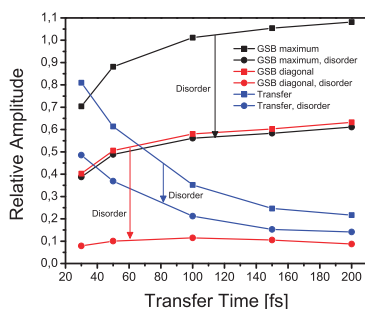

slightly increases at short times, and it stays flat for times up to 200 fs. For longer transfer times, the wavepacket stays for a longer time in the excited state. Because the period of the oscillator is larger than the transfer time, it apparently acquires a larger amplitude when it is projected on the ground state.

Real molecular systems are studied by nonlinear spectroscopy in the form of macroscopic disordered ensembles. The chlorosome that motivates our study of the transfer of vibrational coherence is also a strongly disordered system. It is therefore worth studying the effect of the transition energy disorder on the oscillatory patter observed in 2D spectra. In general, a change in the transition energy results in a displacement of the 2D line shape along the diagonal line of the spectrum. The disorder thus corresponds to an additional elongation of the line shape along the diagonal line. For a line shape that is positive everywhere, this does not mean any significant change in the total amplitude of the spectrum (it should become slightly diminished due to the broadening). For a line shape corresponding to the times $t_2 = 300$ and 400 fs in Fig. 6, however, the displacement may lead to additional canceling of the signal from differently displaced line shapes because the line shapes contain both positive and negative regions. In Fig. 9, we therefore study the influence of the disorder on the amplitude of the transferred oscillations and on the amplitude of the remaining GSB signal. In our calculations, we assume a large Gaussian disorder simulated by a normal distribution of the transition energies with a full width at half maximum of 1000 cm^{-1}. In all studied cases, the disorder leads to a decrease of the relative amplitude of the oscillations. For the oscillation transfer, this decrease is less than 50%. Similarly for the points of the 2D spectrum where the GSB has its maximum at $t_2 = 300$ fs, the decay of the amplitude of the oscillations is less than 50%. On the diagonal, i.e., near the nodal line of the 2D spectrum, the amplitude is decreased almost five times. Nevertheless, the donor signal remains oscillating despite disorder, and the expected amplitude of the oscillations in comparable with or larger than the amplitude of the transferred oscillations.

From the point of view of large aggregates, the results concerning the survival of the bleach signal are the most interesting. In system where each donor has a number of acceptors, the excitation that started on a given donor will be very rarely detected returning to the donor (after it has passed through some other molecules). Even the process in which the excitation passed through its original donor and was then detected on some of the acceptors is much less frequent than the situation in which the

Fig. 9. Influence of electronic disorder on the relative amplitude of the oscillations with frequency $\omega = 150$ cm⁻¹ and reorganization energy $\lambda = 30$ cm⁻¹. The disorder corresponding to a distribution of acceptor and donor transition frequencies with full width at half maximum equal to 1000 cm⁻¹ was applied. The relative amplitude of the transferred coherences (in blue) (color in online version only) is diminished only slightly. At the diagonal of the 2D spectrum, the ground-state bleaching oscillations are reduced by more than a factor of 5 (in red). However, when the amplitude is measured where the bleaching spectrum has its maximum (see lower panels of Fig. 6), the relative amplitude is decreased only by factor of 2, and the beating on the relaxed donor remains larger than the one on the acceptor.

for the case of a resonant energy transfer with constant rates, we find that the nuclear oscillations can be transferred to neighboring molecules. Their amplitude, however, decays with decreasing transfer rates. On the acceptor, the oscillations are solely due to the nuclear wavepacket in the electronically excited state. Interestingly, the amplitude of oscillations that prevail on the donor, after it was deexcited due to energy transfer, does not decrease with the decreasing energy transfer rate. Amplitudes of both types of oscillations decrease in the presence of electronic disorder. In systems where excitation travels away from the original donor, the dominating and surviving contribution after many steps will be the one originating from the electronic ground state of the donor molecule.

excitation leaves the donor and never returns or passes through it. In such a case, the bleaching signal remains oscillating until the vibrational energy relaxes due to processes independent of the energy transfer process. In the same situation, continuing transfer of the excitation to subsequent acceptors will lead to a complete decay of the nuclear oscillations originating in the excited state, i.e., oscillations in the SE and ESA signals.

A. Outlook

The discussion in this paper is only a start of a more extensive research program, which has to incorporate several important effects that were neglected here. First, one has to take into account the excitonic character of the states if one wants to draw some conclusions for the possible vibrational coherence transfer in photosynthetic systems in general. Also, various transition dipole moment borrowing effects including formation of so-called vibronic (vibrational-excitonic) excitons have to be considered in the case where resonance between the energy gap in the heterodimer and the vibrational frequency occurs. These two different effects amount to a study of different model situations. In the present model, however, we have also included several approximations that can be closely investigated. For instance, we assumed constant energy transfer rates, i.e., we assumed certain coarse graining of our problem in time. For fast vibrations, the relaxation rates might still be time dependent during several first periods of the vibrational motion after excitation. The relaxation rates might also be dependent on the vibrational motion itself during this initial time interval. Such effects may change the situation both quantitatively and qualitatively in some cases and will be studied elsewhere.

V. Conclusions

We have investigated the stimulated emission and ground state bleach signals of a molecular dimeric system with pronounced vibrational modes. We have concentrated on the transfer of the vibrational coherence between an excited donor molecule and its neighboring acceptor. Using response function formalism adapted

References

(1) Milota, F.; Sperling, J.; Nemeth, A.; Mančal, T.; Kauffmann, H. F. *Acc. Chem. Res.* **2009**, *42*, 1364. doi:10.1021/ar800282e.
(2) Cheng, Y.-C.; Fleming, G. R. *Annu. Rev. Phys. Chem.* **2009**, *60*, 241. doi:10.1146/annurev.physchem.040808.090259.
(3) Ginsberg, N. S.; Cheng, Y.-C.; Fleming, G. R. *Acc. Chem. Res.* **2009**, *42*, 1352. doi:10.1021/ar9001075.
(4) Collini, E.; Scholes, G. D. *Science* **2009**, *323*, 369.
(5) Turner, D. B.; Nelson, K. A. *Nature* **2010**, *466*, 1089. doi:10.1038/nature09286.
(6) Collini, E.; Wong, C. Y.; Wilk, K. E.; Curmi, P. M. G.; Brumer, P.; Scholes, G. D. *Nature* **2010**, *463*, 644. doi:10.1038/nature08811.
(7) Schlau-Cohen, G. S.; Ishizaki, A.; Fleming, G. R. *Chem. Phys.* **2011**, *386*, 1. doi:10.1016/j.chemphys.2011.04.025.
(8) Wong, C. Y.; Alvey, R. M.; Turner, D. B.; Wilk, K. E.; Bryant, D. A.; Curmi, P. M. G.; Silbey, R. J.; Scholes, G. D. *Nat. Chem.* **2012**, *4*, 396. doi:10.1038/nchem.1302.
(9) Turner, D. B.; Hassan, Y.; Scholes, G. D. *Nano Lett.* **2012**, *12*, 880. doi:10.1021/nl2039502.
(10) Bixner, O.; Lukeš, V.; Mančal, T.; Hauer, J.; Milota, F.; Fischer, M.; Pugliesi, I.; Bradler, M.; Schmidt, W.; Riedle, E.; Kauffmann, H. F.; Christensson, N. *J. Chem. Phys.* **2012**, *136*, 204503.
(11) Dostál, J.; Mančal, T.; Augulis, R.; Vácha, F.; Pšenčík, J.; Zigmantas, D. *J. Am. Chem. Soc.* **2012**, *134*, 11611. doi:10.1021/ja3025627.
(12) Cho, M.; Yu, J.-Y.; Joo, T.; Nagasawa, Y.; Passino, S. A.; Fleming, G. R. *J. Phys. Chem.* **1996**, *100*, 11944. doi:10.1021/jp9601983.
(13) Yang, M.; Fleming, G. R. *J. Chem. Phys.* **1999**, *110*, 2983. doi:10.1063/1.477893.
(14) Mančal, T.; Fleming, G. R. *J. Chem. Phys.* **2004**, *121*, 10556. doi:10.1063/1.1807816.
(15) Brixner, T.; Mančal, T.; Stiopkin, I. V.; Fleming, G. R. *J. Chem. Phys.* **2004**, *121*, 4221. doi:10.1063/1.1776112.
(16) Brixner, T.; Stenger, J.; Vaswani, H. M.; Cho, M.; Blankenship, R. E.; Fleming, G. R. *Nature* **2005**, *434*, 625. doi:10.1038/nature03429.
(17) Kjellberg, P.; Bruggemann, B.; Pullerits, T. *Phys. Rev. B* **2006**, *74*, 024303. doi:10.1103/PhysRevB.74.024303.
(18) Pisliakov, A. V.; Mančal, T.; Fleming, G. R. *J. Chem. Phys.* **2006**, *124*, 234505. doi:10.1063/1.2200705.
(19) Engel, G. S.; Calhoun, T. R.; Read, E. L.; Ahn, T.-K.; Mančal, T.; Cheng, Y.-C.; Blankenship, R. E.; Fleming, G. R. *Nature* **2007**, *446*, 782. doi:10.1038/nature05678.
(20) Egorova, D. *Chem. Phys.* **2008**, *347*, 166. doi:10.1016/j.chemphys.2007.12.019.
(21) Nemeth, A.; Milota, F.; Mančal, T.; Lukeš, V.; Kauffmann, H. F.; Sperling, J. *Chem. Phys. Lett.* **2008**, *459*, 94. doi:10.1016/j.cplett.2008.05.057.
(22) Turner, D. B.; Wilk, K. E.; Curmi, P. M. G.; Scholes, G. D. *J. Phys. Chem. Lett.* **2011**, *2*, 1904. doi:10.1021/jz200811p.
(23) Caram, J. R.; Lewis, N. H. C.; Fidler, A. F.; Engel, G. S. *J. Chem. Phys.* **2012**, *136*, 104505. doi:10.1063/1.3690498.
(24) Mancal, T.; Bixner, O.; Christensson, N.; Hauer, J.; Milota, F.; Nemeth, A.; Sperling, J.; Kauffmann, H. *Procedia Chem.* **2011**, *3*, 105. doi:10.1016/j.proche.2011.08.017.
(25) Butkus, V.; Zigmantas, D.; Valkunas, L.; Abramavičius, D. *Chem. Phys. Lett.* **2012**, *515*, 40. doi:10.1016/j.cplett.2012.07.014.
(26) Butkus, V.; Valkunas, L.; Abramavičius, D. *ArXiv* **2012**, 1205.3383v2. doi:10.1063/1.4737843.
(27) Seibt, J.; Pullerits, T. *J. Phys. Chem. C* **2013**, *117*, 18728. doi:10.1021/jp406103m.
(28) Panitchayangkoon, G.; Hayes, D.; Fransted, K. A.; Caram, J. R.; Harel, E.; Wen, J.; Blankenship, R. E.; Engel, G. S. *Proc. Natl. Acad. Sci. U.S.A.* **2010**, *107*, 12766. doi:10.1073/pnas.1005484107.
(29) Christensson, N.; Kauffmann, H. F.; Pullerits, T.; Mančal, T. *J. Phys. Chem. B* **2012**, *116*, 7449. doi:10.1021/jp304649c.
(30) Tiwari, V.; Peters, W. K.; Jonas, D. M. *Proc. Natl. Acad. Sci. U.S.A.* **2013**, *110*, 1203. doi:10.1073/pnas.1211157110.

(31) Chin, A. W.; Prior, J.; Rosenbach, R.; Caycedo-Soler, F.; Huelga, S. F.; Plenio, M. B. *Nat. Phys.* **2013**, *9*, 113. doi:10.1038/nphys2515.

(32) Chenu, A.; Christensson, N.; Kauffmann, H. F.; Mančal, T. *Scientific Reports* **2013**, *3*, 2029.

(33) Yuen-Zhou, J.; Krich, J. J.; Aspuru-Guzik, A. *J. Chem. Phys.* **2012**, *136*, 234501. doi:10.1063/1.4725498.

(34) Mančal, T.; Christensson, N.; Lukéš, V.; Milota, F.; Bixner, O.; Kauffmann, H. F.; Hauer, J. *J. Phys. Chem. Lett.* **2012**, *3*, 1497. doi:10.1021/jz300362k.

(35) Dostál, J.; Mančal, T.; Vácha, F.; Pšenčík, J.; Zigmantas, D. Submitted **2013**.

(36) Ma, Y. Z.; Aschenbrücker, J.; Miller, M.; Gillbro, T. *Chem. Phys. Lett.* **1999**, *300*, 465. doi:10.1016/S0009-2614(98)01368-2.

(37) Förster, T. *Ann. Phys.* **1948**, *2*, 55. doi:10.1002/andp.19484370105.

(38) Sumi, H. *J. Phys. Chem. B* **1999**, *103*, 252. doi:10.1021/jp983477u.

(39) Jang, S.; Newton, M. D.; Silbey, R. J. *Phys. Rev. Lett.* **2004**, *92*, 218301. doi:10.1103/PhysRevLett.92.218301.

(40) Mančal, T. In *Quantum Effects in Biology*; Mohseni, M., Omar, Y., Engel, G. S., Plenio, M. B., Eds.; Cambridge University Press: Cambridge, UK, 2013; Chapter Principles of Multi-Dimensional Electronic Spectroscopy.

(41) Mukamel, S. *Principles of nonlinear spectroscopy*; Oxford University Press: Oxford, UK, 1995.

(42) Mukamel, S.; Rupasov, V. *Chem. Phys. Lett.* **1995**, *242*, 17. doi:10.1016/0009-2614(95)00648-N.

(43) Yang, M.; Fleming, G. R. *J. Chem. Phys.* **1999**, *111*, 27. doi:10.1063/1.479359.

(44) Jonas, D. M. *Annu. Rev. Phys. Chem.* **2003**, *54*, 425. doi:10.1146/annurev.physchem.54.011002.103907.

(45) Chenu, A.; Maly, P.; Mančal, T. *arXiv:1306.1693*, **2013**.

(46) Jiang, X.-P.; Brumer, P. *J. Chem. Phys.* **1991**, *94*, 5833. doi:10.1063/1.460467.

PAPER IV

2D electronic spectroscopy reveals excitonic structure in the baseplate of a chlorosome

Jakub Dostál[1,2], František Vácha[3], Jakub Pšenčík[2], Donatas Zigmantas[1]

[1]*Department of Chemical Physics, Lund University, P.O. Box 124, 221 00 Lund, Sweden*
[2]*Faculty of Mathematics and Physics, Charles University, Ke Karlovu 3, 121 16 Prague, Czech Republic*
[3]*Faculty of Science, University of South Bohemia, Branišovská 31, 370 05 České Budějovice, Czech Republic*

In green photosynthetic bacteria the chlorosome baseplate mediates excitation energy transfer from the interior of light-harvesting antenna chlorosome towards the reaction centers. However, the electronic states of the baseplate remain unexplored, hindering the mechanistic understanding of the baseplate as an excitation energy collector and mediator. Here we use two-dimensional spectroscopy to study the excited state structure and internal energy relaxation in the baseplate of green sulfur bacterium *Chlorobaculum tepidum*. We resolved an exciton system with four energy states, indicating that the organization of the pigments in the baseplate is more complex than was thought before and constitutes at least four bacteriochlorophyll molecules in a close contact. Based on the finding that the energy of the baseplate states is in the same range as in the Fenna-Matthews-Olson complex we propose a "lateral" energy transfer pathway, where excitation energy can flow through the photosynthetic unit via the lowest states of individual complexes.

Chlorosomes serve the light-harvesting function for representatives of distinct groups of photosynthetic bacteria: green sulfur bacteria, green filamentous bacteria and acidobacteria [1–4]. The main structural and functional properties of the chlorosome are determined by the strong exciton interaction between a large number of self-assembled pigments. Chlorosomes typically contain $\sim 10^5$ bacteriochlorophyll (BChl) *c*, *d* or *e* molecules co-aggregated with smaller amounts of carotenoids, quinones and lipids and it is surrounded by the lipid-protein envelope [1–6].

The baseplate pigment-protein complex is attached to the side of chlorosome facing the cytoplasmic membrane and is built up from the CsmA proteins binding BChls *a* [1–4]. The structure of the CsmA from green sulfur bacterium *Chlorobaculum (Cba.) tepidum* was determined by NMR [7]. The CsmA proteins are arranged in a two-dimensional crystalline lattice with a spacing of 3.2–3.3 nm directly observable by electron cryomicroscopy [6,8]. In *Cba. tepidum* the baseplate lattice intersects the long axis of the chlorosome at an ~40°

angle [6] However, the exact arrangement of the CsmA proteins within the baseplate, the pigment-binding geometry and stoichiometry have not yet been determined. The presence of a single conserved histidine residue in the CsmA sequence suggests there is one BChl *a* molecule per CsmA [9], while the experimentally obtained stoichiometry is 1–3 BChl *a* molecules per CsmA [10–12]. Structural studies suggests that the baseplate building block is a CsmA dimer [13]. Furthermore, based on the circular dichroism studies, the presence of a BChl *a* dimer in the baseplate of green sulfur bacteria was proposed [14,15]. Interestingly, the exciton circular dichroism signal was not observed for the isolated baseplate from green filamentous bacterium *Chloroflexus aurantiacus* [12]. A model of the baseplate based on the available information was built by Pedersen and coworkers [9]. Despite all this progress the energy structure of the baseplate is unknown.

The photosynthetic process in green sulfur bacteria begins with the capture of sunlight by the strongly absorbing BChl *c* aggregate. Initially formed delocalized excitations (excitons) randomly diffuse in the disordered chlorosome interior on the sub-100 fs timescale, as was recently observed in two-dimensional electronic spectroscopy (2DES) studies [16]. This process is followed by relaxation to the lower energy states of the BChl aggregates in 100–1000 fs [17–21] before the excitation is transferred to the baseplate on a 10–100 ps timescale [22,23]. The aggregate to baseplate transfer time depends on the species; for the BChl *c* containing green sulfur bacteria it was determined to be 30–40 ps [22,24]. In green sulfur bacteria and acidobacteria the excitation energy is transferred from the baseplate putatively through the Fenna-Matthews-Olson (FMO) protein to the reaction center (RC).

In this study we used the 2DES technique to explore spectral properties of the baseplate as well as the functional connectivity between the baseplate and the low-lying exciton states of the BChl *c* aggregate. Chlorosomes were isolated from the green sulfur bacterium *Cba. tepidum* and measured at 77 K. The 2DES method utilizes the third order (in the interaction with the laser fields) response of the sample and provides simultaneously high temporal and spectral resolution that is not available in a conventional pump-probe experiment. The real part of the measured 2D spectrum can be interpreted as a collection of transient absorption spectra with an additional spectral resolution along the excitation frequency. The analysis of the obtained 2D spectra of chlorosomes provided information about the energetic structure and excitation dynamics from the low-lying states of BChl *c* aggregate to- and within- the baseplate. Important implications of these

observations for the energy transfer from the baseplate to FMO in the intact photosystems are discussed.

The low temperature (77 K) absorption spectrum of isolated chlorosomes (Fig. 1) is dominated by the BChl *c* aggregate band peaking at 13280 cm^{-1} (753 nm). The weak, relatively broad and structureless absorption band of the baseplate complex with maximum at 12550 cm^{-1} (797 nm) is visible in its red part. This band appears only as a shoulder of the strong aggregate band at the room temperature. In order to avoid the excessive excitation of the BChl *c* aggregate the broad laser spectrum was centered at 12050 cm^{-1} (830 nm). Hence, the blue side of the laser spectrum covered the absorption of the baseplate and only the red edge of the aggregate absorption.
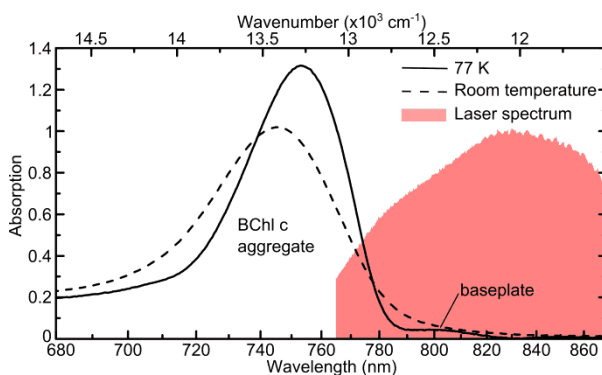
Figure 1: Absorption spectra of isolated chlorosomes from Cba. tepidum *at room temperature (294 K) and at 77 K. The laser spectrum used in the 2DES experiments is also shown.*

Both the baseplate and aggregate are clearly visible in the acquired 2D spectra (Fig. 2). At early population times (Fig. 2, 30 fs spectrum) the positive baseplate signal has the shape resembling a right triangle, filling the space above the diagonal. Along the diagonal it extends between 12120 cm^{-1} and 12700 cm^{-1} with a maximum at ~12500 cm^{-1}, which corresponds well to the absorption spectrum. The shape of the baseplate signal is determined by an overlap of the stimulated emission (SE), ground state bleach (GSB) and excited state absorption (ESA) signals. The positively signed SE from several energy states extends along the diagonal (A1-D4 in Fig. 2). The GSB signal covers a corresponding square area (framed by the lines A, D, 1 and 4 in Fig. 2), and is cancelled by the negative ESA signal below the diagonal. Together the contributions results in a triangular-shaped positive signal with an intense diagonal part. Such signals are typical signatures of excitonic systems of several coupled chromophores (see discussion below).
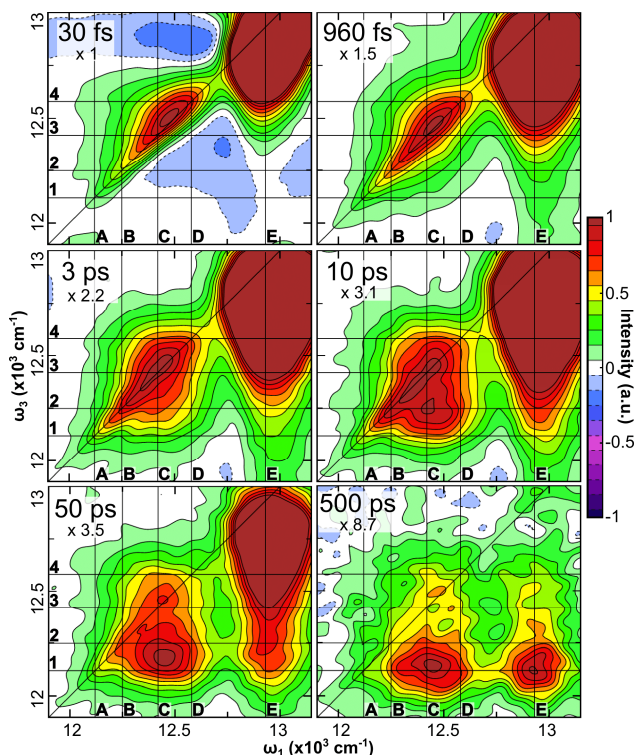
Figure 2: 2D spectra of isolated chlorosomes from Cba. tepidum *measured at 77 K. Each frame is normalized to the baseplate maximum signal and the corresponding multiplication factor is given. Vertical and horizontal lines indicate the presumed positions of the energy states in the baseplate (D4: 12590 cm^{-1} (794 nm), C3: 12420 cm^{-1} (805 nm), B2: 12260 cm^{-1} (816 nm), A1: 12120 cm^{-1} (825 nm)). The additional vertical line E in the chlorosome region is drawn at 12940 cm^{-1} (773 nm).*

Due to the finite laser spectrum and limited measured detection frequency range only the red edge of the BChl *c* aggregate peak is visible in the 2D spectra appearing at excitation frequencies higher than 12700 cm^{-1}. The peak has an asymmetric shape extending below the diagonal, which is caused by the location of the very strong peak close to the spectral detection edge and by its broad line shape. Therefore the low energy tail that is present in the early-time spectrum (Fig. 2, 30 fs spectrum, positions E3 and E4) should not be interpreted as cross-peaks connecting the aggregate and baseplate transitions, which would indicate strong excitonic interaction between the two.

By following the time-evolution of the baseplate 2D spectrum four electronic transitions were identified on the basis of the following arguments. A cross-peak C2 is clearly visible in the 10 ps 2D spectrum at an approximate (ω_1, ω_3) position of (12420, 12260) cm^{-1}, indicating energy transfer between the two states located at the corresponding energies (lines 2 and 3). Energy relaxation then

continues on a longer timescale into an almost dark low-lying state located at approximately 12120 cm^{-1} (see 500 ps 2D spectrum, line 1), allowing us to assign the lowest exciton state. Lastly, upon inspection of the 30 fs 2D spectrum it is clear that the three states identified so far are not sufficient to explain the baseplate signal, that extends to much higher energies, indicating the presence of at least one additional energy state, tentatively located at 12590 cm^{-1} (line 4 in Fig. 2).
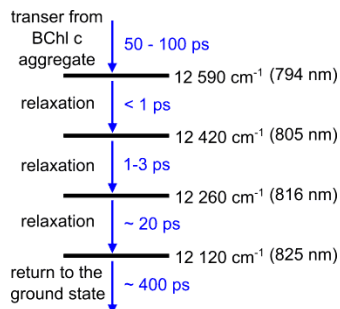
Figure 3: Proposed scheme of the exciton relaxation in the baseplate complex.

To evaluate the energy transfer dynamics in the observed spectral region the kinetic traces in individual points of the 2D spectrum were fitted by a sum of exponentials. Quantitative analysis of the transfer rates between the individual energy states is relatively difficult, as all points in the 2D spectrum exhibit complex multiexponential decays (see Fig. S1 and S2 of the Supporting Information). However, a few salient conclusions can be made. In the baseplate part of the 2D spectra the longest timescale (~400 ps) can be associated with the baseplate returning to the ground state. This causes a decay of the GSB contribution that extends below the entire 2D spectrum due to the excitonic interactions. The fastest processes (spanning the range of 0.3–20 ps), on the other hand, can be connected to population relaxation between individual excitonic states of the baseplate. This transfer is reflected in the 2D spectra as redistribution of the SE signals (fading of the diagonal peaks and appearance of the cross-peaks below the diagonal), accompanied by shifting of the ESA towards higher energies. The tentative assignment of the rate constants to particular energy transfer steps is carried out by comparing the rise and decay components of the individual fits. We estimate that the first exciton relaxation step in the baseplate occurs on the time scale of few hundred femtoseconds, the second step in a few picoseconds, and the last step in ~20 ps (see Fig. 3).

Now we examine the energy transfer from BChl *c* aggregate to the baseplate, which is clearly visible in the time-evolution of the 2D spectrum. The

diagonal peak of the aggregate does not completely disappear before ~200 ps (see Fig. S1 of the Supporting Information), indicating slow energy transfer. This peak decays multiexponentially, which is caused by a combination of several processes: i) exciton annihilation due to multiple photon excitations, ii) exciton relaxation within the aggregate and iii) energy transfer to the baseplate. Superimposed on the population dynamics oscillatory quantum coherence dynamics (identical to the observations in [25]) are visible during the initial 1.8 ps (see Fig. S3 of the Supporting Information). Since the energy transfer from the BChl c aggregate to the baseplate is much slower than the relaxation within the baseplate exciton manifold, the transient populations in the higher baseplate states are rather low, as evidenced by the weak cross-peaks E2–4 (Fig. 2). On the other hand, appearance of energy transfer cross-peak at the baseplate lowest energy state (E1) is evident. All baseplate cross-peaks indicating energy flow from the aggregate to the baseplate (E1–4) exhibit significantly longer rise times than the corresponding cross-peaks appearing after direct baseplate excitation (D1–3, C1, C2, B1) (see Fig. S2 of the Supporting Information). This confirms that the BChl c aggregate feed the baseplate with energy on rather long timescales, here estimated to be in the order of 50–100 ps, well in the range of previously reported observations [22–24].

The baseplate 2D spectrum exhibits all features of a complex exciton system of at least four coupled pigments. As discussed above, the presence of four energy states of a single exciton band was identified based on their different energies and distinct dynamical properties. The most prominent feature is that all excitonic states share a common ground state and are therefore connected by an off-diagonal GSB signal. The ESA falls almost into the same region as it corresponds to transitions to the double exciton band.

We can thus deduce that at least four excitonically coupled BChl a molecules are in close contact within the baseplate structure. This is in contrast to previously presented models where a BChl a dimer was assumed [9,14,15]. However, it is not clear whether two BChl a molecules are bound by a single CsmA protein, which then form a dimer as previously proposed [9,13], or if the proteins form a tetramer (or even more complicated structure) binding a single BChl a each.

The relative orientations of the four transition dipole moments of the tetramer constituents determine the distribution of oscillator strength among the individual excitonic transitions. The baseplate 2D signal is concentrated in two higher lying states (see Fig. 2, 30 fs spectrum). In agreement with the exciton

theory [26] these states exhibit the strongest ESA to the double exciton band, which explains the location of the ESA signal below the diagonal and consequently the upper-triangular shape of the 2D spectrum at early times. This indicates that the arrangement of transition dipole moments in the tetramer is closer to the H aggregate (parallel) than J-aggregate (head-to-tail) arrangement. However, the structure seems to be more complicated since the transition to the highest lying single exciton state would be the only allowed one, if the tetramer was an ideal H-aggregate.

It is instructive to discuss the electronic transitions (energy states) of the baseplate in a context of the light capture function of green sulfur bacteria. We find that the baseplate states are located in the same spectral region as the states of the FMO complex (Fig. 4). It has been assumed that the FMO protein acts as a "molecular wire" by receiving an excitation to its high energy states located in a close proximity to the baseplate. Excitations then relax through the exciton manifold of FMO to the lowest state located on the other side of the complex, close to the RC, thus facilitating energy trapping by RC [27,28]. However, observations presented here suggest an alternative design and function of the excitation energy transfer network. We find that even the highest energy state in the baseplate is of comparable energy to the highest states in FMO, which are usually placed in the range of 12620–12890 cm^{-1} (for a review see [28]). A similar match is found for the lowest energy states of the baseplate and FMO (the FMO lowest state is located at 12110–12140 cm^{-1} [28]). The energy relaxation within the baseplate observed in this study would thus be a competing process to the energy transfer directly to the highest energy states of FMO. The fraction of excitations that relax to the low-lying baseplate states in the intact photosynthetic unit depends on the energy transfer rate to FMO, which is not known. It is reasonable to expect that excitations that end up in the lower baseplate states are not lost but are "laterally" transferred into the lower FMO states (Fig. 4). Interestingly, the energy states of the RC internal antenna are also located in a similar energy range as the states in FMO and the baseplate [29,30]. Therefore the presence of FMO does not seem to be necessary from the energetic point of view. Perhaps it has a dual function, as a spacer, which allows ferredoxin to access RCs putatively located under the chlorosome, and at the same time, as the energy conduit, transferring excitation energy from the baseplate to the RCs. Ferredoxins are water soluble electron acceptors employed by type I RC, which are found in green sulfur bacteria and acidobacteria, but not by type II RCs, which might explain the absence of FMO in green filamentous bacteria.
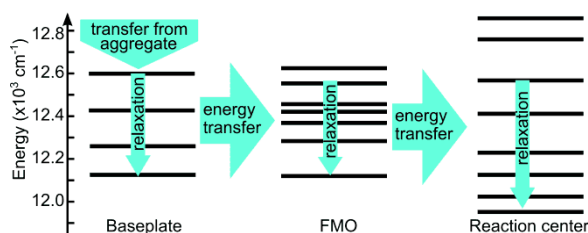
Figure 4: Proposed scheme of energy transfer within the photosynthetic apparatus of Cba. tepidum. *The positions of energy states in FMO and RC are based on the values reported in* [31] *and* [29] *respectively.*

The overall energy flow through the photosynthetic unit of green sulfur bacteria is apparently very complex and depends on the relaxation rates within subunits and of energy transfer rates between the different states in the subunits. We expect that the 2DES experiments on the intact photosynthetic units should be able to unravel the complexity of the energy collection function.

In conclusions, the energy structure of the baseplate exhibits spectroscopic features typical of an excitonic system of four coupled molecules, implying that the baseplate structure is more complex than it was believed before. After the excitation energy is transferred to the baseplate from the BChl *c* aggregate on a 50–100 ps timescale excitation relaxes between the individual states; each energy transfer step occurring on a distinctive timescale. The energy of the baseplate states suggests an alternative energy flow pathway in the photosynthetic unit of green sulfur bacteria where the excitations captured by the chlorosome is transferred via the lowest states of the baseplate and FMO complexes to the RC.

EXPERIMETAL METHODS

The *Chlorobaculum tepidum* cell culture was grown as described previously [32] and chlorosomes were isolated and purified according to the standard procedure using two successive sucrose gradient ultracentrifugation steps [33] Prior to experiments, the chlorosome solution was dissolved in 1:2 (v/v) ratio in glycerol, reduced by 20 mM sodium dithionite and incubated for 2 hour in an air-tight vessel. The sample optical density was approximately 0.05 in the baseplate region at 12500 cm^{-1} in the 0.5 mm optical path demountable cell. All 2DES experiments were carried at 77 K in an optical cryostat (Oxford Optistat DN). The energy of excitation pulses was 1.5 nJ per pulse and the beams were focused to the spot size of ~100 μm in diameter.

The 2D spectra were obtained using a setup described in detail elsewhere [34,35]. Briefly, a solid state KGW amplified laser system (Pharos, Light

Conversion) pumped a homemade NOPA producing 17-fs pulses centered at 12050 cm^{-1} (FWHM 1380 cm^{-1}) at 20 kHz repetition rate. Each pulse was split into four equal parts by a beamsplitter and a transmissive diffractive grating. The resulting four pulses were ordered in time using conventional optical delay lines (for the population time delays) and by inserting variable amount of fused silica in their optical paths (for the coherence time delays). One beam, serving as the local oscillator (LO), was further attenuated by an OD 3 neutral density filter, and all four pulses were focused in box-car geometry on a single spot at the sample. As the result of the sample interaction with the three laser pulses the signal pulse is emitted into the phase matching direction coinciding with the direction of LO, it is mixed with the LO and after passing through the spectrometer is detected by a CCD camera. Two of the excitation pulses were modulated by optomechanical choppers operating at different frequencies. Lock-in detection on the sum and difference frequency was used to discriminate the signal against scattered light. During the experiments the time delay between the first two pulses (coherence time) was systematically scanned from −200 fs to 250 fs with 2 fs steps giving spectral resolution of about 65 cm^{-1} along the excitation axis. 50 cm^{-1} spectral resolution was achieved along the detection frequency axis, as determined by the time domain window used in the Fourier analysis.

ACKNOWLEDGEMENT

REFERENCES

1. Frigaard N-U, Bryant DA (2006) Chlorosomes: Antenna Organelles in Photosynthetic Green Bacteria. In Shively J (ed.), *Complex Intracellular Structures in Prokaryotes* pp 79–114. Springer Berlin / Heidelberg.

2. Bryant DA, Costas AMG, Maresca JA, Chew AGM, Klatt CG, Bateson MM, Tallon LJ, Hostetler J, Nelson WC, Heidelberg JF, et al. (2007) Candidatus Chloracidobacterium thermophilum: An aerobic phototrophic acidobacterium. *Science* **317**: 523–526.

3. Blankenship RE, Matsuura K (2003) Antenna complexes from green photsynthetic bacteria. In Green BR, Parson WW (eds.), *Light-harvesting antennas in photosynthesis* pp 195–217. Kluwer Academic Publishers, Dordrecht.

4. Blankenship RE, Olson JM, Miller M (1995) Antenna Complexes from Green Photosynthetic Bacteria. In Blankenship R, Madigan M, Bauer C (eds.), *Anoxygenic Photosynthetic Bacteria* pp 399–435. Springer Netherlands.

5. Orf GS, Blankenship RE (2013) Chlorosome antenna complexes from green photosynthetic bacteria. *Photosynth Res* **116**: 315–331.

6. Oostergetel GT, van Amerongen H, Boekema EJ (2010) The chlorosome: a prototype for efficient light harvesting in photosynthesis. *Photosynth Res* **104**: 245–255.

7. Pedersen MØ, Underhaug J, Dittmer J, Miller M, Nielsen NC (2008) The three-dimensional structure of CsmA: a small antenna protein from the green sulfur bacterium Chlorobium tepidum. *FEBS Lett* **582**: 2869–2874.

8. Pšenčík J, Collins AM, Liljeroos L, Torkkeli M, Laurinmäki P, Ansink HM, Ikonen TP, Serimaa RE, Blankenship RE, Tuma R, et al. (2009) Structure of chlorosomes from the green filamentous bacterium Chloroflexus aurantiacus. *J Bacteriol* **191**: 6701–6708.

9. Pedersen MØ, Linnanto J, Frigaard N-U, Nielsen NC, Miller M (2010) A model of the protein – pigment baseplate complex in chlorosomes of photosynthetic green bacteria. *Photosynth Res* **104**: 233–243.

10. Bryant DA, Vassilieva E V, Frigaard N, Li H (2002) Selective protein extraction from Chlorobium tepidum chlorosomes using detergents. Evidence that CsmA forms multimers and binds bacteriochlorophyll a. *Biochemistry* **41**: 14403–14411.

11. Sakuragi Y, Frigaard N, Shimada K, Matsuura K (1999) Association of bacteriochlorophyll a with the CsmA protein in chlorosomes of the photosynthetic green filamentous bacterium Chloroflexus aurantiacus. *Biochim Biophys Acta* **1413**: 172–180.

12. Montaño GA, Wu H-M, Lin S, Brune DC, Blankenship RE (2003) Isolation and characterization of the B798 light-harvesting baseplate from the chlorosomes of Chloroflexus aurantiacus. *Biochemistry* **42**: 10246–10251.

13. Vassilieva E V, Stirewalt VL, Jakobs CU, Frigaard N-U, Inoue-Sakamoto K, Baker M a, Sotak A, Bryant D a (2002) Subcellular localization of chlorosome proteins in Chlorobium tepidum and characterization of three new chlorosome proteins: CsmF, CsmH, and CsmX. *Biochemistry* **41**: 4358–4370.

14. Gerola PD, Olson JM (1986) A new bacteriochlorophyll a-protein complex associated with chlorosomes of green sulfur bacteria. *Biochim Biophys Acta - Bioenerg* **848**: 69–76.

15. Pedersen MØ, Pham L, Steensgaard DB, Miller M (2008) A reconstituted light-harvesting complex from the green sulfur bacterium Chlorobium tepidum containing CsmA and bacteriochlorophyll a. *Biochemistry* **47**: 1435–1441.

16. Dostál J, Mančal T, Augulis R, Vácha F, Pšenčík J, Zigmantas D (2012) Two-dimensional electronic spectroscopy reveals ultrafast energy diffusion in chlorosomes. *J Am Chem Soc* **134**: 11611–11617.

17. Savikhin S, Zhu Y, Blankenship RE, Struve WS (1996) Intraband energy transfers in the BChl c antenna of chlorosomes from the green photosynthetic bacterium Chloroflexus aurantiacus. *J Phys Chem* **100**: 17978–17980.

18. Martiskainen J, Linnanto J, Kananavičius R, Lehtovuori V, Korppi-Tommola J (2009) Excitation energy transfer in isolated chlorosomes from Chloroflexus aurantiacus. *Chem Phys Lett* **477**: 216–220.

19. Martiskainen J, Linnanto J, Aumanen V, Myllyperkiö P, Korppi-Tommola J (2012) Excitation energy transfer in isolated chlorosomes from Chlorobaculum tepidum and Prosthecochloris aestuarii. *Photochem Photobiol* **88**: 675–683.

20. Savikhin S, van Noort PI, Zhu Y, Lin S, Blankenship RE, Struve WS (1995) Ultrafast energy transfer in light-harvesting chlorosomes from the green sulfur bacterium Chlorobium tepidum. *Chem Phys* **194**: 245–258.

21. Pšenčík J, Ma Y-Z, Arellano JB, Hála J, Gillbro T (2003) Excitation energy transfer dynamics and excited-state structure in chlorosomes of Chlorobium phaeobacteroides. *Biophys J* **84**: 1161–1179.

22. Causgrove TP, Brune DC, Blankenship RE (1992) Förster energy transfer in chlorosomes of green photosynthetic bacteria. *J Photochem Photobiol B Biol* **15**: 171–179.

23. Causgrove TP, Brune DC, Wang J, Wittmershaus BP, Blankenship RE (1990) Energy transfer kinetics in whole cells and isolated chlorosomes of green photosynthetic bacteria. *Photosynth Res* **26**: 39–48.

24. Van Noort PI, Zhu Y, LoBrutto R, Blankenship RE (1997) Redox effects on the excited-state lifetime in chlorosomes and bacteriochlorophyll c oligomers. *Biophys J* **72**: 316–325.

25. Dostál J, Mančal T, Vácha F, Augulis R, Pšenčík J, Zigmantas D (2013) Fast exciton dynamics and coherent oscillations revealed by coherent 2D spectroscopy in chlorosomes. *EPJ Web Conf* **41**: 08015.

26. Van Amerongen H, Valkunas L, Van Grondelle R (2000) *Photosynthetic Excitons*. World Scientific.

27. Schmidt Am Busch M, Müh F, El-Amine Madjet M, Renger T (2011) The eighth bacteriochlorophyll completes the excitation energy funnel in the FMO protein. *J Phys Chem Lett* **2**: 93–98.

28. Milder MTW, Brüggemann B, van Grondelle R, Herek JL (2010) Revisiting the optical properties of the FMO protein. *Photosynth Res* **104**: 257–274.

29. Hauska G, Schoedl T, Remigy H, Tsiotis G (2001) The reaction center of green sulfur bacteria. *Biochim Biophys Acta* **1507**: 260–277.

30. Permentier HP, Schmidt KA, Kobayashi M, Akiyama M, Hager-Braun C, Neerken S, Miller M, Amesz J (2000) Composition and optical properties of reaction centre core complexes from the green sulfur bacteria Prosthecochloris aestuarii and Chlorobium tepidum. *Photosynth Res* **64**: 27–39.

31. Abramavicius D, Voronine D V, Mukamel S (2008) Double-quantum resonances and exciton-scattering in coherent 2D spectroscopy of photosynthetic complexes. *Proc Natl Acad Sci U S A* **105**: 8525–8530.

32. Pšenčík J, Ikonen TP, Laurinmäki P, Merckel MC, Butcher SJ, Serimaa RE, Tuma R (2004) Lamellar organization of pigments in chlorosomes, the light harvesting complexes of green photosynthetic bacteria. *Biophys J* **87**: 1165–1172.

33.   Steensgaard DB, Matsuura K, Cox RP, Miller M (1997) Changes in bacteriochlorophyll c organization during acid treatment of chlorosomes from Chlorobium tepidum. *Photochem Photobiol* **65**: 129–134.

34.   Augulis R, Zigmantas D (2011) Two-dimensional electronic spectroscopy with double modulation lock-in detection: enhancement of sensitivity and noise resistance. *Opt Express* **19**: 13126–13133.

35.   Augulis R, Zigmantas D (2013) Detector and dispersive delay calibration issues in broadband 2D electronic spectroscopy. *J Opt Soc Am B* **30**: 1770–1774.

2D electronic spectroscopy reveals excitonic structure in the baseplate of a chlorosome

Jakub Dostál[1,2], František Vácha[3], Jakub Pšenčík[2], Donatas Zigmantas[1]

[1]*Department of Chemical Physics, Lund University, P.O. Box 124, 221 00 Lund, Sweden*
[2]*Faculty of Mathematics and Physics, Charles University, Ke Karlovu 3, 121 16 Prague, Czech Republic*
[3]*Faculty of Science, University of South Bohemia, Branišovská 31, 370 05 České Budějovice, Czech Republic*
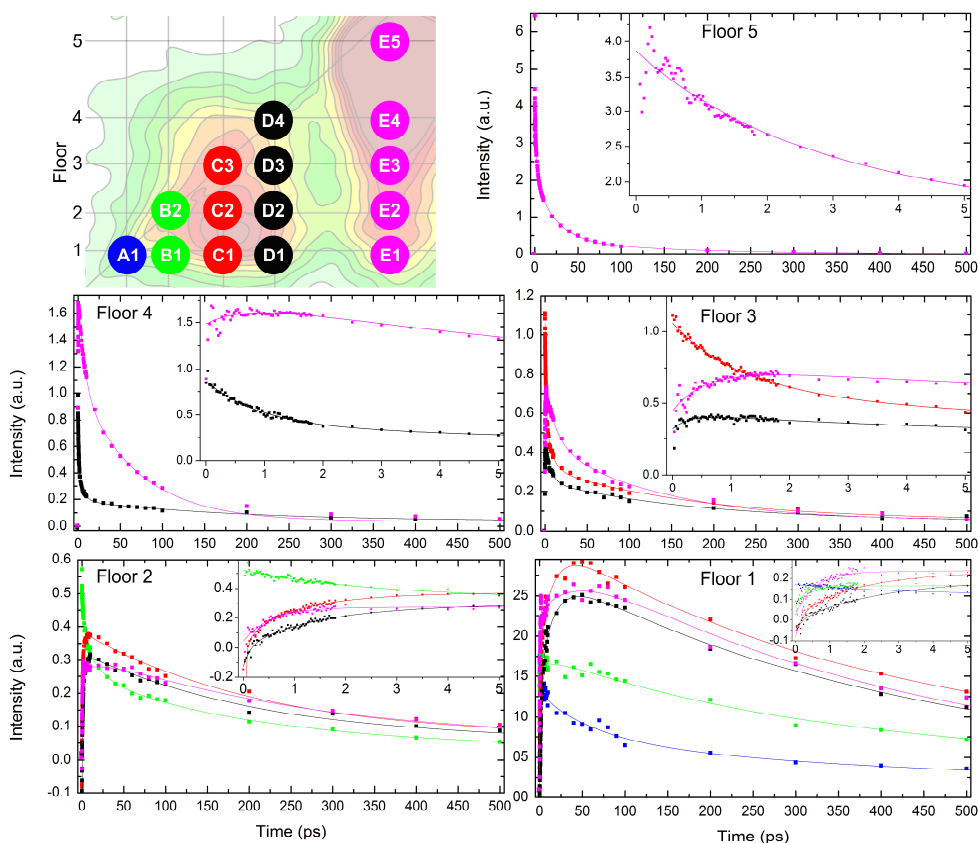
Figure S1: Time evolution of the individual points in the 2D spectrum fit by multiple decaying exponentials. Each graph contains time evolution curves of a set of distinctive peaks at the same detection frequency (ω₃) and different excitation frequency (ω₁). The color coding of curves is according to the legend in the top-left-handed corner, where each color disc corresponds to one

SUPPORTING INFORMATION

diagonal peak or cross-peak arranged as in the experimental 2D spectrum and denoted by the gridline markers (Fig. 2).

				Chlorosome
				(2.3 ± 0.4) ps ↓ 46% of 3.87 (20 ± 10) ps ↓ 43% (140 ± 200) ps ↓ 11%
			(0.89 ± 0.09) ps ↓ 51% of 0.86 (6 ± 1) ps ↓ 27% (185 ± 60) ps ↓ 18% ∞ 4%	(0.7 ± 0.2) ps ↑ -17% of 1.79 (7 ± 2) ps ↓ 39% (67 ± 8) ps ↓ 59% 2%
		(1.2 ± 0.1) ps ↓ 44% of 1.06 (7 ± 2) ps ↓ 25% (170 ± 30) ps ↓ 25% 5%	(0.26 ± 0.05) ps ↑ -24% of 0.43 (7.5 ± 0.9) ps ↓ 42% (180 ± 30) ps ↓ 47% ∞ 11%	(0.59 ± 0.08) ps ↑ -41% of 0.76 (12 ± 3) ps ↑ -40% (130 ± 30) ps ↓ 53% ∞ 7%
	(2.0 ± 0.4) ps ↓ 25% of 0.52 (17 ± 7) ps ↓ 25% (210 ± 50) ps ↓ 43% ∞ 7%	(0.03 ± 0.01) ps ↑ -205% of 0.38 (0.4 ± 0.2) ps ↑ -42% (1.5 ± 0.4) ps ↑ -57% (220 ± 20) ps ↓ 84% ∞ 16%	(0.13 ± 0.07) ps ↑ -40% of 0.32 (1 ± 1) ps ↑ -57% (3 ± 3) ps ↑ -42% (220 ± 30) ps ↓ 84% ∞ 16%	(0.55 ± 0.05) ps ↑ -71% of 0.32 (30 ± 30) ps ↑ -15% (280 ± 90) ps ↓ 84% ∞ 16%
Baseplate: (2.8 ± 0.8) ps ↓ 25% of 0.17 (60 ± 60) ps ↓ 31% (400 ± 800) ↓ 14% ∞ 11%	(0.26 ± 0.03) ps ↑ -62% of 0.18 17 ps ↑ -7% (400 ± 100) ps ↓ 78% ∞ 22%	(0.16 ± 0.06) ps ↑ -31% of 0.32 (1.4 ± 0.3) ps ↑ -55% (16 ± 5) ps ↑ -40% (390 ± 90) ps ↓ 83% ∞ 17%	(0.2 ± 0.2) ps ↑ -15% of 0.29 (1.9 ± 0.5) ps ↑ -55% (17 ± 7) ps ↑ -48% (400 ± 100) ps ↓ 88% ∞ 12%	(0.53 ± 0.05) ps ↑ -65% of 0.32 (40 ± 30) ps ↑ -27% (400 ± 200) ps ↓ 88% ∞ 12%

Figure S2: Time constants of and relative amplitudes obtained from multiexponential fits of individual points in the 2D spectrum. Each cell contains information about the evolution of the single distinct peak in the 2D spectrum. The cells are arranged in the way the peaks appear in the 2D spectrum. The color-coding is identical as in Supplementary Fig. 1. Decaying and rising components are marked by the black and red colors, correspondingly. The total amplitude of each curve is marked at the right side of each cell.

Figure S3: Coherent oscillations observed in the diagonal peak of the BChl c aggregate.

PAPER V

Tracking energy flow through the intact photosynthetic apparatus in vivo

[1,2]Jakub Dostál, [2]Jakub Pšenčík, [1]Donatas Zigmantas

[1]*Department of Chemical Physics, Lund University, P.O. Box 124, SE-22100 Lund, Sweden*
[2]*Faculty of Mathematics and Physics, Charles University, Ke Karlovu 3, 121 16 Prague, Czech Republic*

Sunlight absorption by a photosynthetic unit is the first step in photosynthesis that provides energy for the vast majority of living organisms on Earth. The photophysical processes in complexes extracted from photosynthetic organisms have been studied in great detail using various spectroscopic techniques including two-dimensional electronic spectroscopy [1,2]. Energy and electron transfer rates and efficiencies have been determined for a variety of isolated light-harvesting complexes and reaction centers. At the same time, the energy transfer within the complete photosynthetic apparatus has never been monitored, preventing comprehensive understanding of these processes. We present direct observation of the energy flow through entire photosynthetic system in the intact green sulfur bacteria. By using two-dimensional electronic spectroscopy we directly mapped connections between the light-harvesting antenna chlorosome, intermediate Fenna-Matthews-Olson complex and reaction center. We show that whereas energy transfer within individual complexes proceeds on a sub-picosecond scale, energy flows with moderate speed of tens of picoseconds between the subunits. Our study provides hitherto unavailable information about connectivity and organization of photosynthetic unit in green sulfur bacteria and opens new venues for modeling intact photosynthetic systems [3]. We envision that intact photosynthetic machinery of variety of organism will be explored in vivo with the two-dimensional spectroscopy and will eventually enable to complete the picture of energy capture and funneling in photosynthesis.

Green sulfur bacteria are photosynthetic organisms adapted to energy-limited conditions and can be found in the aqueous environments at the depth below 100 m and even in the proximity of the black smokers at two and half kilometers below the ocean surface [4,5]. Very low light environments necessitated these organisms to develop highly efficient light-capture machinery. The photosynthetic apparatus of a model organism for green sulfur bacterium, *Chlorobaculum* (*Cba*.) *tepidum* consists of an assembly of several complexes: chlorosome, Fenna-Matthews-Olson (FMO) proteins and reaction centers (RCs) that significantly differ in their architecture (Fig.1 inset). The bulk of the gigantic antenna chlorosome is composed of many thousands of bacteriochlorophyll (BChl) *c* molecules [6]. In contrast, the baseplate of the chlorosome is a pigment-protein complex containing BChl *a* and carotenoid molecules [7]. Its function is to mediate the energy transfer from the BChl *c* aggregate (the bulk of the

chlorosome) to the FMO proteins. FMO is a homotrimeric water-soluble protein where each subunit binds eight excitonically coupled BChl *a* molecules [8]. Even though it is widely assumed that FMO serves as the energy transfer linker between the chlorosome baseplate and the reaction centers, it has never been demonstrated experimentally [9]. Accordingly, energy transfer from the chlorosome to FMO or from FMO to the RC has not been measured in vivo. It has been suggested that several FMO trimers are in a close contact with the PSI-type RC core complex possessing altogether 22 pigments (16 BChl *a*, 4 chlorophyll *a* and 2 carotenoid molecules) [10]. Two BChl *a* molecules form so-called special pair where the charge separation takes place starting the chain of photosynthetic reactions.
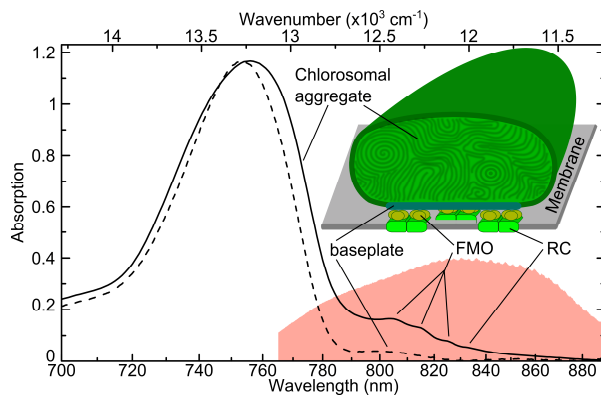

Fig.1: The absorption spectrum of the intact Cba. tepidum cells (solid line), the spectrum of isolated chlorosomes (dashed line) at 77 K and the laser spectrum used in the 2DES experiments (red). In the inset: schematic representation of the photosynthetic apparatus of green sulfur bacteria.

Most of the photosynthetic complexes are readily identifiable in the absorption spectrum of green sulfur bacteria cells at 77 K (Fig. 1). Prominent band of chlorosomal aggregate with an absorption maximum at ~745 nm (13420 cm^{-1}) dominates the spectrum. Three weak peaks at 806 nm (12410 cm^{-1}), 816 nm (12250cm^{-1}) and 825 nm (12120 cm^{-1}) are associated with FMO. Most of the absorption from the baseplate (see the isolated chlorosome absorption in the range of 785-825 nm in Fig. 1) and a core RC complex (750-840 nm) [10] falls into the same region, however their absorption is substantially weaker (see Fig. 1 and ref [11]). The rather weak peak in the most red side of the spectrum at 833 nm (12000 cm^{-1}) belongs to the RC [12]. The fact that absorption of different constituent complexes of the photosynthetic unit is distinguishable enables us to address separate complexes independently.

To map the energy flow through the entire photosynthetic unit we employed coherent two-dimensional electronic spectroscopy (2DES). The main

advantage of the 2DES is that it provides high spectral resolution in excitation and probe frequencies, while retaining high temporal resolution [13]. The real part of the two-dimensional (2D) spectrum can be interpreted as a set of transient absorption spectra. Here we show that the additional dimension in 2DES enables to resolve individual energy transfer steps within and between the light-harvesting complexes and RCs in vivo.
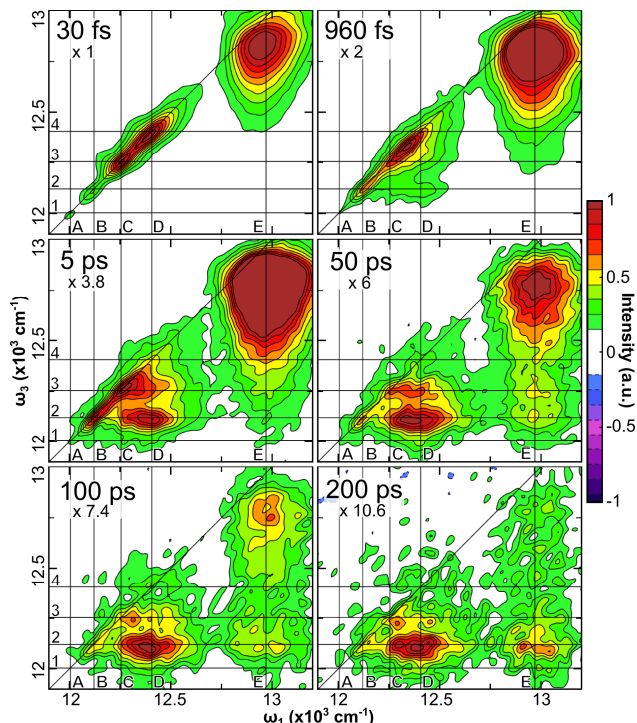

Fig.2: The selected 2D spectra (real part) of the intact cells of green sulfur bacterium Cba. tepidum measured between 11900 – 13200 cm^{-1} (760-840 nm) at indicated population times at 77 K. The spectra are normalized to the maximum of the FMO signal (the relative amplitude is shown in the top left corner). The vertical and horizontal lines show positions of the distinct peaks (from left to right: reaction center - 12000 cm^{-1}; FMO - 12120 cm^{-1}, 12250 cm^{-1} and 12410 cm^{-1}; an extra line in the chlorosome region at 12940cm^{-1}). The letters and numbers associated with the lines are to facilitate location of individual peaks. The same grid is used in the following figures.

The spectrum of laser pulses was centered at 830 nm and covered all the near infrared absorption bands of the photosynthetic apparatus (Fig. 1). Care was taken not to overexcite the strong chlorosomal aggregate band at 745 nm, which signal would otherwise overwhelm the other spectral features. Experiments were performed at anaerobic conditions at 77 K, where spectroscopic features of individual complexes in photosynthetic unit are clearly identifiable. The 2DES spectrum acquired at 30 fs delay time after the excitation (population times)

consists of a series of diagonal peaks that correspond to the linear absorption spectrum (Fig.2). The red-side slope of the chlorosome band, three main FMO peaks and a weak RC peak are clearly visible. The elongated featureless shape of the chlorosome band extending below the diagonal peak is the part of the overwhelming chlorosome peak lineshape and not a cross-peak indicating exciton coupling between the chlorosome and FMO complexes.

The excitation energy flow within and between the individual complexes in the photosynthetic unit are clearly revealed by the time evolution of the 2D spectrum as formation (and decay) of the cross-peaks bellow the diagonal (Fig. 2). Individual points in the 2D spectrum evolve in a complex multiexponential manner with the timescales ranging from 100 fs to 200 ps. To facilitate quantitative analysis the 2D spectra were split into two parts corresponding to the FMO-RC and chlorosome excitation regions and were globally fitted with four decaying exponentials. Amplitudes of all components are plotted in Fig. 3 and 4 as the two-dimensional decay associated spectra (DAS) [14]. Since the positive signals, corresponding to the ground state bleach (GSB) and stimulated emission (SE) dominate the 2D spectra (Fig. 2), it can be concluded that the excited state absorption, which would appear as negative signal, plays only a minor role. Consequently the positive and negative peaks in the DAS spectra (Fig. 3 and 4) can be interpreted as decay and rise of the SE/GSB signals, and indicate energy transfer pathways in the photosynthetic unit.

First, we review the energy relaxation in the FMO complex in vivo. The peaks of the FMO spectrum in the intact cells (Fig. 2) appear at similar positions as the corresponding peaks reported previously in the isolated FMO complexes [1]. The two diagonal FMO peaks at 12410 cm^{-1} and 12250 cm^{-1} decay on a 150 fs timescale transferring energy to the lower levels (Fig 3). Weaker state located in between them at ~12330 cm^{-1} decay ten to hundred times slower transferring energy mostly to the lowest FMO level. This is clearly indicated by a rise (blue color) of the 1.4 ps component at the lowest FMO level (D2 cross-peak in Fig. 3). Interestingly, this intermediate energy relaxation occurs on the slower time scale in vivo than what was observed in the isolated complexes [1]. E.g., the 2D spectrum in our measurement at 5 ps (Fig. 2) is similar to the 2D spectrum at 1 ps of isolated FMO [1]. The third 17 ps component (Fig. 3) is connected with the energy transfer through intermediate levels to the bottom of FMO and with a decay of the lowest FMO level. The latter is identified as the energy transfer from the lowest FMO level to RC and will be discussed below. The relaxation within FMO is completed in ~50 ps. Equilibration on a similar timescale in the isolated

FMO complexes at cryogenic temperatures has been observed previously in the transient absorption experiments [15,16]. Later on the FMO spectrum uniformly decays without any changes of the shape, as demonstrated by the 250 ps component in Fig. 3. The part of the FMO signal that is still visible at the diagonal C3 peak and the cross-peak D3 on the long timescales (see 50 – 200 ps 2D spectra in Fig.2) comes from the GSB signal. This signifies that when the lowest FMO state at 12120 cm^{-1} is populated, the absorption of the state at 12250 cm^{-1} is bleached. This observation confirms that the BChl *a* with the lowest energy in FMO is excitonically coupled to the other pigment(s) [17–19].
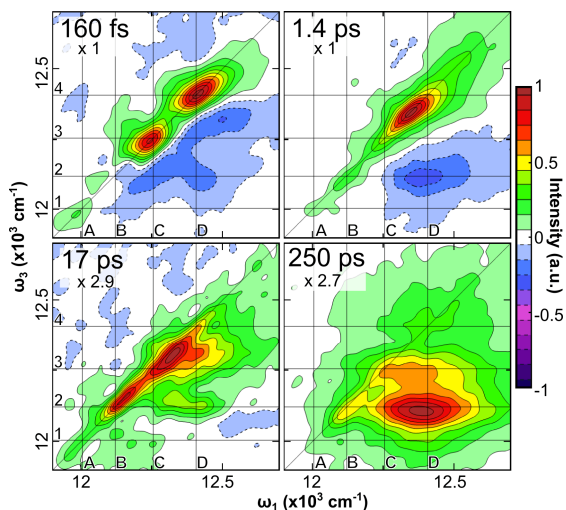

Fig.3: Decay associated spectra of the FMO-RC spectral region. The spectra characterize the energy relaxation within FMO and FMO-RC energy transfer on indicated timescales. All spectra are normalized (the relative amplitude is shown in the bottom right corner).

Now we focus on the energy transfer through the whole photosynthetic unit. The connectivity and energy transfer between the different complexes are clearly observed in the sequence of the 2D spectra presented in Fig. 2. Appearance of the cross-peaks below the chlorosome diagonal peak at E2, E3 positions implies energy transfer from the chlorosome to FMO and cross-peaks appearing at D1 and E1 positions reveal the energy transfer from FMO to RC. Thus, we unequivocally show that the FMO complex serves as the energy conduit between the chlorosome and RC.

To get more quantitative information on each energy transfer step we analyze global fitting results. The DAS components of the chlorosome part are determined by the evolution of chlorosome diagonal and cross-peak, providing insights into the clorosome connectivity to the rest of the photosynthetic unit

(Fig.4). The fastest ~1 ps process (940 fs component in Fig. 4) can be attributed to the relaxation within the chlorosome band [20]. On 10 ps timescale the exciton annihilation in the chlorosome is resolved as a decaying component without corresponding rise. The chlorosome to FMO energy transfer proceeds with the 70 ps time constant. Lastly, the population from the lowest FMO level leaves with 250 ps time constant. Whereas the rise on the lowest long-lived FMO level (at E2) is clearly visible in the 70 ps component (Fig. 4), the rise of the higher FMO level signal, i.e. E3 is not observed, because of the fast internal relaxation in FMO. In our measurement energy transfer between the baseplate and FMO is not apparent. This can be explained as follows. First, the absence of additional dynamics in our measurements indicates that the equilibrium between the baseplate and FMO is very fast. Second, the baseplate absorption is much weaker than absorption of FMO (Fig. 1) and thus baseplate signals cannot be clearly disentangled.
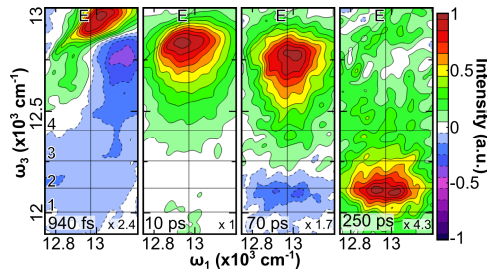

Fig.4: Decay associated spectra of the chlorosome excitation region. The spectra characterize the energy transfer through the whole photosynthetic system after chlorosome excitation. All spectra are normalized (the relative amplitude is shown in the bottom right corner).

Next we evaluate the energy transfer from FMO to the RC after direct FMO excitation that appears as the D1 cross-peak (Fig. 2). The intrinsic RC dynamics can be analyzed at the RC diagonal peak A1. This peak decays mainly on the 160 fs and 1.4 ps timescale (Fig. 3). These time constants correspond to the electron transfer and likely other processes in RC. The FMO-RC energy-transfer cross-peak D1 rises on the same timescales and decays with the 17 ps time constant (Fig 3). Such a sign inversion indicates that the energy leaves the RC state at 12000 cm^{-1} faster than it is populated by the energy transfer from FMO. The 17 ps component thus should be assigned to the FMO-RC energy transfer. However, it is clear from the significant amplitude of the cross-peaks at D2 and E2 in 200 ps 2D spectrum in Fig. 2 that some fraction of the excitation energy stays in the lowest FMO level at much longer timescales. Based on the analysis of peak amplitudes we estimate that around ~25% of the energy originally absorbed by FMO is still present in the lowest state after 200 ps.

Efficiency of the FMO-RC energy transfer in green sulfur bacteria is a long-standing question. It has been consistently demonstrated that the FMO-RC energy transfer in the isolated complexes or membrane preparations is <30% [21–24], for which isolation procedures were held responsible. Our estimate from in vivo measurements points to 75 % efficiency; however there are two factors that could affect this number. First, the estimation is sensitive to the annihilation processes in FMO, which would lead to the efficiency overestimation. On the other hand the FMO-RC energy transfer efficiency could be underestimated, because of excitation congestion in the photosynthetic apparatus due to multiple excitations competing for the entry into RC. Then only the first excitation would be transferred to the RC, effectively closing it for the others.

Here we demonstrate how 2DES is used to directly monitor the primary photosynthetic processes in the intact photosynthetic organisms, avoiding all ambiguities and possible pitfalls of inferring the total energy collection functionality in vivo from the data obtained on isolated subunits.

METHODS SUMMARY

The detailed description of the experimental setup used to obtain 2DES spectra can be found in [25]. During experiments the coherence time was scanned from −170 fs to 450 fs with 2 fs step, which ensured the resolution of 40 cm^{-1} along the excitation (coherence) frequency axis. The same resolution was achieved along the detection frequency axis, determined by the time domain window used in Fourier analysis. The laser repetition rate was 20 kHz and the excitation energy was 1nJ per single pulse focused to the 0.1 mm spot.

The *Cba. tepidum* cells were grown as described in [26] and chlorosomes were isolated as described in [27]. Prior the measurements the cell suspension was concentrated by centrifugation and diluted in 1:2 (v/v) ratio with glycerol to obtain absorbance of about 0.2 at 800 nm in the 0.2 mm sample cell. The sample was reduced by sodium dithionite (concentration of 20 mM) and incubated for at least 2 hours in air-tight vessel at the room temperature. All experiments were carried at 77 K in the optical cryostat (Oxford Optistat DN).

REFERENCES

1. Brixner T, Stenger J, Vaswani HM, Cho M, Blankenship RE, Fleming GR (2005) Two-dimensional spectroscopy of electronic couplings in photosynthesis. *Nature* **434**: 625–628.

2. Zigmantas D, Read EL, Mančal T, Brixner T, Gardiner AT, Cogdell RJ, Fleming GR (2006) Two-dimensional electronic spectroscopy of the B800–B820 light-harvesting complex. *Proc Natl Acad Sci U S A* **103**: 12672–12677.

3. Huh J, Saikin S ~K., Brookes J ~C., Valleau S, Fujita T, Aspuru-Guzik A (2013) Atomistic study of energy funneling in the light-harvesting complex of green sulfur bacteria. *ArXiv e-prints*.

4. Overmann J, Cypionka H, Pfennig N (1992) An extremely low-light-adapted phototrophic sulfur bacterium from the Black Sea. *Limnol Oceanogr* **37**: 150–155.

5. Beatty JT, Overmann J, Lince MT, Manske AK, Lang AS, Blankenship RE, Van Dover CL, Martinson T a, Plumley FG (2005) An obligately photosynthetic bacterial anaerobe from a deep-sea hydrothermal vent. *Proc Natl Acad Sci U S A* **102**: 9306–9310.

6. Blankenship RE, Matsuura K (2003) Antenna complexes from green photsynthetic bacteria. In Green BR, Parson WW (eds.), *Light-harvesting antennas in photosynthesis* pp 195–217. Kluwer Academic Publishers, Dordrecht.

7. Pedersen MØ, Linnanto J, Frigaard N-U, Nielsen NC, Miller M (2010) A model of the protein – pigment baseplate complex in chlorosomes of photosynthetic green bacteria. *Photosynth Res* **104**: 233–243.

8. Milder MTW, Brüggemann B, van Grondelle R, Herek JL (2010) Revisiting the optical properties of the FMO protein. *Photosynth Res* **104**: 257–274.

9. Amesz J, Neerken S (2002) Excitation energy trapping in anoxygenic photosynthetic bacteria. *Photosynth Res* **73**: 73–81.

10. Hauska G, Schoedl T, Remigy H, Tsiotis G (2001) The reaction center of green sulfur bacteria. *Biochim Biophys Acta* **1507**: 260–277.

11. Permentier HP, Schmidt KA, Kobayashi M, Akiyama M, Hager-Braun C, Neerken S, Miller M, Amesz J (2000) Composition and optical properties of reaction centre core complexes from the green sulfur bacteria Prosthecochloris aestuarii and Chlorobium tepidum. *Photosynth Res* **64**: 27–39.

12. Otte SC, Heiden JC van der, Pfennig N, Amesz J (1991) A comparative study of the optical characteristics of intact cells of photosynthetic green sulfur bacteria containing bacteriochlorophyll c, d or e. *Photosynth Res* **28**: 77–87.

13. Hamm P, Zanni M (2011) *Concepts and methods of 2D infrared spectroscopy.* Cambridge University Press, New York.

14. Van Stokkum IHM, Larsen DS, van Grondelle R (2004) Global and target analysis of time-resolved spectra. *Biochim Biophys Acta* **1657**: 82–104.

15. Vulto SIE, Streltsov AM, Aartsma TJ (1997) Excited state energy relaxation in the FMO complexes of the green bacterium Prosthecochloris aestuarii at low temperatures. *J Phys Chem B* **101**: 4845–4850.

16. Zhou W, LoBrutto R, Lin S, Blankenship RE (1994) Redox effects on the bacteriochlorophyll a-containing Fenna-Matthews-Olson protein from Chlorobium tepidum. *Photosynth Res* **41**: 89–96.

17. Adolphs J, Renger T (2006) How proteins trigger excitation energy transfer in the FMO complex of green sulfur bacteria. *Biophys J* **91**: 2778–2797.

18. Vulto SIE, de Baat MA, Louwe RJW, Permentier HP, Neef T, Miller M, Van Amerongen H, Aartsma TJ (1998) Exciton simulations of optical spectra of the FMO complex from the green sulfur bacterium Chlorobium tepidum at 6 K. *J Phys Chem B* **102**: 9577–9582.

19. Cho M, Vaswani HM, Brixner T, Stenger J, Fleming GR (2005) Exciton analysis in 2D electronic spectroscopy. *J Phys Chem B* **109**: 10542–10556.

20. Pšenčík J, Ma Y-Z, Arellano JB, Hála J, Gillbro T (2003) Excitation energy transfer dynamics and excited-state structure in chlorosomes of Chlorobium phaeobacteroides. *Biophys J* **84**: 1161–1179.

21. Oh-oka H, Kamei S, Matsubara H, Lin S, van Noort PI, Blankenship RE (1998) Transient Absorption Spectroscopy of Energy-Transfer and Trapping Processes in the Reaction Center Complex of Chlorobium tepidum. **102**: 8190–8195.

22. Kramer H, Kingma H, Swarthoff T, Amesz J (1982) Prompt and delayed fluorescence in pigment-protein complexes of a green photosynthetic bacterium. *Biochim Biophys Acta* **681**: 359–364.

23. Francke C, Otte SC, Miller M, Amesz J, Olson JM (1996) Energy transfer from carotenoid and FMO-protein in subcellular preparations from green sulfur bacteria. Spectroscopic characterization of an FMO-reaction center core complex at low temperature. *Photosynth Res* **50**: 71–77.

24. Neerken S, Permentier HP, Francke C, Aartsma TJ, Amesz J (1998) Excited states and trapping in reaction center complexes of the green sulfur bacterium Prosthecochloris aestuarii. *Biochemistry* **37**: 10792–10797.

25. Augulis R, Zigmantas D (2011) Two-dimensional electronic spectroscopy with double modulation lock-in detection: enhancement of sensitivity and noise resistance. *Opt Express* **19**: 13126–13133.

26. Pšenčík J, Ikonen TP, Laurinmäki P, Merckel MC, Butcher SJ, Serimaa RE, Tuma R (2004) Lamellar organization of pigments in chlorosomes, the light harvesting complexes of green photosynthetic bacteria. *Biophys J* **87**: 1165–1172.

27. Steensgaard DB, Matsuura K, Cox RP, Miller M (1997) Changes in bacteriochlorophyll c organization during acid treatment of chlorosomes from Chlorobium tepidum. *Photochem Photobiol* **65**: 129–134.